Development of Stable Leader-Follower Tracking System for Agricultural Vehicles

January 2015

Linhuan ZHANG

Development of Stable Leader-Follower Tracking System for Agricultural Vehicles

A Dissertation Submitted to
the Graduate School of Life and Environmental Sciences,
the University of Tsukuba
in Partial Fulfillment of the Requirements
for the Degree of Doctor of philosophy in Agricultural Science
(Doctoral Program in Biosphere Resource Science and Technology)

Linhuan ZHANG

Abstract

Multiple robotic vehicle technology potentially has significantly important in agricultural operation with the requirement of higher working efficiency and tendency of land concentration. When compared with large size agricultural vehicles, the multiple small size autonomous agricultural vehicles can work in leader-follower mode owns its advantages from view of cost and working flexibility. By tracking a leader vehicle one or more autonomous follower vehicles could form a group to carry out tasks with higher efficiency. Additionally, under soft and wet land condition small tire and lighter weight of small size agricultural vehicles will cause less land tearing which is important to solve soil compaction. Also by adjusting the tracking formation and trajectory between the leader and follower vehicles, composed of the multiple small size leader-follower agricultural vehicles would be more adaptable to variegated terrain land and road conditions in hilly Asian countries.

The core work of this thesis concerns defining of the leader vehicle position using local sensors and landmark under the follower vehicle based on local coordinate, and driving the follower vehicle tracks the leader vehicle for safety driving and precision agriculture task operation. To meet the requirements of variant tasks, the Laser Ranger Finder (LRF)-landmark based and monocular camera-marker based local sensing system, and the leader-follower formation tracking and leader trajectory tracking algorithm were developed.

For verifying the performance of developed tracking system five major experiments were conducted: the discrimination and location of marker using

camera vision, dynamically detection and measurement the leader-follower relative position using the camera-marker sensing system, fusion local sensing system observation with odometry, tracking a required leader-follower vehicle formation and tracking the leader vehicle trajectory.

In the first experiment, by used of shape feature and known size of the marker to ensure the stable recognition and accuracy measurement. In the scope of 4 m the RMSEs of distance, orientation and relative angle observation were 0.036 m, 0.239˚ and 3.01˚, respectively.

Second, both of the camera and marker was installed on driving vehicles and then measured the relative position between the camera and the marker which could define the relative position between two vehicles. By compensating vehicle rolling angle the relative position observation could avoid suffering from uneven ground condition. Camera servo system composed of servo motor and rotary encoder was designed to solve the problem of limited camera view field. Least square method based data smooth method was used to smooth the camera observation. As a result, RMSEs of the relative distance and relative angle was 0.046 m and 2.87˚, respectively, standard deviation of the relative distance and relative angle was 0.042 m and 2.55˚, respectively, on the zigzag path driving and maximum relative distance was up to 4.3 m. The experimental data showed the camera-marker sensing system have enough stability and accuracy to measure the relative position between the leader and the follower.

Third, simulators were developed to evaluate performance of the designed leader-follower formation tracking and leader trajectory tracking algorithm. The simulated vehicles reference parameters of Kubota KL 21 tractor. Simulations

were conducted for longitudinal 2 m and lateral 3 m leader-follower relative formation tracking and 5 m longitudinal distance and 3 m lateral trajectory interval leader trajectory tracking. The simulation results showed that the follower vehicle could track the required formation and leader trajectory accuracy and smoothly. During the leader-follower formation tracking the RMSEs of lateral, longitudinal, and heading tracking error on small curved path was 0.166 m, 0.104 m, and 4.045˚, respectively; on large curved path was 0.195 m, 0.234 m, and 13.613˚, respectively. During the leader trajectory tracking the RMSEs of trajectory tracking error for linear and parallel tracking on small curved path was 0.051 m, and 0.066 m, respectively, on large curved path was 0.041 m, and 0.256 m, respectively.

Fourth, an Extend Kalman Filter (EKF) was used to estimate the leader-follower relative position by fusing the local sensing system observation and odometry. Computer simulation was conducted based on the previous knowledge of LRF and the odometry. It was confirmed and the developed EKF model has good performance for reducing noise. The EKF helped to improve observation accuracy, velocity, and steering angle stability of the follower. On the small sinusoidal curved path, the RMSEs of the lateral, longitudinal, and heading observation error reduced from 0.181 to 0.173 m, 0.166 to 0.053 m, and 4.373 to 1.807˚, respectively; and RMSEs of the velocity and steering angle was reduced from 0.167 to 0.053 m/s and 6.029 to 2.406 º, respectively. On the large sinusoidal curved path, the RMSEs of the lateral, longitudinal, and heading observation error were reduced from 0.191 to 0.126 m, 0.175 to 0.045 m, and 4.672 to 1.718˚, respectively; and RMSEs of the velocity and steering angle was

reduced from 0.176 to 0.039 m/s and 7.659 to 3.157 º, respectively. As a result of the improved accuracy of observation and motion action, the tracking performance for lateral, longitudinal, and bearing were also improved after the EKF was implemented in the tracking system.

Finally, field experiment was conducted to tracking the leader trajectory based the camera-marker sensing system for 4m longitudinal distance and 2m lateral trajectory interval. The experimental leader and the follower vehicle were modified from electric vehicle EJ-20 produced by CHIKUSUI CANYCOM Company. The autonomous vehicle as a follower was equipped with computer, electric cylinder, camera, linear encoder, and two incremental rotary encoders were used in the experimental vehicle. The results of the field experiments showed that the leader trajectory tracking algorithm could control the follower stably and realize accurate tracking. When tracking on straight path, the maximum and RMS tracking error between the trajectory of leader and the follower vehicle was 0.167 m and 0.067 m, 0.142 m and 0.072 m for linear tracking and parallel tracking; When tracking on turning path, the maximum and RMS tracking error between the trajectory of the leader and the follower vehicle was 0.19 m and 0.092 m, 0.352 m and 0.158 m for linear tracking and parallel tracking; and when tracking on zigzag path, the maximum and RMS tracking error between the trajectory of leader and the follower vehicle was 0.351 m and 0.162 m, 0.285 m and 0.142 m for linear tracking and parallel tracking, respectively. By smooth the camera observation of the leader-follower relative position the stability of velocity and steering angle was also significantly improved during tracking.

The experimental results confirmed that the designed sensing and tracking system could ensure accuracy and stable tracking control of the leader-follower multiple robotic vehicles. Thus, low-cost and reliable navigation system for the leader-follower multiple robotic vehicles could be available to realize precise agricultural operation, improve working efficiency and ensure driving safety.

Table of Contents

Nomenclature

x_l, y_l : Global position of the leader (m)

x_f, y_f : Global position of the follower (m)

θ_l, θ_f : Global heading angle of the leader, and follower (˚)

x_{l_F}, y_{l_F} : Local position of the leader based on the follower

θ_{l_F} : Local heading angle of the leader based on the follower (˚)

L : Length of wheelbase (m)

l_1, l_2, l_3 : Distances between first and second landmarks; second and third landmarks; and first and third landmarks (m)

d_1, d_2, d_3 : Distances from LRF to first landmark, to second landmark and third landmark, respectively (m)

$\alpha_1, \alpha_2, \alpha_3$: Detected angles between LRF axle and first landmark, LRF axle and second landmark, and LRF axle and third landmark, respectively (˚)

β : Relative heading angle between the leader and the follower (˚)

H : Side of squares on marker (m)

h : Length of square centerline in the image plane (m)

x_c, y_c : Square centers under image coordinate (m)

X_C, Y_C, Z_c : Square centers under camera based coordinate (m)

f, f_x, c_x : Camera parameter

X_{CN}, Y_{CN}, Z_{CN} : Square centers under camera based coordinate (m)

x, y : Position of vehicle based on center rear axle (m)

δ : Steering angle (˚)

v : Velocity (m s-1)

w : Steering angular velocity (rad s-1)

x_{vf}, y_{vf} : Global position of the virtual follower (m)

θ_{vf} : Global heading angle of the virtual follower (˚)

$\delta_l, \delta_{vf}, \delta_f$: Steering angle of leader, virtual follower and follower (˚)

v_l, v_{vf}, v_f : Velocity of the leader, virtual follower and follower (m s-1)

w_l, wv_f, w_f : Steering angular speed of the leader, virtual follower and follower (rad s-1)

d_{01} : Required relative distance between the leader and the follower (m)

Φ_{01} : Required relative angle between the leader and follower (˚)

d_{12} : Relative distance between the leader and the follower (m)

Φ_{12} : Required relative angle between the leader and follower (˚)

x_e : Lateral formation tracking error (m)

y_e : Longitudinal formation tracking error (m)

θ_e : Heading formation tracking error (˚)

x_{f_L}, y_{f_L} : Local position of the follower based on the leader

x_{vf_L}, y_{vf_L} : Local position of the virtual follower based on the leader (m)

θ_{f_L} : Local heading of the follower based on the leader (˚)

θ_{vf_L} : Local heading of the virtual follower based on the leader (˚)

θ_{l_L} : Local heading angle of the leader based on local coordinate of the leader (˚)

x_{req_L}, y_{req_L}: Local position of the required position based on the leader (m)

θ_{req_L}: Local heading of the required position based on the leader (˚)

L_c: Distance from rear wheel axle center to control point (m)

x_{c_L}, y_{c_L} : Local position of the control point based on the leader

θ_{c_L}: Local heading of the control point based on the leader (˚)

x_{e_c} : Lateral position tracking error (m)

y_{e_c} : Longitudinal position tracking error (m)

θ_{e_c} : heading position tracking error (˚)

$f(\cdot)$: Nonlinear system function

$h(\cdot)$: Observation function

X_k: State of leader-follower relative state at time instant k

Z_k: Observation of leader-follower relative state at time instant k

$\tilde{X}, \hat{X}$: Prediction and corrected state of leader-follower relative state

$\tilde{P}_k, \hat{P}_k$: Prediction state error covariance matrix and correction state error covariance matrix

$J_{x,k}, J_{v,k}$: Jacobeans of system function $f(\cdot)$ with respect to state X and input U

$H_k, J_{w,k}$: Jacobeans of observation function $h(\cdot)$ with respect to prediction state $\tilde{X}_k$ and observation Z_k

K_k : Kalman gain

I : Identity matrix

U: Control input

V : Noise and disturbance of control input

W : LRF measurement noise

Q, R : Covariance matrices for control input noise and LRF measurement noise

T_s : Time interval (ms)

θ_{flaser} : Heading angle of the follower based on the leader local coordinate using LRF (˚)

d_{laser} : Relative distance between the leader and the follower using LRF (m)

Φ_{laser} : Relative angle between the leader and the follower using LRF (˚)

σ_{vl}, σ_{vf} : Variances of measurement noise from encoders (m s-1)

$\sigma_{\delta l}, \sigma_{\delta f}$: Variances of measurement noise from encoders (rad s-1)

σ_d : Variances of distance measurement noise from the LRF (m)

σ_{ang} : Variances of angle measurement noise from the LRF (rad)

X_{CH}, Y_{CH}, Z_{CH} : Square centers under horizon surface (m)

α_s : Angle from between square center to camera optic axis (˚)

α_{En} : Angle between optic axis and follower centerline (˚)

X_{VN}, Y_{VN} : Square centers under follower vehicle local coordinate (m)

$Q(s)$: Sequence of stored observation data

q_{Raw} : Raw vision data

q_{Fit} : Fitted data

q_{store_i} : Stored i_{th} observation data

M_1, M_2 : Threshold value

List of Tables

List of Figures

Chapter 1

Introduction

The agricultural labor in Japan has been greatly changed recently. With the rapidly decreasing of agricultural labor, by 2020s more than 60% and 45% of people engaged in farming are expected older than 60 and 70. Furthermore, half of them will be women. Lacking of farming workforce and aging population also became a global problem.

Development of autonomous agricultural machinery creates opportunity to change the traditional agricultural production system and shift to an intelligent agricultural system. Autonomous agricultural machinery could ensure precise operation, increase productivity, minimize required workforce, and improve production. Numerous studies have been performed on navigation of autonomous tractors, including positioning, driving, and steering control functions (Kise et al., 2001; Sutiarso et al., 2002; Han et al. 2004; Fu et al., 2013). Advanced sensing technologies, control theories, and high accuracy control of autonomous tractors have been developed. However, most of the previous research focused on the navigation of a single tractor. Agricultural operate by the multiple autonomous vehicles could further improve working efficiency, save workforce and perform various labor consuming tasks. And there is in fact a strong need for cooperation between multiple machines in agricultural operation (Noguchi et al., 2011).

1.1 Navigation of multiple vehicles

Considering farming task style, a common operational method of multiple autonomous vehicles would be effective when taking the leader-follower

formation. Requested performance in agricultural task somewhat differ from one another. The content of leader-follower vehicle system navigation mainly considers the controls of the follower vehicle include: leader-follower relative formation tracking and leader trajectory tracking.

Tracking the leader-follower relative formation request the follower vehicle to tracking a required formation by maintaining a certain longitudinal and lateral with the leader vehicle. One of the typical applications of leader-follower relative formation tracking could be observed in harvest operations. During harvesting operations, a follower tractor is required to maintain a short distance and parallel motion with a leader combine or other harvesters (Fig 1.1). This was an arduous and dangerous task for drivers who have to focus their attention for long time. An autonomous follower could replace the human driver to realize safety and accuracy tracking.

Fig. 1.1 Track a requirement formation with the harvester

Tracking the leader trajectory request the follower vehicle to track an identical or parallel trajectory with the leader vehicle (Fig 1.2). Such performance owns significant meaning under the complex farmland condition. For example, follower vehicles track linear formation with the leader could drive as the leader

to keep safety when driving on narrow road with obstacles; while working on the farmland, follower vehicles track parallel formation with the leader could drive parallel trajectories with the leader trajectory to conduct farming task without overlap or leak. When driving on a curve road or working on an irregular farmland tracking the leader vehicle trajectory would show its special advantage.

(a)

(b)

Fig. 1.2 Track the trajectory of leader vehicle

(a) Track an identical trajectory (b) Track a parallel trajectory

1.2 Sensors for leader-follower vehicle tracking control

To ensure the tracking stability and safety, constant and precise observation of

the relative position of between the leader and follower vehicles was essential. Under the irregularities farmland ground swing and vibration of vehicles would affect sensing accuracy. The sensing system should be competent under changing movement and posture of the leader and follower vehicles. In an adverse environment such as agricultural operations, a proper sensing and control system alone was insufficient to ensure the stability and safety tracking of the leader and the follower. Because there are sources of noise from sensors, for example, farmland surface conditions cause a large odometry error, dust, flog and strong sunshine would make optic sensors difficult to detect or even blind. The limited detection rang and distance would also lead to losing of target, and low update frequency of sensor data would cause the follower vehicle impossible to tack sensitive response. Thus, the integrity of sensors and fusing of sensor data was essential for obtaining correct observation information from noisy signals as another key issue for stability and safety tracking.

1.3 Objects

This study addresses the issues of stable and accuracy navigation a follower vehicle using reliable sensing system for stable operation in the multiple agricultural vehicles. The goal of this thesis is to develop accuracy and stable tracking system including sensing systems and tracking algorithms to complete the leader-follower multiple vehicles tracking project from road driving and field operation. The objectives of this thesis in order to reach this goal are:

1) To develop a formation tracking system for multiple agricultural machinery combinations, with a leader and a follower, including virtual follower-based feedback control.

2) To develop an accuracy leader vehicle trajectory tracking system for multiple agricultural machinery combinations, with a human-driven leader and an autonomous follower using a feedback control.

3) To construct a robust and accuracy landmark based laser and monocular vision local sensing system can identify relative position between a leader and a follower.

4) To introduce an EKF fusing system to improve accuracy of the leader-follower relative position in the virtual follower-based feedback control system.

1.4 The Structure of this Thesis

This thesis was organized as follow: In chapter 2, control theories and the use of sensors for robot navigation and multiple robotics control was described. In chapter 3, sensing method for leader-follower relative position observation was discussed. The designed laser-landmark based and monocular camera-marker based local sensing system was described. In chapter 4, the virtual follower based leader-follower formation tracking algorithm and the leader trajectory tracking algorithm was preprocessed. The performance of development controllers were then tested through computer simulation. In chapter 5, model for local sensing observation and odometry date fusing using an EKF was designed and the performance was evaluated through computer simulation. In chapter 6, a description of electronic and control devices used in the experiment was explained. In chapter 7, the results of camera-marker sensing system and the leader vehicle trajectory tracking performance evaluation experiments were described. Finally, some conclusions and recommendations were given in chapter 8,

Chapter 2

Literature Review

With the improvement of sensors device and deeper understand of control theory high performance field autonomous vehicle systems could be designed. However, compare with the robotic applied on structured environment or industrial sectors the autonomous agricultural machines request higher performance of sensing system and robust controller. Take the car like robot as example it is convenient to navigation in structured environment, while in case of agricultural condition wheel slip, field undulation and dusty would disturbance control model and sensor accuracy and cause large navigation error or even fail (Wu et al., 1999). In the multi-robot navigation, as a dynamic tracking system except above disturbance the follower also required quickly and correctly responds to tracking error (Madhavan et al., 2004).

In this chapter, the follower sections discuss the contributions regarding leader-follower tracking system.

2.1 Tracking control of a leader-follower system

2.1.1 Feedback control

Feedback control was popular in robot control, and the control of nonholonomic wheel mobile can be divided into two main groups: open-loop and closed-loop strategies. Open-loop (feed forward) controls are regarded as synonyms as opposed to feedback control. A closed-loop controller results from superposition of a feedback action to a coherent feed forward term. The feed forward term is determined based on a priori knowledge about the motion task and the

environment. Instead the feedback control is computed in real-time based on sensor data.

Zhang et al (2010) designed a feedback controller to control a master-slaver tractor for an auto tracking system. In the research system was developed based on RTK-GPS and gyroscope which provide positional information. The system was tested on real condition using Fendt 936 Vario model tractors. In field experiment it could obtain tracking error less than 20cm on curve path.

Yang et al (2007) designed a time-varying feedback control law with asymptotic stability has been achieved by using the integrator back stepping method for the dynamically. It was succeed applied for collaboratively mooring control of nonholonomic AUVs in chained form. The feedback control law that gives asymptotical convergence to the origin of the formation error dynamics has been presented for the nonlinear formation-keeping control of multiple nonholonomic AUVs. The design of this formation-keeping control law was based on the nonlinear changes of states and the Lyapunov direct method. The stability of the formation system has been analyzed. Under some additional conditions on the inputs of the leader, the asymptotical convergence can be guaranteed. With some assumptions and constraints on the reference inputs, the bounded stability and asymptotical convergence were also available. The motion of the leader is time-varying. Besides the desired separations with respect to the leader, the orientation of the follower can also be steered to the same as the leader in both formation-keeping and dynamically mooring control.

Yamaguchi et al (2003) proposed a path following feedback control method with a variable velocity for a cooperative transportation system with two car-like

mobile robots was designed. All state variables of the transportation system are controlled by feedback and their asymptotical stability is guaranteed and furthermore, the deviation of its position from is compensated and converged into zero by a new feedback control loop in which its moving velocity along the path is variable. The experiment apparatus of the transportation system and verified the validity of the feedback control method with a variable velocity.

2.1.2 Sliding mode control

Sliding mode control is a nonlinear control method that alters the dynamics of a nonlinear system by application of a discontinuous control signal that forces the system to "slide" along a cross-section of the system's normal behavior. The state-feedback control law is not a continuous function of time. Instead, it can switch from one continuous structure to another based on the current position in the state space. Hence, sliding mode control is a variable structure control method. Sliding mode control has many applications in robotics.

Noguchi et al (2004) designed a sliding mode controller and was adopted for both the spacing control and the lateral offset control for a master-slave follow control. During the simulation, the master traveled on a predetermined path and changed speed according to a schedule. The slave controlled its own speed and angle of direction to follow the path of the master. When the slave was controlled by the sliding mode controllers, the following performance was better compared to the when it was controlled by a conventional PD controller because the sliding mode control was suitable for control on a highly nonlinear system. The advantage showed on smaller tracking error and stable motion. In the research the sliding mode controller realized 0.134 m RMSE for lateral and 0.106 m

RMSE for longitudinal. They concluded that the sliding mode controller that was developed using the sliding mode control had better performance for both lateral and spacing controls.

Morbidi et al (2008) proposed a sliding mode control scheme for asymptotically stabilizing the vehicles to a time-varying desired formation. In the research, the follower is a car-like vehicle and the leader is a tractor pulling a trailer. The leader moves along assigned trajectories and the follower is to maintain a desired distance and orientation to the trailer. The attitude angles of the follower and the tractor are estimated via global exponential observers based on the invariant manifold technique. Simulation experiments illustrate the theory and show the effectiveness of the control method.

However, the sliding mode control must be applied with more care than other forms of nonlinear control that have more moderate control action. In particular, because actuators have delays and other imperfections, the hard sliding-mode-control action can lead to chatter, energy loss, plant damage, and excitation of unmolded dynamics. Continuous control design methods are not as susceptible to these problems and can be made to mimic sliding-mode controllers.

2.1.3 Receding horizon control

The prediction horizon keeps being shifted forward and for this reason MPC is also called receding horizon control. Although this approach is not optimal, in practice it has given very good results. Much academic research has been done to find fast methods of solution of Euler–Lagrange type equations, to understand the global stability properties of MPC's local optimization, and in general to

improve the MPC method.

Dunbar et al (2007) considered cooperative control problems using receding horizon optimal control. For a cost function whose coupling reflects the communication constraints of the vehicles, he generates distributed optimal control problems for each subsystem and establishes that the distributed receding horizon implementation is asymptotically stabilizing. The communication requirements between subsystems with coupling in the cost function are that each subsystem obtains the previous optimal control trajectory of those subsystems at each receding horizon update. The key requirements for stability are that each distributed optimal control not deviate too far from the previous optimal control, and that the receding horizon updates happen sufficiently fast.

Chen et al (2008) presented a receding-horizon leader-follower (RH-LF) controller for addressing formation control problem of multiple nonholonomic mobile robots. The follower robots are controlled with given separation, bearing, and relative orientation deviation to the leader. Two formation control strategies, Separation-Bearing-Orientation Controller (SBOC) and Separation- Separation – Orientation Controller (SSOC) were proposed in. The system stability can be guaranteed if a terminal state penalty term is added to the cost function and a terminal state inequality constraint can be satisfied the proposed RH-LF controller guarantees asymptotic stability of the robot system. The proposed control strategy also ensures that the velocity input generates suboptimal solutions to the formation tracking system. Simulations are performed and demonstrated the effectiveness of the proposed RH-LF formation controller.

2.2 Sensors

2.2.1 GPS

Global Positioning System (GPS) receivers have been widely used as global guidance sensors. GPS-based guidance technology can be used for many field operations such as sowing, tilling, planting, cultivating, weeding and harvesting. GPS-based navigation systems are the only navigation technologies that have become commercially available for farm vehicles (Li et al., 2009).

Van Zuydam et al (1999) measured the actual position of the implement using Real Time Kinematic DGPS. The calculated error was used to control a correction device that moved the implement to its predetermined path, with in a control band of ±20 cm. thereby providing a steering aid for the driver. Field tests with a full size tractor the followed a winding guide rail with ±12 cm lateral undulations, while the implement was programmed to cover a straight track, showed an average error of 2 cm. when moving at a speed of 5.2 km/h.

Nagasaka et al (2002) employed a Real Time Kinematic DGPS for precise positioning (2 cm precision at 10 HZ data output rate), fiber optic gyroscope (FOG) sensors for measuring direction and maintain vehicle inclination, and actuators to control steering, engine throttle, clutch, brake, etc. The field experiment showed that root mean square deviation from the desired straight path after correcting for the yaw angle offset was approximately 5.5 cm at a speed of 0.7m/s. the maximum deviation from the desired path was less than 12 cm.

Zhou et al (2013) designed a GPS based navigation system for wheel-type agricultural vehicles with mechanism steering system. By responding the heading angle error and cross track error using fuzzy controller, an incremental PID control method was used for front wheels steering control. Filed experiment

showed cross track error of line track less than 0.12m, and the average cross track error as 0.04m was realized.

The above contribution related with GPS sensors could provide high accuracy, however the GPS signal was easy suffered the limitation of signal availability due to interference like trees and buildings.

2.2.2 Odometry and inertial sensors

Navigation using the odometry and inertial sensors was named as dead reckoning. This method was reliable for the short traveling, while error was easy accumulated. The odometry and Inertial sensors are mainly used to measure the monitor the internal state of the vehicle, for example; velocity, acceleration, attitude, current, voltage, temperature, pressure, balance etc.

Hague et al (2000) summarized that a common limitation suffers dead reckoning sensors. This is not so much a failing of the sensors themselves, but in the method; since motion information is integrated to give position, any small bias in the sensor output will accumulate and result in position drift. However, odometers and inertial system have a high bandwidth, and are fairly reliable in the short term.

Barshan et al (1995) explained that the dead reckoning using odometry is not very robust localization technique for robots that cover long distance and are in continuous operation over extended periods. This occurred due to errors in odometry accumulate over time, in accuracies in the kinematic model, precision limitations of encoders, unobservable factors like wheel slippages that are accounted in the kinematic model.

Cho et al (2011) designed a dead reckoning localization system for mobile robots

using inertial sensors and wheel revolution encoding. The mobile robot position estimation reduced the accumulation errors through a Kalman filter by combining odometry and INS. The system estimates the orientation of the mobile robot using inertial sensors, therefore it can compensate for the inclination of the ground. By correcting Inertial sensors errors and compensates for the yaw angle errors that generate position errors in odometry, the system shows liable of position estimation. The dead reckoning period that estimates the position without any external position data from an absolute positioning system has been extended.

Thus the odometry and inertial sensors was very important devise for robot location but their drawbacks come from accumulated errors and they are sensitive to slope and uneven surface (Maeyama et al., 1997), and should deal with its error accumulate problem by cooperate using of other sensor system.

2.2.3 Laser Ranger Finder

Laser ranger finder owns the advantage for distance and angle measurement. As its long range and high resolution many works have been contributed for the mobile robots for indoor and outdoor localization using laser ranger finder.

Núñez et al (2008) proposed a geometrical feature detection system which was to be used with conventional 2D laser ranger finders. It consisted of three main modules: data acquisition and pre-processing, segmentation and landmark extraction and characterization. The novelty of the system was a new approach for laser data approach divided the laser scan into line and curve segments. Then, these items were used to directly extract several types of landmarks associated with real and virtual features of the environment (corners, center of tree like

objects, line segments and edges). For each landmark, characterization provided not only the parameter vector, but also complete statistical information, suitable to be used in a localization and mapping algorithm. Experiment results showed that the proposed approach is efficient to detect landmarks for structured and semi-structured environments.

Barawid et al (2007) developed an automatic guidance system capable of navigating an autonomous vehicle travelling between tree rows in a real-time application. The study focused solely on straight line recognition of the tree rows using a laser scanner as a navigation sensor. A 52 kW agricultural tractor was used as the algorithm to recognize the tree row. Hough transform was used as the algorithm to recognize the tree row. An auto-regression method eliminated the white Gaussian noise in the laser scanner data. And calibration method was used to select the offset position of the laser scanner and to correct the heading and lateral error evaluation. An appropriate speed for tractor was also determined. By obtaining an accuracy of 0.11 m lateral error and 1.5˚ heading error, it was possible to navigate the robot tractor autonomously between the orchard row crops.

Chen et al (2004) applied a SICK laser ranger finder worked in 2D mode for recognizing a leader vehicle under jungle environment. Utilizing the width of leader vehicle and geometrical calculation the leader vehicle could be found from laser data segments. A Kalman Filter and Nearest-Neighbor (NN) approach was introduced to ensure the stable recognizing the real lead vehicle from noise observation. The cooperation of GPS and odometry could ensure the stable tracking when traveling distances up to 2 km with the leading vehicle moving up

to a maximum speed of 15km/h.

The disadvantage of laser ranger finder was considered that the information provided under 2D mode is too poor to describe the environment and usually an artificial landmark was required; model could be established to describe environment when under 3D mode while the cost of computation would be greatly enlarged; under the farmland condition the information from laser ranger finder was fragile and noisy.

2.2.4 Vision sensors

The vision sensors as camera were also popularly utilized on robot control. Relaying on rich vision information such as colors the technology of computer vision could be used to recognize of plant rows, task boundary, obstacles and objects to service for vehicle navigation.

Torii et al (1996) developed an image-processing algorithm for crop. This algorithm has been applied to vision guided navigation of a tractor for use in row crop husbandry, including mechanical weeding and the precise application of chemicals. For accurate vision guidance, image analysis of the crop row field is essential. Discrimination of the crop area was performed using color transformation of HIS transform. The least square method was used for boundary detection between crop row and soil area, and a three dimensional perspective view transformation was used for position identification. Results show that the offset error within 0.02 m at speed of 0.25 m/s. the attitude angle error was within 0.5˚; these values are sufficient for guidance in the field.

Kannan et al (2011) presents a summary of a subset of the extensive vision-based tracking methods developed at Georgia Tech. The problem of a follower aircraft

tracking an uncooperative leader, using vision information only, is addressed. In all the results presented, a single monocular camera is used as the sole source of information used to maintain formation with the leader. The leader motion in the image plane was estimates using a Kalman filter. The subtended angle, also available from computer vision algorithm is used to improve range estimation accuracy. In situations where subtended angle information is not available, an optimal trajectory is generated that improves range estimation accuracy.

However the camera was easily affected by light condition, also the limited view field, image distortion and high cost of computation was problem showed be deal with when using a computer vision on navigation.

2.3 Data fusing

A signal sensor system usually incompetence to handle variety of conditions, a stable sensor system should own performance to select and switch suitable sensors or rationally use data from different sensors.

Tofael et al (2006, 2009) developed a multiple sensor based sensing system for autonomous tractor navigation system with a laser range finder, RTK GPS and gyroscope. Through sensor switch between laser ranger finder, RTK GPS and IMU sensor system and the tractor could navigation under local and global positioning. And the navigation system could confirm task as hitching, parking and back into garage. The results of field experiments using the laser range finder showed a lateral error of less than 2 cm and a heading error of less than 1˚. Noguchi. et al (1998) developed a guidance system by the sensor fusion integration with machine vision, RTK-GPS and GDS sensors. An Extended Kalman Filter (EKF) and statistical method based on a two-dimensional

probability density function were adopted as fusion integration methodology. To achieve the navigation planner based on sensor fusion integration, four types of control strategies were built by changing combination of the three kinds of sensors. The developed navigation planner selected from a priority scheme of the control strategies using knowledge based-approach. The average lateral error of the vehicle guidance based on the fusion of the RTK-GPS and GDS was 8.4 cm. The developed sensor fusion methodology with the EKF performed with satisfactory precision, given that the lateral error was less than the precision of the RTK-GPS.

Guo et al (2002) established a real-time tractor position estimations system, which consists of a six-axis inertial measurement unit (IMU) and a Garmin global positioning system (GPS) was developed. A Kalman filter was designed to integrate the signals from both errors so that the noise in GPS signal was smoothed out, the redundant information fused and a high update rate of output signals obtained. The drift error of IMU was also compensated. By using this system, a low cost GPS can be used to replace expensive one with a high accuracy. Test and fusion results showed that the positioning error of the tractor estimated using this system was greatly reduced from a GPS-only system. At a tractor speed of about 1.34 *m/s*, the mean bias in easting axis of the system was 0. 48 m, comparing to the GPS mean bias of 1. 28 m, and the mean bias in northing axis was reduced from 1.48 m to 0.32m. The update frequency of the GPS system was increased from 1 to 9 Hz.

Compare with the solution of multiple sensors switching, the EKF as an effective method could provide rather stable sensing. Especially in the cost sensitive

agricultural application the EKF could reduce cost of system by fusion low cost sensors.

2.4 Concluding Remarks

The receding horizon control cannot be able of explicitly dealing with plant model uncertainties. For the sliding model control the hard sliding mode control action can lead to chatter, energy loss, plant damage, and excitation of un-modeled dynamics, because of actuators delays and other imperfections. The feedback control was complex but can usually obtain accuracy control. For sensing system of solving the tracking problem, both GPS, odometry, laser and vison sensor were possible for multiple vehicle control. However, under the farmland condition each sensor system owns its drawback and the sensor data was easily suffered by noise. The data fusion should be done for data smooth and noise reduction, and an effective could be the EKF.

Chapter 3

Leader-follower Relative Position Observation

3.1 Leader-follower relative position

To fulfill the tracking task and ensure tracking stability and safety a suitable sensing system showed be primarily designed. As a suitable sensing system it was required to provide constant and precise observation of the relative position of two vehicles. Under the uneven ground condition of agricultural environment the sensing system should further competent the changing movement and posture of the two vehicles.

The relative position between the leader vehicle and the follower vehicle can be described as Fig 3.1. By identifying the relative handing angle β, relative distance D and orientation angle α of the leader vehicle relative to the follower vehicle, the follower vehicle could identify the position of the leader vehicle on its local coordinate. For obtaining the relative position between the leader and the follower vehicles, two kinds of solution could be approach: the global sensor based observation and the local sensor based observation.

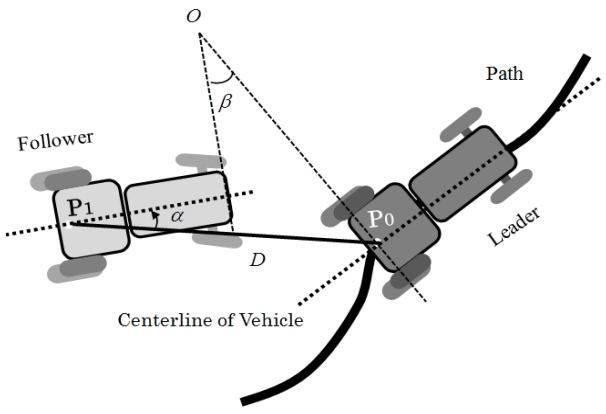

Fig. 3.1 Leader-follower relative position

3.2 Global sensor based relative position observation

For global observation usually a GPS could be utilized to obtain their global positon and a Gyroscope (Gyro) to obtain their heading angle. As figure 3.2 once the global position of $P_0(x_l, y_l)$ and $P_1(x_f, y_f)$, and the heading of two vehicle θ_l and θ_f could be determined the leader-follower relative position under the follower-based local coordinate could be easily calculated as follow.

$$\begin{bmatrix} x_{l\_F} \\ y_{l\_F} \\ \theta_{l\_F} \end{bmatrix} = \begin{bmatrix} (x_l - x_f)\cos\theta_f + (y_l - y_f)\sin\theta_f \\ (y_l - y_f)\cos\theta_f - (x_l - x_f)\sin\theta_f \\ \theta_l - \theta_f \end{bmatrix} \qquad (3\text{-}1)$$

Where, the (x_l, y_l, θ_l) and (x_f, y_f, θ_f) were global position of the leader and the follower vehicle, respectively. The $(x_{l\_F}, y_{l\_F}, \theta_{l\_F})$ means the leader position under the follower-based local coordinate.

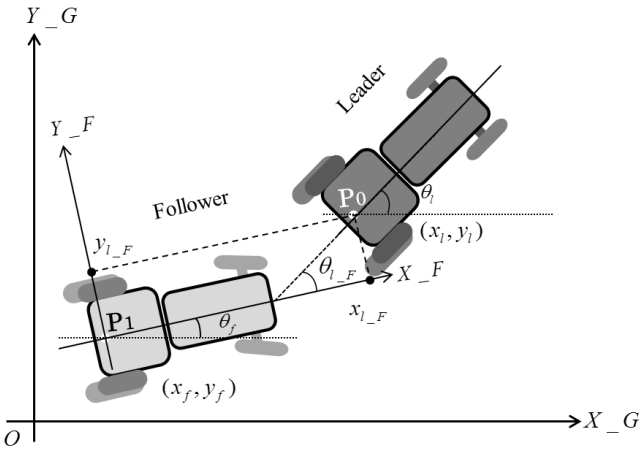

Fig. 3.2 Global sensor based leader-follower relative position

However, in this case both of the leader and the follower vehicle should equipment with the GPS and Gyro system. It was well known that the GPS single was easy to be interrupted by cloud, building and high tree, and the drift error of Gyro would also be accumulated with the time. If the GPS signal is interrupted or

existing of large Gyro error, there is a possibility of collision in tracking, or the development of a large offset due to the loss of updated positional information. Thus, the lack of signal correction during interruptions and the additional cost of a GPS and Gyro made the global sensing solution suboptimal for solving the tracking problem.

3.3 Local sensor based relative position observation

To overcome the limitations of relative position measurement using global sensor as GPS and Gyro and safety concerns, local sensor such as LRF, camera and ultrasonic sensor and so on could be utilized to design a local sensor based sensing system. As described above the ultrasonic sensor was incapable for this study, because of the short detection distance and limited detection angle of the ultrasonic sensor often resulted in loss of the target. LRF and camera were thought to be proper approaches, and have been successfully applied for tracking both on indoor and outdoor condition. Both the LRF and the camera own their advantage and disadvantage: the LRF was accuracy in distance measurement over a wide detection angle while poor information was conclude in 2-D scanning mode and time-consume in 3-D mode; the camera could provide richer information to describe the surroundings while it was low accuracy for distance measurement, sensitive to light condition and distance limited.

Thus, kindly research and design was required to enable obtaining rapid and stable observation for the tracking task utilizing the advantage and avoiding disadvantage of the LRF and camera.

3.3.1 Laser and landmark sensing system

The LRF-landmark-based method could be used to detect the relative position

between the leader and the follower. The LRF could be implemented on the follower, and reflectors mounted on the leader can be used as landmarks. Utilizing the geometric relationship between the LRF and the landmarks, the relative position between the leader and the follower could easily be calculated. Landmark detection has already been utilized and has proven to have high precision and stability in our previous research.

Three landmarks were considered on the leader (shown in the red dotted circle) (Fig 3.3), and an LRF was on the follower. According to the principle of triangulation interval between adjacent landmarks should as large as possible to improve the accuracy of leader-follower realtive position estimate. Thus the three landmarks were consider to arrange along the center line of the leader vehicle. To facilitate the calculation, we mounted the first landmark on the middle point of front axles and the third landmark on the middle point of the leader vehicle rear axles P_0. The LRF was placed at the middle point of the follower vehicle rear axles P_1. The distance from the first landmark to the third landmark is equal to the length of the leader vehicle ($l_3 = L$). The location of the third landmark can be used to represent the location of the leader vehicle, and the location of the LRF can be used to represent the location of the follower vehicle. It is clear that the laser detection of d_3 and α_3 represents the relative distance and the relative angle between the leader and the follower vehicles. Thus, under follower-based local coordinate the position of the leader vehicle could be obtained as:

$$\begin{bmatrix} x_{l\_F} \\ y_{l\_F} \end{bmatrix} = \begin{bmatrix} d_3 \cos\alpha_3 \\ d_3 \sin\alpha_3 \end{bmatrix} \tag{3-2}$$

Using the geometrical relationship between the LRF and the landmarks, the relative heading angle β between the leader and the follower could also be calculated as:

$$\beta = \pi + \alpha_3 - arc\cos(\frac{l_3^2 + d_3^2 - d_1^2}{2l_3 d_3}) \tag{3-3}$$

Obviously, the follower-based local heading angle of the leader is equal to the relative heading angle was given by

$$\theta_{l\_F} = \beta \tag{3-4}$$

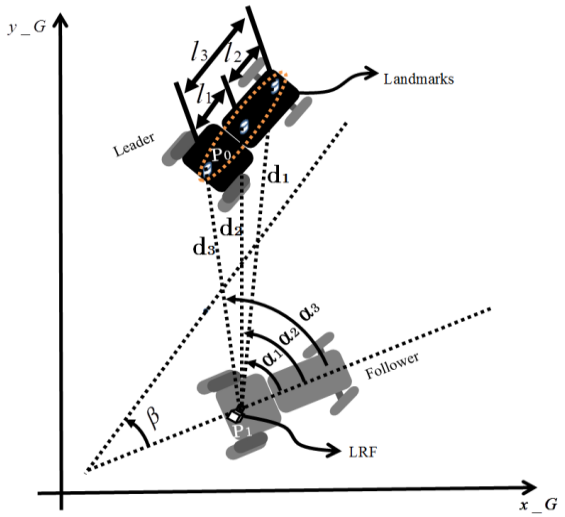

Fig. 3.3 Laser-landmark detection model.

3.3.2 Camera-marker sensing system

Compare with the LRF, camera was relative low cost and with the development of technology even low-end camera own high resolution. Recognize and measurement of a tracking object mainly relay on its appearance feature or artificial marker. Compare with marker-based method the feature-based method seems more flexibly but it also sensitive to light condition, limit of distance and

time expansive. The marker-based method was stable on object recognize and could accurately estimate the object state by comparing the known geometry of the marker with its perceived geometry. In this study a monocular vision system based camera-marker sensing was equipped for estimate the leader-follower relative position. Where, the camera was equipment on the follower vehicle and the marker was composed by three lineally aligned black squares on a white background plane, installed on rear part of the leader vehicle vertical with its heading Fig 3.4.

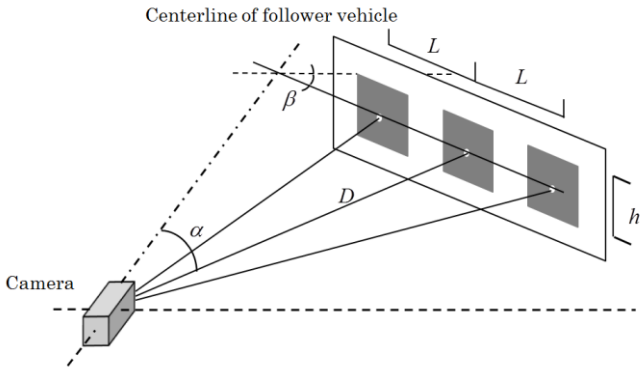

Fig. 3.4 Relative position between camera and marker plane

Also, the camera was equipment on the point P_1 of the follower vehicle, the optical axis of the camera was parallel with the centerline of the follower. The marker was installed perpendicular to the centerline of the leader vehicle, and the position of the middle square of the marker was at the rear wheel axle center point P_0. The relative distance D could be described using the distance from camera to the center point of middle square, orientation angle α could be described using the angle between the follower centerline and the center point of middle square, and relative handing angle β could be described using the

gradient angle of a straight line joining the center points of the squares in the follower's local coordinates. The side length of each square was H and interval between square centers was L. Thus, by relying on the camera-marker sensing system the leader-follower relative position could be calculated for further tracking.

3.3.2.1 Marker detection and location

The marker was detected based on its pre-known geometry information including the square shape features and relative spatial relationship between squares in the marker plane. The flow of image processing comprises four steps: to transform an original RGB image into a grayscale image, and then enhance the contrast ratio, extract contours, find rectangles from the contour image and determine the marker (Fig 3.5).

Low computational of pre-known geometry information based method could satisfy real-time detection. Also, the high contrast ratio between the black squares and the white background conduced to generating acutance contours and made it easy to detect the marker, using the shape feature of squares. Contour extracting was influenced by illumination conditions and similarly shaped objects on the background. For example, low-light condition or the camera facing the sun would reduce the contrast ratio of grayscale image (Fig 3.5a) and cause the contour of squares be corroded and reason of fail of marker detection. To expand the scope for adapting various illumination conditions, a commonly used normal distribution of the image histogram method was utilized to enhance the image contrast (Fig 3.5b).

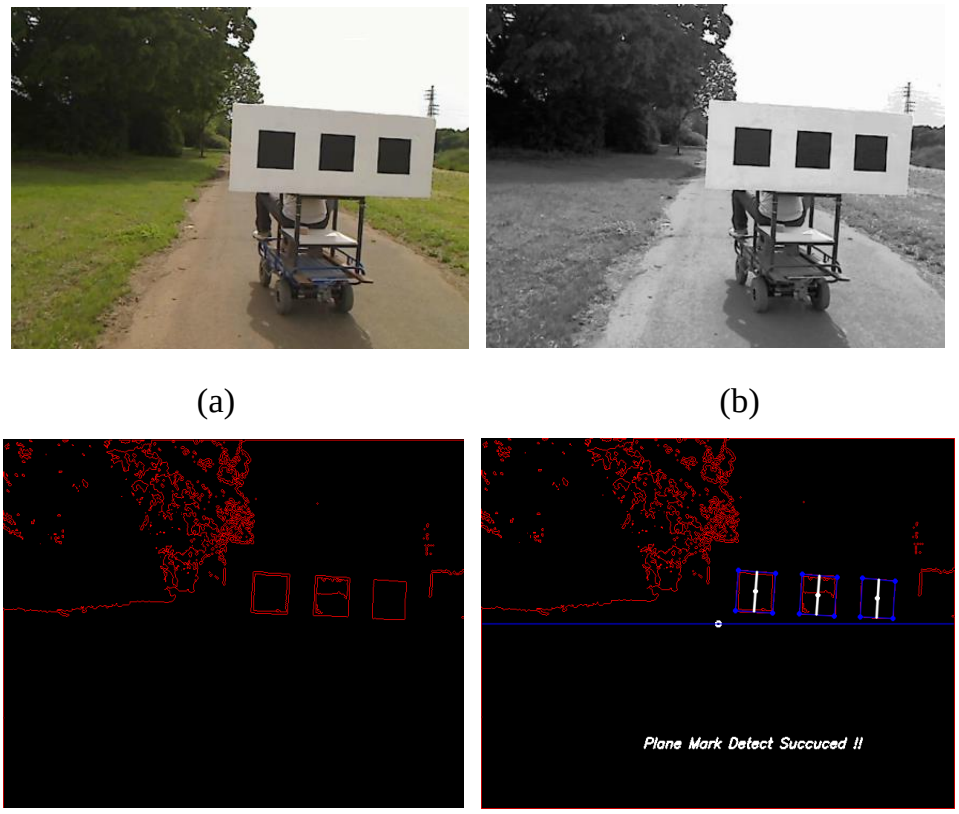

(a) (b)

(c) (d)

Fig. 3.5 Image processing for marker detection. (a) Grayscale image. (b) Contrast enhanced image. (c) Contour image. (d) Detected marker.

Affected by posture changes of the vehicles, squares projected on the image plane would show the shapes of rectangles. Thus, in the contour image rectangles were recognized and selected. For example, all rectangles have four sides and opposite sides are parallel and the ratios of two diagonal lines and of two adjacent sides should fall within a certain range for rectangles that were probably projected as squares. Relying on the relative spatial relationship between the three squares, false targets with rectangular shapes such as rooms and windows could be excluded and squares belonging to the marker could be identified.

Given that the vision data were obtained from a single camera, the relative

position between the marker and the camera was estimated by the known side length of the squares. The position of each square in the marker plane could be described by its center point. Under a pinhole model, the geometric relationship of similar triangles could be established for relative position estimation (Fig 3.6). Neglecting the pitch angle of the vehicle body, the image plane was hypothesized always to be parallel to the marker plane, meaning that sides of squares in the vertical direction would not be affected by posture changes of the leader and follower vehicles when projected on the image plane. For this reason, the centerline of the squares in the vertical direction could be used to estimate the relative position between the camera and marker plane. As shown in figure 3.6a, the image plane was parallel with the pinhole plane and the target plane, and the angle formed between the target plane and the marker plane was equal to the relative heading angle β between the leader vehicle and the follower vehicle. Taking the middle square as an example, point P_C was the square center point located on the marker plane and p_c was its mapping point located on the image plane. The centerline $\overline{ab}$ in the image plane was the projection of centerline $\overline{AB}$ in the marker plane. The triangle ΔabO_C was similar to the triangle ΔABO_C. The distance from the square center P_C in the marker plane to the camera could be calculated using the relationship of similar triangles:

$$D = \frac{H}{h} d = \sqrt{m^2 + f^2} \tag{3-5}$$

Where d was the distance from O_C to p_c mean distance from the pinhole center to the square center in the image plane, m was the distance from p_c to O_1 equal to the distance from the square center to the optical axis; f was the

focal length obtained by camera calibration, h was the length of the square centerline in the image plane and H was the length of the square centerline in the marker plane .

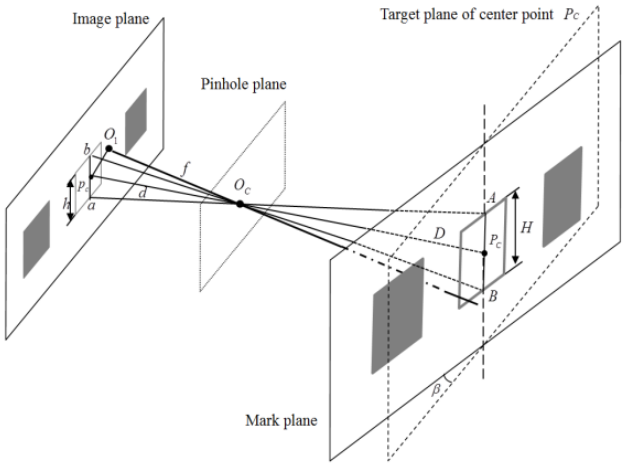

(a)

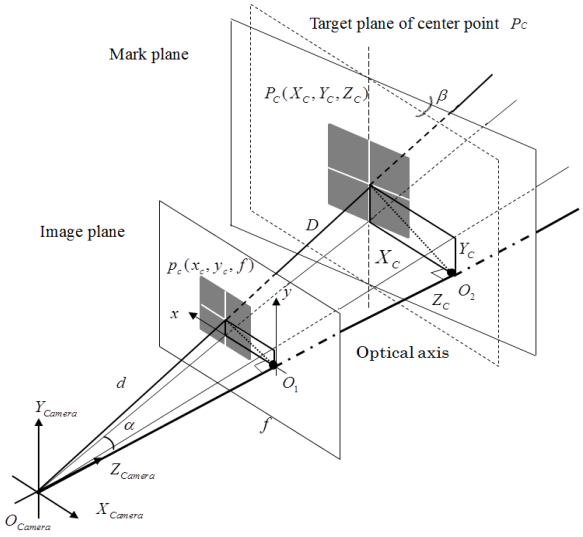

(b)

Fig. 3.6 Relative position calculation.

(a) Pinhole model. (b)Perspective model.

Transforming the pinhole model to the perspective model (Fig 3.6 b) and from

the similarity of triangles between the image plane and the target plane, the following relation could be established:

$$x_c = f_x \frac{X_C}{Z_C} + c_x \tag{3-6}$$

Where, the coordinates of the square center under the image coordinate and under the camera based coordinates could be written as $p_c(x_c, y_c, f)$ and $P_C(X_C, Y_C, Z_C)$ separately. The f_x and c_x was camera parameter obtain by camera calibration.

From equation (3-5) and (3-6), position of square center P_C in camera based coordinates could be estimated:

$$X_C = \frac{x - c_x}{f_x} Z_C \tag{3-7}$$

$$Z_C = \frac{D}{d} f = \frac{H}{h} f \tag{3-8}$$

$$\alpha = \arctan(\frac{X_C}{Z_C}) \tag{3-9}$$

Thus, the position of marker relative to the camera could be estimated from the position of the squares in the marker plane.

3.3.2.2 Compensate of vehicle rolling

On uneven farm ground, rolling of the camera or the marker plane would occur owing to swing of vehicles. Under this condition, calculation of the relative position between the leader and the follower vehicle should be considered and should offset the rolling effect of the camera or the marker plane. For convenience of illustration, suppose the leader vehicle is driven on a horizontal

surface, while the follower vehicle forms a roll angle with the horizontal surface. The camera rotates on an angle γ around its optical axis from the horizontal surface (Fig 3.7 a), and the same dip angle γ of the straight line composed by the square centers of p_{cn} on the image plane coordinates (Fig 3.7 b).

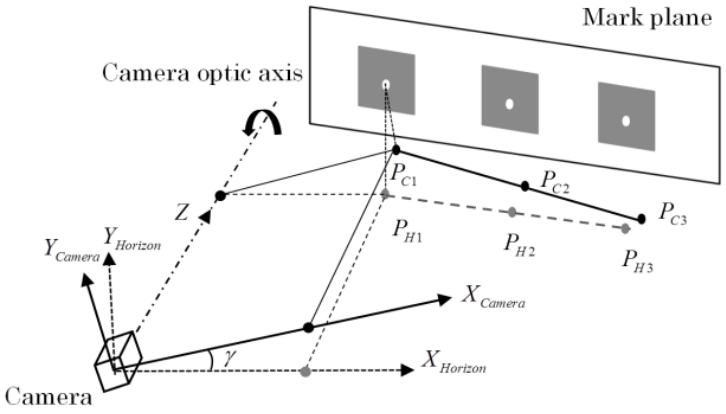

(a)

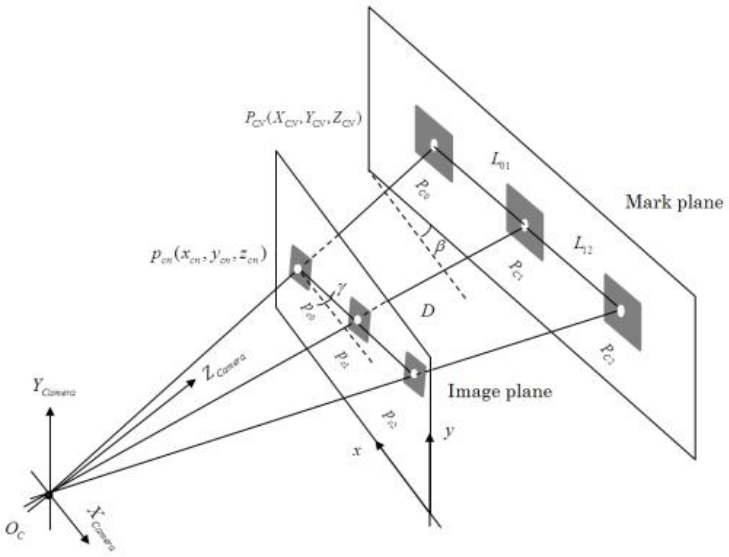

(b)

Fig. 3.7 Model for offsetting vehicle roll effect.

(a) Effect of the camera roll angle.

(b) Effect of the camera roll angle on image plane coordinate.

As illustrated in Figure 3.7 (a), $P_{CN}\left(X_{CN},Y_{CN},Z_{CN}\right)$ were coordinates of square

centers based on the camera coordinate system and $P_{HN}\left(X_{HN},Y_{CN},Z_{HN}\right)$ were coordinates of square centers according to the horizontal surface. Clearly, the position of P_{CN} represents the relative position between the camera and the marker plane, and the position P_{HN} represents the relative position between the follower and the leader vehicles.

Following the imaging law and camera based coordinate calculation principles the relationship between P_{CN} and P_{HN} could be written as:

$$X_{CN} = X_{HN}\cos\gamma - Y_{HN}\sin\gamma \tag{3-10}$$

$$Z_{CN} = Z_{HN} \tag{3-11}$$

As the relative position between the leader and follower vehicle corresponds only to the *X*-*Z* surface, the square centers could be supposed to lie on the horizontal surface. Thus, equation (3-10) can be rewritten as:

$$X_{HN} = \frac{X_{CN}}{\cos\gamma} \tag{3-12}$$

Where, the angle γ could be calculated from the image plane coordinate, which equals dip angle of straight line composed by p_{cn}.

Correspond with equation (3-11) and (3-12), under the follower-based local coordinate the leader-follower relative position could be written as:

$$x_{l\_F} = Z_{CN} \tag{3-13}$$

$$y_{l\_F} = X_{CN} \tag{3-14}$$

$$\theta_{l\_F} = \beta \tag{3-15}$$

Where, β was calculated from the dip angle of straight line composed by P_{VN} under the follower vehicle local coordinate.

3.4 Conclusion

Analyzed possible methods could be used for leader-follower vehicle relative position observation. The LRF-landmark based sensing system and the camera-marker based monocular vision system was designed. Mathematic models utilizing the relationship between the LRF/camera and landmarks were established to calculate the leader-follower vehicle relative position.

Chapter 4

Coordinate Navigation of the Autonomous Follower Vehicle

When considering farming task style, a common operational method of multiple autonomous vehicles will be effective when taking the leader–follower format. While, different performance of the tracking system was require for different task, there were tracking a formation with the leader vehicle and tracking the trajectory of the leader vehicle. Tack harvesting for example, a truck would be required to maintain a special formation with a harvester for loading and also for safety driving. On other condition such as driving on road or simultaneous operation of multiple same kinds of machineries would require the follower vehicle to tracking a special trajectory according to the trajectory of the leader vehicle, and the formation maintaining would not strictly required. Consequently algorithm for the leader-follower formation tracking and trajectory tracking were designed and discussed in this chapter.

4.1 Formation tracking and leader trajectory tracking

The most fundamental difference could be considered to be the different requirements for the position of the follower that is required to track (Fig 4.1). As shown in figure 4.1, the position of the vehicle shown in broken outline is the required position of the follower on the leader trajectory tracking task, whereas in the formation tracking task the follower is required to track the position of the vehicle shown in solid outline.

The leader-follower formation tracking was aim to control the follower tracking a parallel formation for conforming requirement as harvesting tasks. The leader

trajectory tracking intend to control the follower tracking an identical or parallel trajectory with the leader for ensuring safety driving on complex farmland condition or conduct precision farming task without overlapping or leaking.

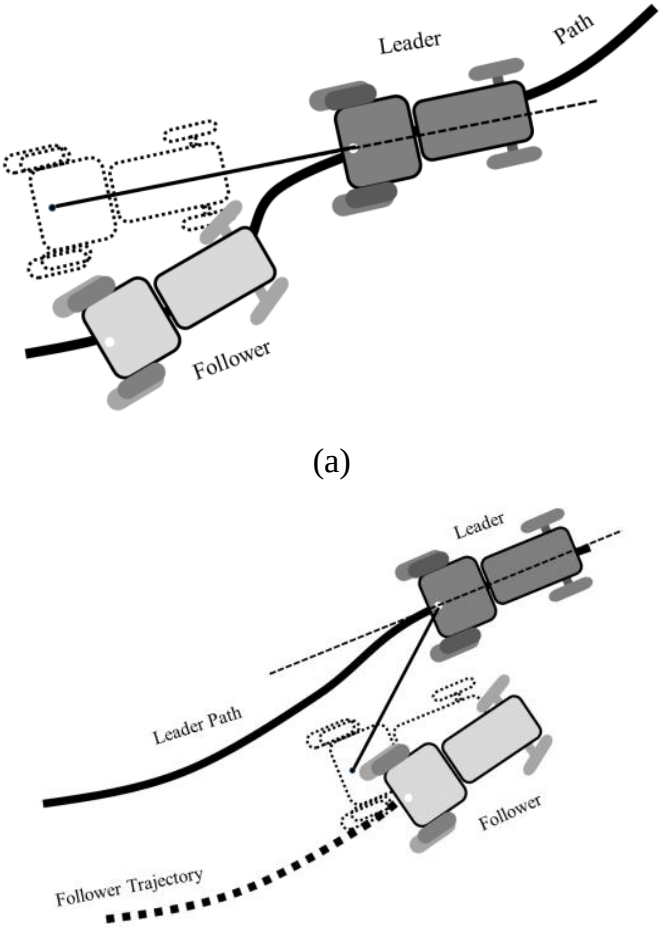

Fig. 4.1 Formation tracking and leader trajectory tracking.

(a) Linear tracking. (b) Parallel tracking.

4.2 Kinematic Model

According to the car-like kinematic model, the rear-wheel drive and front wheel steering vehicle model was describle as Fig 4.2.

The center of the gravity of the vehicle was located at the center of the rear axle

to simplify the model. In this study both of the leader and follower was consider to own same Technical and structure Parameters. Thus, kinematic equation for both the leader and the follower is given by the following expression:

$$\begin{bmatrix} \dot{x} \\ \dot{y} \\ \dot{\theta} \\ \dot{\delta} \end{bmatrix} = \begin{bmatrix} v\cos\theta \\ v\sin\theta \\ \dfrac{\tan\delta}{L}v \\ w \end{bmatrix} \tag{4-1}$$

Where v is the velocity and w is the steering angular velocity of the vehicle and L is the length of the wheelbase.

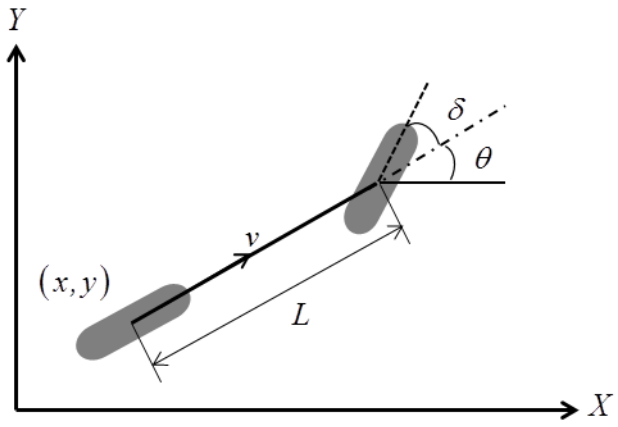

Fig. 4.2 Rear-wheel drive and front wheel steering vehicle model

4.3 Feedback control for leader-follower formation tracking

A virtual follower was imaged at P_2 represent the required position of the follower (Fig.4.3). The relative position between the leader and virtual follower was set to a constant. By tracking the position of virtual follower, safety and required formation between the leader and the follower could be obtained. In addition, the information about the velocity and steering angular velocity of the leader could be sent from the leader to the follower.

Considering the operational mode and working style of agricultural operation, the formation-keeping problem in this research can be stated as follows: the leader is driving on a given path and asks the follower to keep a relative distance d_{01} and a relative angle Φ_{01}; this required state is the virtual follower. If the state deviation (x_e, y_e, θ_e) between the follower and the virtual follower can always converge to zero, then the required formation between the leader and the follower could be maintained. By changing the relative distance of d_{01} and a relative angle Φ_{01}, formation can be varied.

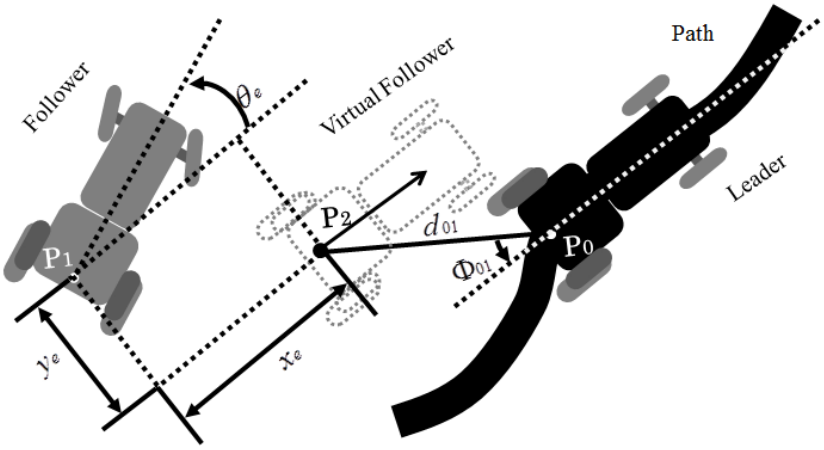

Fig. 4.3 Leader-follower formation tracking model.

The state of the virtual follower depends on the global coordinates and relative position (Fig 4.3). The state of the virtual follower can be expressed as:

$$\begin{bmatrix} x_{vf} \\ y_{vf} \\ \theta_{vf} \\ \delta_{vf} \\ v_{vf} \\ w_{vf} \end{bmatrix} = \begin{bmatrix} x_l - d_{01}\cos(\theta_l - \Phi_{01}) \\ y_l - d_{01}\sin(\theta_l - \Phi_{01}) \\ \theta_l \\ \delta_l \\ v_l \\ w_l \end{bmatrix} \tag{4-2}$$

As mentioned above, the formation-tracking problem can be thought as the

tracking problem of the follower and the virtual follower, and if the state error (x_e, y_e, θ_e) asymptotically approaches zero, the desired formation can be kept. The formation-tracking error between the follower and the virtual follower can be expressed as

$$\begin{bmatrix} x_e \\ y_e \\ \theta_e \end{bmatrix} = \begin{bmatrix} \cos\theta_{vf} & \sin\theta_{vf} & 0 \\ -\sin\theta_{vf} & \cos\theta_{vf} & 0 \\ 0 & 0 & 1 \end{bmatrix} = \begin{bmatrix} x_f - x_{vf} \\ y_f - y_{vf} \\ \theta_f - \theta_{vf} \end{bmatrix} \tag{4-3}$$

The formation-tracking error (x_e, y_e, θ_e) could be easily calculated under the leader-based local coordinate system, following the relationship of coordinates between the leader, the follower, and the virtual follower (Fig 4.4).

$$\begin{bmatrix} x_e \\ y_e \\ \theta_e \end{bmatrix} = \begin{bmatrix} x_{f\_L} \\ y_{f\_L} \\ \theta_{f\_L} \end{bmatrix} - \begin{bmatrix} x_{vf\_L} \\ y_{vf\_L} \\ \theta_{vf\_L} \end{bmatrix} \tag{4-4}$$

Where $(x_{f\_L}, y_{f\_L}, \theta_{f\_L})$ represents the local state of the follower under the leader-based local coordinate system.

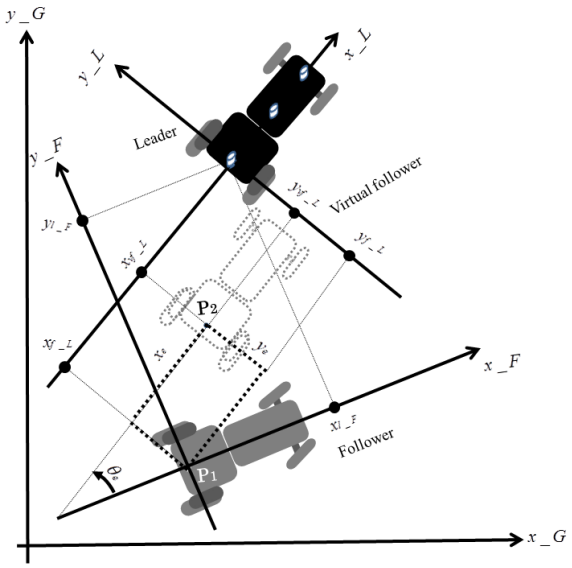

Fig. 4.4 Coordinates of the leader and the follower tracking system.

The state of virtual follower under the leader-based local coordinate could be writen as:

$$\begin{bmatrix} x_{vf\_L} \\ y_{vf\_L} \\ \theta_{vf\_L} \end{bmatrix} = \begin{bmatrix} d_{01}\cos\Phi_{01} \\ d_{01}\sin\Phi_{01} \\ 0 \end{bmatrix} \tag{4-5}$$

The above equation (4-4) can further transform to the follower-based local coordinate and described as:

$$\begin{bmatrix} x_e \\ y_e \\ \theta_e \end{bmatrix} = -\begin{bmatrix} \cos\beta & \sin\beta & 0 \\ -\sin\beta & \cos\beta & 0 \\ 0 & 0 & 1 \end{bmatrix}\begin{bmatrix} x_{l\_F} \\ y_{l\_F} \\ \theta_{l\_F} \end{bmatrix} + \begin{bmatrix} d_{01}\cos\Phi_{01} \\ d_{01}\sin\Phi_{01} \\ 0 \end{bmatrix} \tag{4-6}$$

A feedback control law can be obtained according to the formation-tracking error and control input of the virtual follower. The expression of feedback control can be referred to as (Morin et al 2008):

$$(v_f, w_f) = f(x_e, y_e, \theta_e, v_{vf}, w_{vf}) = f(x_e, y_e, \theta_e, v_l, w_l) \tag{4-7}$$

Where (v_f, w_f) is the control input of the follower. The virtual follower control input (v_{vf}, w_{vf}) was equal to the leader control input (v_l, w_l) and transmitted from the leader to the follower.

4.4 Feedback control for leader trajectory tracking

The feedback control algorithm for leader trajectory tracking would be designed under hypothesis of that there was no data exchange between the leader and follower vehicles, and the tracking would only relay on the leader-follower relative position. Free of communication between the leader and the follower would improve safety of the tracking system, while also improved the difficulty for accuracy tracking. Because, lacking of information exchange and absolute reference position made the leader trajectory became thoroughly uncertain for the

follower, and the tracking position for the follower was ambiguous.

A control point C located on the centerline of the follower vehicle was introduced, and the distance from the rear wheel axle center to the control point C was defined as:

$$L_c = k_0 L \tag{4-8}$$

Where, L_c was length of the follower vehicle from its control point to the rear wheel axle center; the parameter k_0 was not limited to positive value.

Then, the position of the control point C in the leader based local coordinates could be written as:

$$\begin{bmatrix} x_{c\_L} \\ y_{c\_L} \\ \theta_{c\_L} \end{bmatrix} = -\begin{bmatrix} \cos\beta & \sin\beta & 0 \\ -\sin\beta & \cos\beta & 0 \\ 0 & 0 & 1 \end{bmatrix} \begin{bmatrix} x_{l\_F} \\ y_{l\_F} \\ \theta_{l\_F} \end{bmatrix} + \begin{bmatrix} L_c \cos\beta \\ -L_c \sin\beta \\ 0 \end{bmatrix} \tag{4-9}$$

Figure 4.5 shows that the position error between the follower and the required position could easily be calculated in the lead based coordinates, which could be obtained by subtracting the local position of required position P_2 from local position of control point C.

Combining with equations (3-13, 14, 15), the position error between the follower and the required position could be calculated as:

$$\begin{aligned} \begin{bmatrix} x_{e\_c} \\ y_{e\_c} \\ \theta_{e\_c} \end{bmatrix} &= \begin{bmatrix} x_{c\_L} \\ y_{c\_L} \\ \theta_{c\_L} \end{bmatrix} - \begin{bmatrix} x_{req\_L} \\ y_{req\_L} \\ \theta_{req\_L} \end{bmatrix} \\ &= -\begin{bmatrix} cos\beta & sin\beta & 0 \\ -sin\beta & cos\beta & 0 \\ 0 & 0 & 1 \end{bmatrix} \begin{bmatrix} X_{V2} \\ X_{V2} \\ \beta \end{bmatrix} + \begin{bmatrix} L_c cos\beta \\ -L_c sin\beta \\ 0 \end{bmatrix} - \begin{bmatrix} d_{01} cos\Phi_{01} \\ d_{01} sin\Phi_{01} \\ 0 \end{bmatrix} \end{aligned} \tag{4-10}$$

Note that the position error between the follower and the required position was

calculated from pre-known elements and camera estimated results.

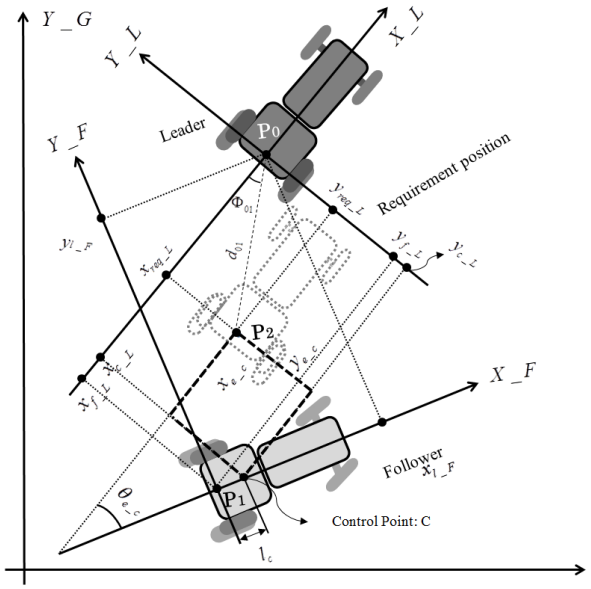

Fig. 4.5 Relationship and coordinate transformation between leader and follower vehicle.

A simple steering strategy to respond to longitudinal and heading error between the follower and the required position was given as:

$$\delta = k_1 y_{e\_c} + k_2 \sin\left(\theta_{e\_c}\right) \tag{4-11}$$

An additional element was introduced to stabilize the tracking when there was large position error between the follower and the required position. The above equation could be modified as:

$$\delta = k_1 y_{e\_c} + k_2 \sin\left(\theta_{e\_c}\right) + k_3 \, sgn\left(y_{e\_c}\right) \left| \frac{1 - e^{D - d_{01}}}{1 + e^{D - d_{01}}} \right| \left(D - d_{01}\right) \tag{4-12}$$

Where

$$sgn\left(y_{e\_c}\right) = \begin{cases} 1 & y_{e\_c} > 0 \\ 0 & y_{e\_c} = 0 \\ -1 & y_{e\_c} < 0 \end{cases} \tag{4-13}$$

Maintaining of the required distance between the leader and the follower vehicle, and controlling of the follower velocity could be given as:

$$v = k_4(D - d_{01}) \tag{4-14}$$

Where, k_0, k_1, k_2, k_3, k_4 were control parameters corresponding to a required position of the follower relative to the leader vehicle. Thus, once the required value of distance d_{01} and angle Φ_{01} for the follower vehicle relative to the leader vehicle were altered, the control parameters must also be adjusted.

4.5 Simulation

Computer simulation was conducted to evaluate the performance of designed algorithm. The simulator was designed using C++ builder XE3. The leader trajectory was given as a small and a large curvatures sinusoidal path. The speed of the leader was set at 1.2 m/s when on the small curvatures and 0.8 *m/s* on the large curvatures. The wheelbase length both of the leader and the follower were set at 1.53 m, equal to the reference parameter of the Kubota KL21 model tractor. Additionally, the limits of speed, steering angular velocity and steering angle were defined as $|v_{\max}| \le 1.6$ m/s, $|w_{\max}| \le 0.38$ rad/s, and $|\delta| \le 45.0^{\circ}$, respectively.

4.5.1 Formation tracking accuracy

At the initial states, there were position errors for lateral, longitudinal, and heading of 1.68 m, 0.25 m, and 1.26˚, respectively, in the small curved path. The position error in the large curved path was 0.82 m, 0.47 m, and 10.37˚ for lateral, longitudinal, and headring, respectively. Meanwhile, the formation required the follower to maintain was longitudinal 2 m and lateral 3 m to ensure harvest operation.

From the simulation results it could found that the leader-follower formation could convergence to the required formation both on small and large curved path. And showed high accuracy of the formation tracking. Affected by the path curve the tracking accuracy on small curved path was higher than on the large curved path.

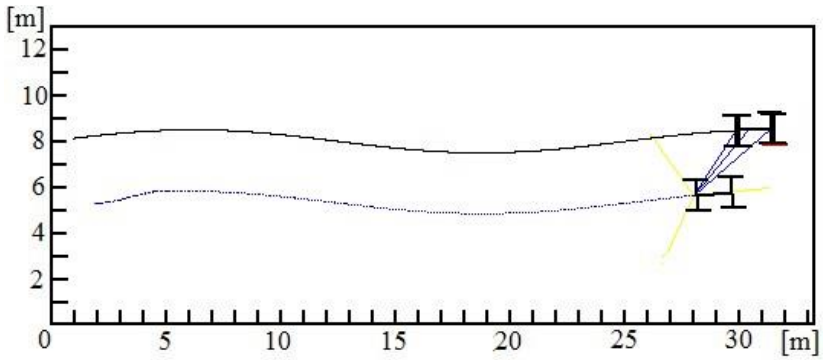

Fig.4.6 Leader-follower formation tracking on small sinusoidal curved path.

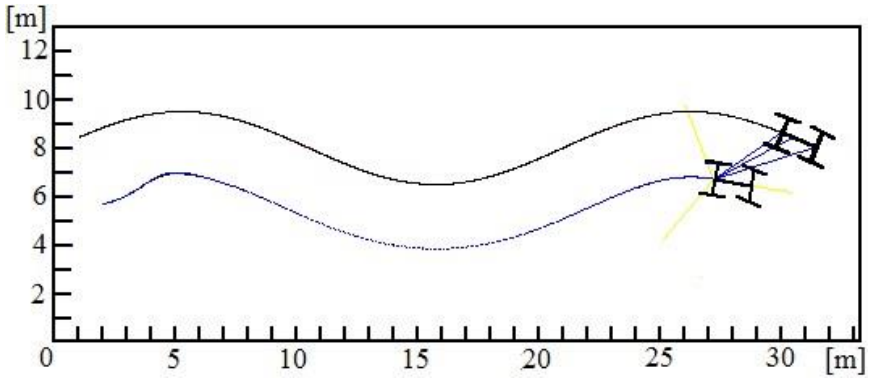

Fig. 4.7 Leader-follower formation tracking on large sinusoidal curved path.

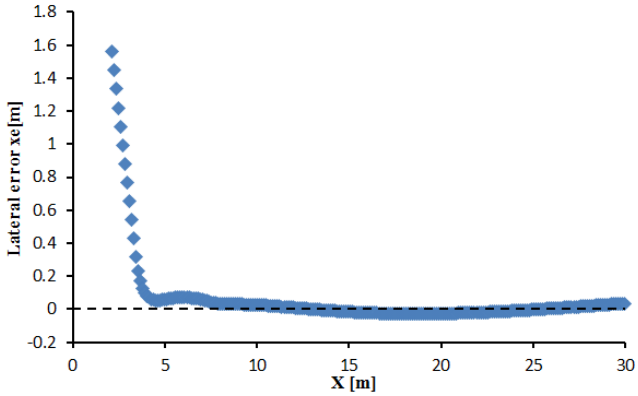

(a)

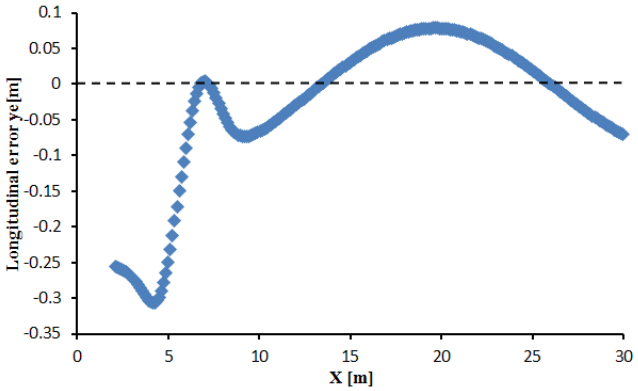

(b)

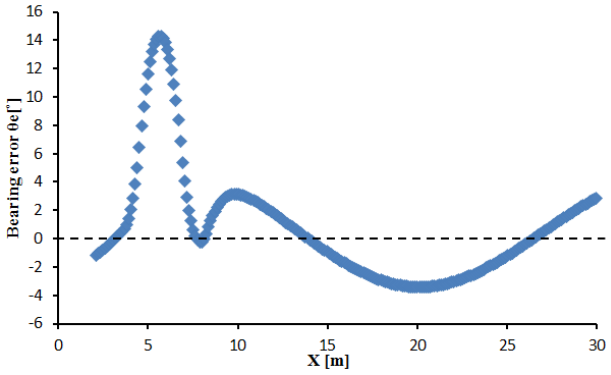

(c)

Fig. 4.8 Leader-follower relative position error on small sinusoidal curved path. (a) Lateral error; (b) Longitudinal error; and (c) Heading error.

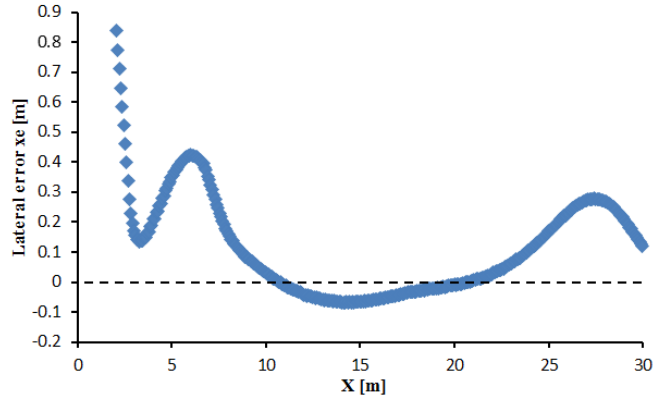

(a)

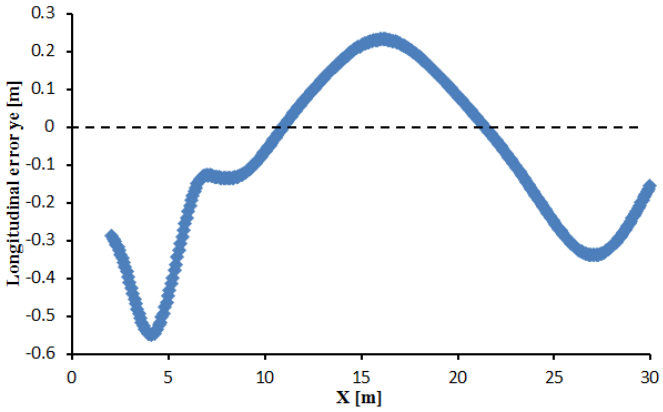

(b)

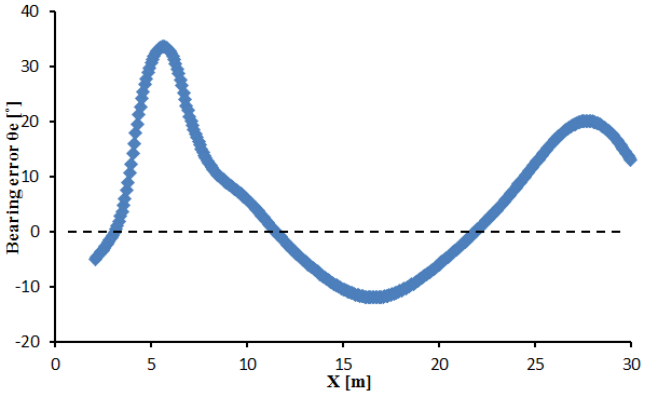

(c)

Fig. 4.9 Leader-follower relative position error on small sinusoidal curved path. (a) Lateral error; (b) Longitudinal error; and (c) Heading error.

The RMSEs of lateral, longitudinal, and heading tracking error on small curved path was 0.166 m, 0.104 m, and 4.045˚, and on large curved path was 0.195 m, 0.234 m, and 13.613˚, respectively.

4.5.2 Leader trajectory tracking accuracy

At the initial states, there were position deviate for lateral, longitudinal, and heading of 5.1 m, 2.53 m, and 14.8˚ between the leader and the followlwer vehicle, respectively, in the small curved path. The position deviate in the large curved path was 4.63 m, 1.78 m, and 24.9˚ for lateral, longitudinal, and headring, respectively. Considering the vehicle size and task characteristics, 5 m longitudinal distance between the leader and the follower vehicle and 3 m lateral distance between the leader and the follower trajecory was required to maintain.

The simulation result showed that on larger curvature leader trajectory the larger tracking error would occure between the leader and the follower trajectory. This was caused by the follower vehicle could only obtain limitated information about the leader vehicle and inevitably led to problem such as short cut.

The RMSEs of trajectory tracking error for linear and parallel tracking on small curved path was 0.051 m, and 0.066 m, and on large curved path was 0.041 m, and 0.256 m, respectively.

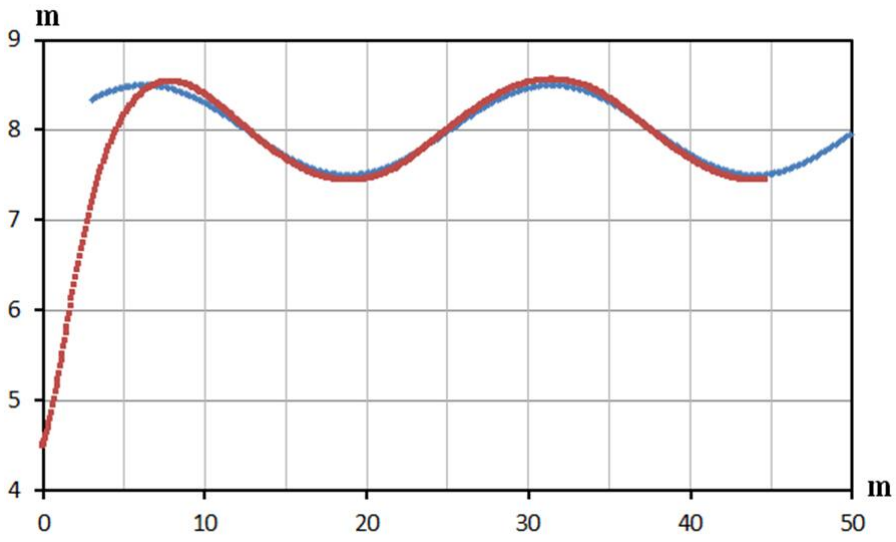

(a)

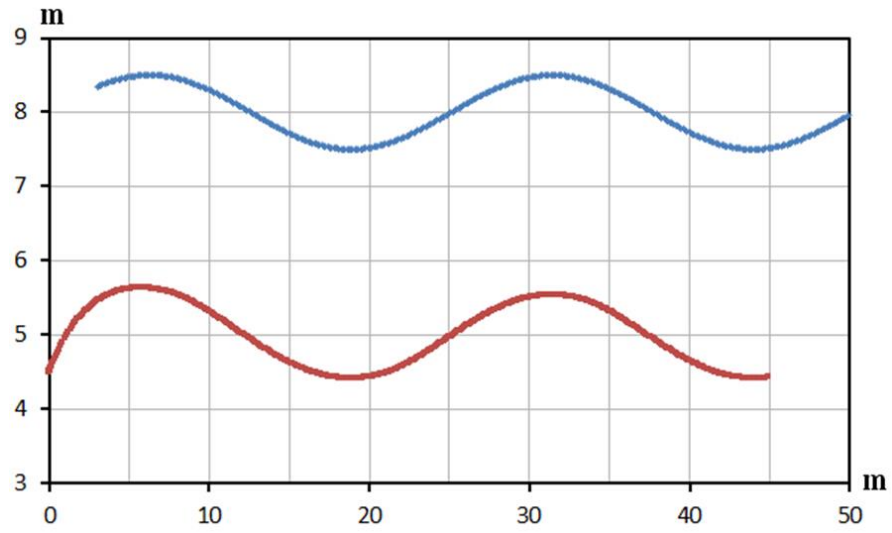

(b)

Fig. 4.10 Leader trajectory tracking on small sinusoidal curved path.

(a) Linear tracking; (b) Parallel tracking.

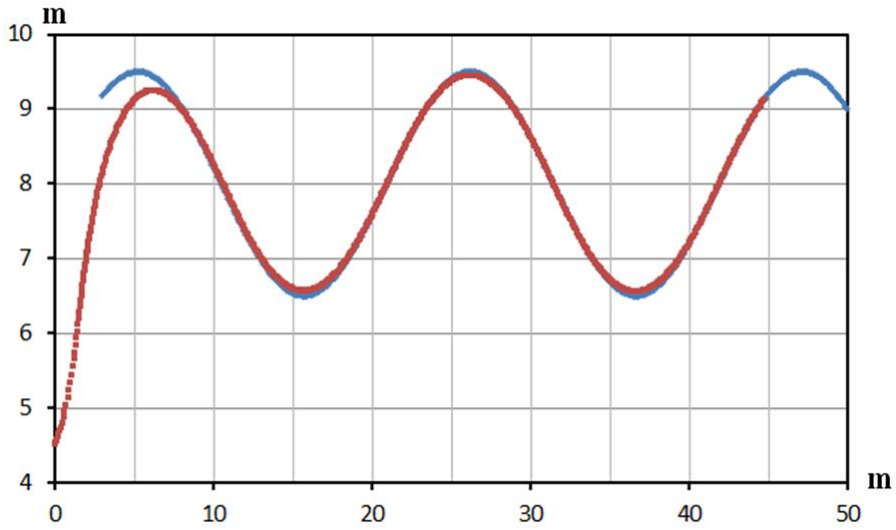

(a)

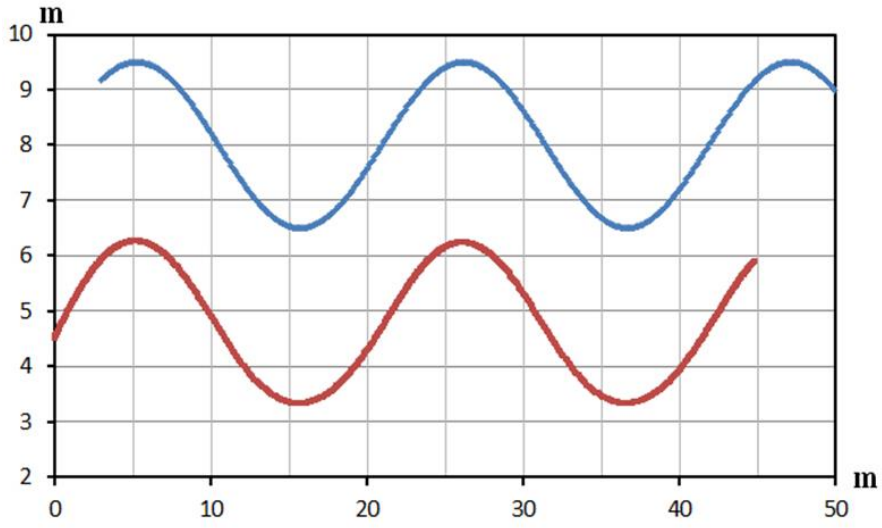

(b)

Fig. 4.11 Leader trajectory tracking on large sinusoidal curved path.

(a) Linear tracking; (b) Parallel tracking.

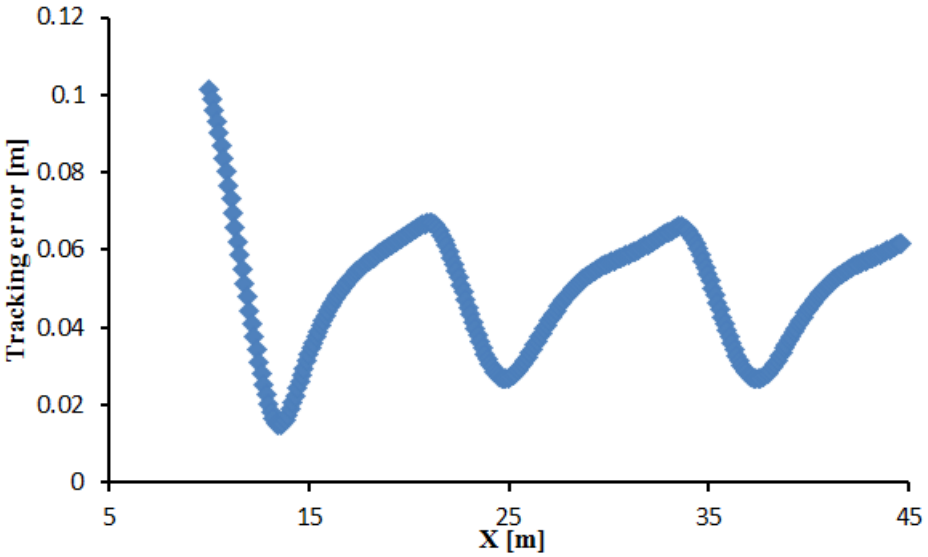

(a)

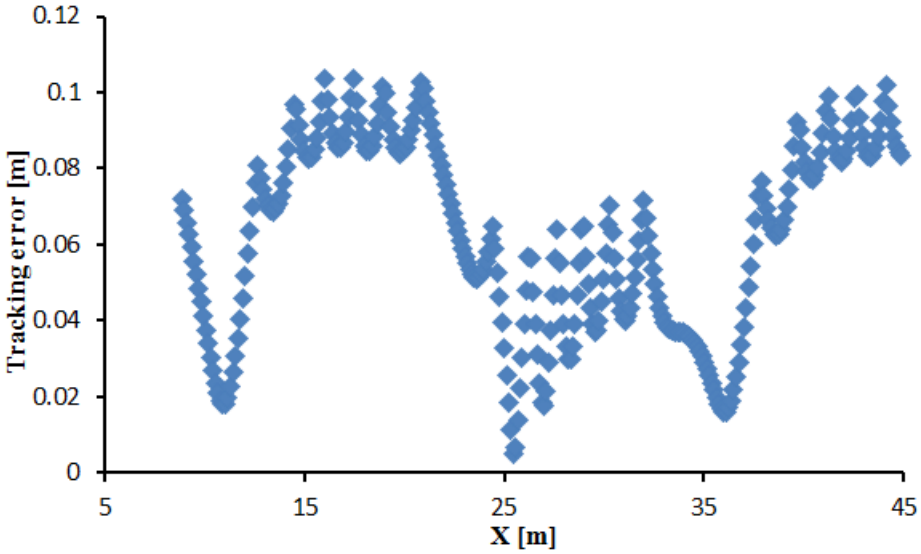

(b)

Fig. 4.12 Leader trajectory tracking error on small sinusoidal curved path.

(a) Linear tracking; (b) Parallel tracking.

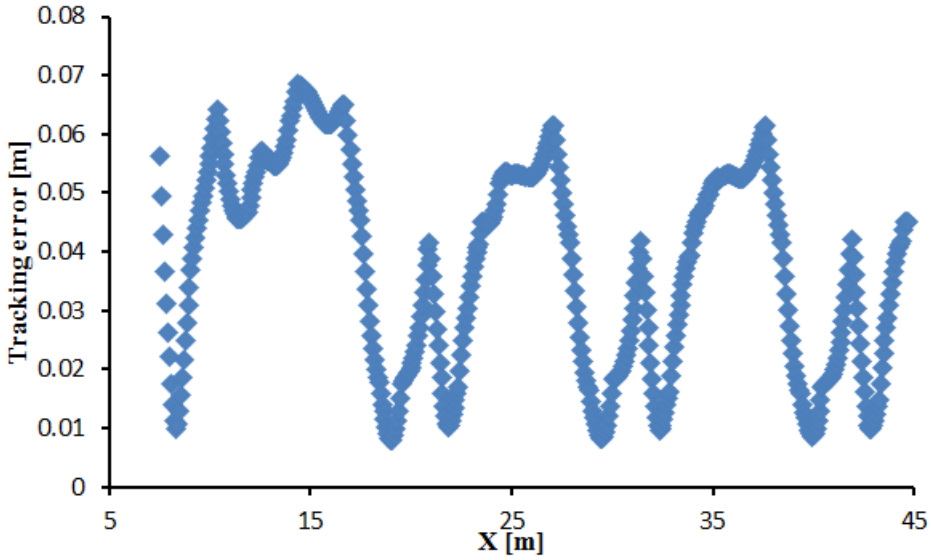

(a)

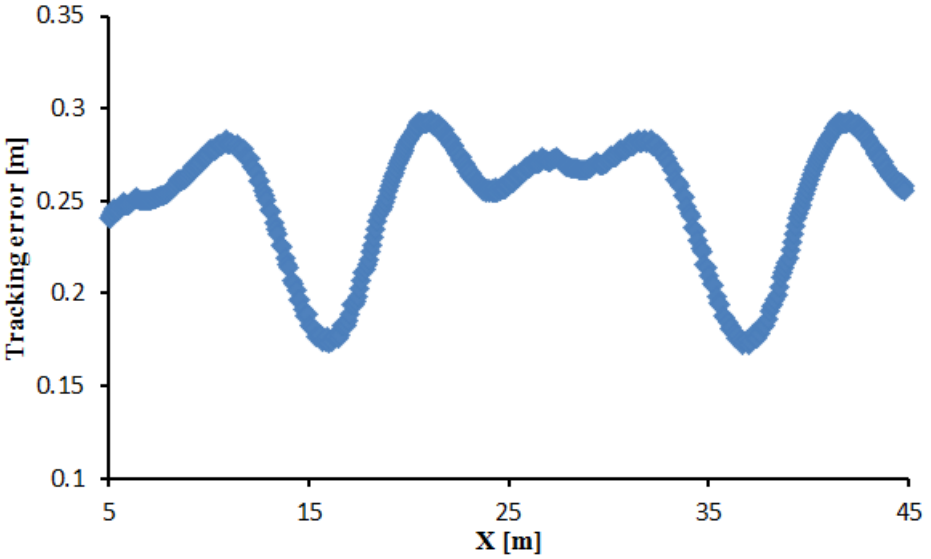

(b)

Fig. 4.13 Leader trajectory tracking error on large sinusoidal curved path.

(a) Linear tracking; (b) Parallel tracking.

4.6 Conclusion

In order to meet the requirement of different farm tasks, algorithm for formation tracking and leader trajectory tracking were developed. The formation tracking algorithm was strict feedback, and the leader trajectory tracking algorithm was simple feedback only relay on the leader-follower vehicle relative position. Simulation showed tracking accuracy was high when driving on small curvature path and even under the larger curvature path the tracking accuracy was enough to support the safty driving and pricision farming operation.

Chapter 5

Stable Tracking Using an Extended Kalman Filter

Feedback control law on chapter 4 was established under the ideal kinematic assumption of no sensor noise and disturbance. In real conditions, the leader-follower relative position detected by the LRF/Camera and odometer data of the leader and odometer data of the follower vehicle velocity and steering angle were corrupted with errors and noise. Additionally, the LRF/Camera data are low update frequency, and they are also noisy in an adverse environment. To improve the stability of the tracking controller of follower vehicle, an EKF was introduced to reduce the model error and fuse the LRF/Camera observation and odometer data.

5.1 Estimate the leader-follower relative position using EKF

The nonlinear leader-follower model described the state transition under a control input, and observation model described the observation under current state, can be expressed respectively as follows:

$$X_k = f(X_{k-1}, U_k, V_k) \tag{5-1}$$

$$Z_k = h(X_k, W_k) \tag{5-2}$$

Where X_k is the current state vector representing the leader-follower relative state at time instant k; X_{k-1} is the previous state vector at time instant $k-1$; U_k is the input vector including the input of leader (v_l, w_l) and follower (v_f, w_f); Z_k is estimate observation vector from LRF/Camera at time instant *k*; V_k and W_k are noises from odometer data and LRF/Camera observation, and

their covariance matrices were defined as Q_k and R_k.

The EKF include two steps which are prediction step and correction step, and data fusion was practiced through recursive the two steps. The prediction step predicts the current leader-follower relative state $\tilde{X}_k$ based on the nonlinear system model $f(\cdot)$; estimated the observation $\tilde{Z}_k$ from the current estimate state $\tilde{X}_k$ based on the observation model $h(\cdot)$; and prediction the state error covariance matrix $\tilde{P}_k$:

$$\tilde{X}_k = f(\hat{X}_{k-1}, U_k, 0) \tag{5-3}$$

$$\tilde{Z}_k = h(\tilde{X}_k, 0) \tag{5-4}$$

$$\tilde{P}_k = J_{x,k}\hat{P}_{k-1}J_{x,k}^T + J_{v,k}Q_k J_{v,k}^T \tag{5-5}$$

The correction step updates the Kalman gain K_k. The estimate $\hat{X}_k$ and state error covariance matrix $\hat{P}_k$ were corrected by integrating the observation function $h(\cdot)$ when the LRF/Camera observation is available:

$$K_k = \tilde{P}_k H_k^T (H_k \tilde{P}_k H_k^T + J_{w,k} R_k J_{w,k}^T)^{-1} \tag{5-6}$$

$$\hat{X}_k = \tilde{X}_k + K_k[Z_k - h(\tilde{X}_k, 0)] \tag{5-7}$$

$$\hat{P}_k = (I - K_k H_k)\tilde{P}_k \tag{5-8}$$

Where $\hat{X}_{k-1}$ represent the corrected state and $\hat{P}_{k-1}$ represent the corrected state error covariance matrix at previous time. $J_{x,k}$ and H_k represent the Jacobeans of system function $f(\cdot)$ and observation function $h(\cdot)$ with respect to state X_k and observation Z_k, $J_{v,k}$ and $J_{w,k}$ are Jacobeans of system function $f(\cdot)$ and observation function $h(\cdot)$ with respect to input U_k and observation

Z_k, and I is defined as an identity matrix.

5.2 Accomplishment of the EKF

From the result of chapter 3 it could found that both of the LRF-landmark-based observation and the Camera-marker-based observation method own same triangulation principle, and the leader-follower relative position was defined by the relative distance, relative orientation angle and relative heading angle.

On this chapter, tracking system based LRF-landmark would be further studied. The leader-follower relative state vector assuming no noise is defined as:

$$X_k = f(\hat{X}_{k-1}, U_k, 0) = [\theta_{l,k}, \theta_{f,k}, d_{12,k}, \Phi_{12,k}]^T \tag{5-9}$$

The LRF-landmark-based observation vector assuming no noise is defined as:

$$Z_k = h(\tilde{X}_k, 0) = [\theta_{flaser,k}, d_{laser,k}, \Phi_{laser,k}]^T \tag{5-10}$$

Where $\theta_{l,k}$ is heading angle of the leader; $\theta_{f,k}$ and $\theta_{flaser,k}$ is the heading angle of the follower; $d_{12,k}$ and $d_{laser,k}$ is the relative distance from P_0 to P_2; and $\Phi_{12,k}$ and $\Phi_{laser,k}$ is the relative angle between line $\overline{P_0P_2}$ and heading position of the follower (Fig 5.1).

By analyzing the relation between the leader and the follower, could get the following equations:

$$\begin{bmatrix} x_l \\ y_l \end{bmatrix} = \begin{bmatrix} x_f + d_{12}\cos(\theta_f + \Phi_{12}) \\ y_f + d_{12}\sin(\theta_f + \Phi_{12}) \end{bmatrix} \tag{5-11}$$

Differentiation of the above equations with respect to time and combining equation (4-1) yields

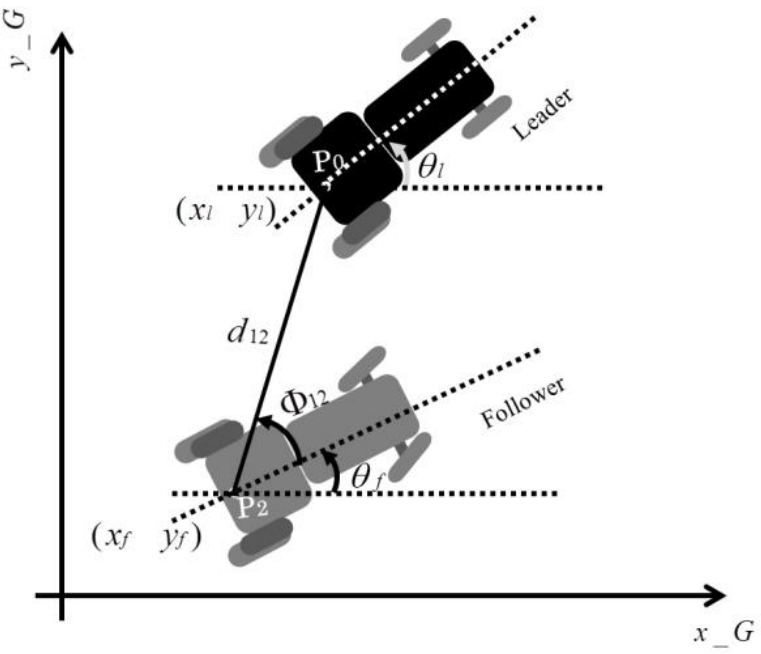

(a)

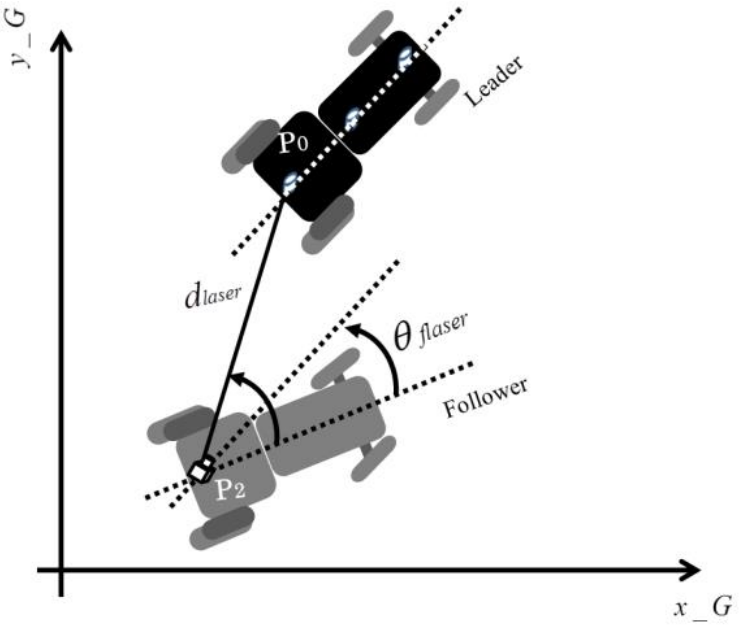

(b)

Fig. 5.1 Leader-follower tracking model:

(a) Relative position under odometry; (b) Relative position under LRF.

$$\begin{bmatrix} \dot{\theta}_l \\ \dot{\theta}_f \\ \dot{d}_{12} \\ \dot{\Phi}_{12} \end{bmatrix} = \begin{bmatrix} \dfrac{\tan\delta_l}{L} v_l \\ \dfrac{\tan\delta_f}{L} v_f \\ \sin(\theta_f + \Phi_{12})(v_l \sin\theta_l - v_f \sin\theta_f) \\ \quad + \cos(\theta_f + \Phi_{12})(v_l \cos\theta_l - v_f \cos\theta_f) \\ \dfrac{1}{d_{12}}[\cos(\theta_f + \Phi_{12})(v_l \sin\theta_l - v_f \sin\theta_f) \\ \quad - \sin(\theta_f + \Phi_{12})(v_l \cos\theta_l - v_f \cos\theta_f)] - \dfrac{v_f}{L}\tan\delta_f \end{bmatrix} \quad (5\text{-}12)$$

The above equations show the leader-follower relative state based on odometer. Note that the heading angles of the leader and the follower θ_l and θ_f in equation (5-12) are in global coordinates. As discussed above, it is impossible to obtain the global coordinates in this research due to the absence of GPS and Gyroscope. Transforming the leader-follower relative state function of equation (5-12) to leader-based local coordinates, the estimate of leader-follower relative state at time instant k can be modified as equation (5-13). The state evolution from time instant *k-1* to *k+1*, in which left-side vehicles represent the corrected state $\hat{X}_{k-1}$ at the previous time instant and right-side vehicles represent the prettiest state $\tilde{X}_k$ at current (Fig 5.2).

$$\tilde{X}_k = \begin{bmatrix} \tilde{\theta}_{f\_L,k} \\ \tilde{d}_{12,k} \\ \tilde{\Phi}_{12,k} \end{bmatrix}$$

$$= \begin{bmatrix} \hat{\theta}_{f\_L,k-1} + \Delta\theta_{f\_L,k} - \Delta\theta_{l\_L,k} \\ \hat{d}_{12,k-1} + \Delta d_{12,k} \\ \hat{\Phi}_{12,k-1} + \Delta\Phi_{12,k} \end{bmatrix}$$

$$= \begin{bmatrix} \hat{\theta}_{f\_L,k-1} + (\frac{\tan\delta_{f,k}}{L} v_{f,k} - \frac{\tan\delta_{l,k}}{L} v_{l,k})T_s \\ \hat{d}_{12,k-1} + (ac+bd)T_s \\ \hat{\Phi}_{12,k-1} + \frac{1}{\hat{d}_{12,k-1}}(ac+bd - \frac{v_{f,k}}{L}\tan\delta_{f,k})T_s \end{bmatrix} \qquad (5-13)$$

where

$$a = \sin(\tilde{\theta}_{f\_L,k} + \hat{\Phi}_{12,k-1}) \quad , b = \cos(\tilde{\theta}_{f\_L,k} + \hat{\Phi}_{12,k-1})$$
$$c = -v_{f,k}\sin\tilde{\theta}_{f\_L,k} \quad , d = v_{l,k} - v_{f,k}\cos\tilde{\theta}_{f\_L,k}$$

Where $v_{l,k}$ and $v_{f,k}$ is the velocity of the leader and the follower; $\delta_{l,k}$ and $\delta_{f,k}$ is the steering angle of the leader and the follower. Both velocity and steering angles are obtained from encoders at time instant *k*. T_s is the time interval.

As an important step, the leader-based local coordinates were updated at each prediction step, which meant that the heading angle of the leader under the leader-based local coordinates was a constant equal to zero:

$$\hat{\theta}_{l\_L,k} \equiv \tilde{\theta}_{l\_L,k-1} \equiv 0 \qquad (5\text{-}14)$$

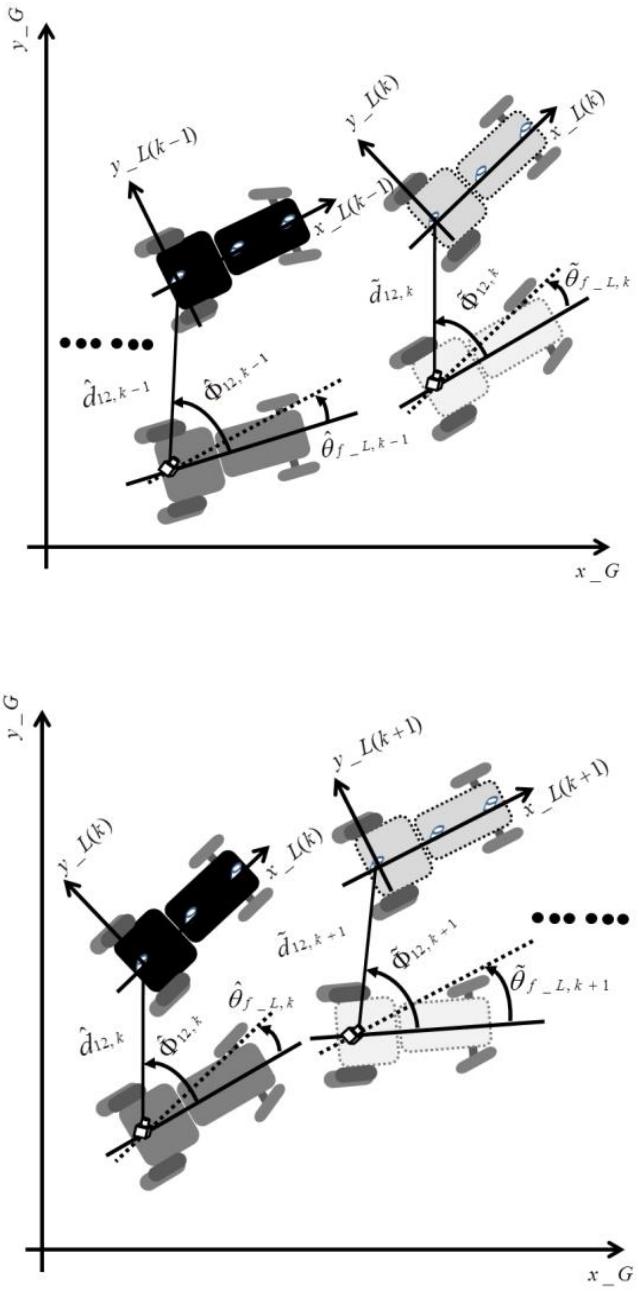

Fig. 5.2 Leader-Follower relative state evolution:

(a) From time *k-1* to *k*; (b) From time *k* to *k+1*.

During the time interval T_s, both the leader and the follower changed their state. Equation (5-13) expressed updated information of leader-based local coordinates, and estimation of the leader-follower relative state in the leader-based local

coordinate system from time *k-1* to *k*. Establishing and updating the leader-based coordinates in a timely manner made tracking possible even though there were no GPS and Gyroscope in the follower and helped to eliminate the effect of incremental error of encoders.

Following the odometry-based state estimate equation (5-13), the system and input Jacobeans $J_{x,k}$ and $J_{v,k}$ can be given:

$$J_{x,k}=\begin{bmatrix} \frac{\partial\tilde{\theta}_{f\_L,k}}{\partial\hat{\theta}_{f\_L,k-1}} & \frac{\partial\tilde{\theta}_{f\_L,k}}{\partial\hat{d}_{12,k-1}} & \frac{\partial\tilde{\theta}_{f\_L,k}}{\partial\hat{\Phi}_{12,k-1}} \\ \frac{\partial\tilde{d}_{12,k}}{\partial\hat{\theta}_{f\_L,k-1}} & \frac{\partial\tilde{d}_{12,k}}{\partial\hat{d}_{12,k-1}} & \frac{\partial\tilde{d}_{12,k}}{\partial\hat{\Phi}_{12,k-1}} \\ \frac{\partial\tilde{\Phi}_{12,k}}{\partial\hat{\theta}_{f\_L,k-1}} & \frac{\partial\tilde{\Phi}_{12,k}}{\partial\hat{d}_{12,k-1}} & \frac{\partial\tilde{\Phi}_{12,k}}{\partial\hat{\Phi}_{12,k-1}} \end{bmatrix}=\begin{bmatrix} 1 & 0 & 0 \\ f_{21} & 1 & f_{23} \\ f_{31} & f_{32} & f_{33} \end{bmatrix} \qquad (5\text{-}15)$$

where

$$f_{21}=[bc-av_{f,k}\cos\tilde{\theta}_{f\_L,k}-ad+bv_{f,k}\sin\tilde{\theta}_{f\_L,k}]T_s \quad , f_{23}=[bc-ad]T_s$$

$$f_{31}=-\frac{1}{\hat{d}_{12,k-1}}[ac+bv_{f,k}\cos\tilde{\theta}_{f\_L,k}+bd+av_{f,k}\sin\tilde{\theta}_{f\_L,k}]T_s$$

$$f_{32}=-\frac{1}{\hat{d}^2_{12,k-1}}[bc-ad]T_s \quad , f_{33}=1-\frac{1}{\hat{d}_{12,k-1}}[ac+bd]T_s$$

And

$$J_{v,k}=\begin{bmatrix} \frac{\partial\tilde{\theta}_{f\_L,k}}{\partial v_{l,k}} & \frac{\partial\tilde{\theta}_{f\_L,k}}{\partial v_{f,k}} & \frac{\partial\tilde{\theta}_{f\_L,k}}{\partial\delta_{l,k}} & \frac{\partial\tilde{\theta}_{f\_L,k}}{\partial\delta_{f,k}} \\ \frac{\partial\tilde{d}_{12,k}}{\partial v_{l,k}} & \frac{\partial\tilde{d}_{12,k}}{\partial v_{f,k}} & \frac{\partial\tilde{d}_{12,k}}{\partial\delta_{l,k}} & \frac{\partial\tilde{d}_{12,k}}{\partial\delta_{f,k}} \\ \frac{\partial\tilde{\Phi}_{12,k}}{\partial v_{l,k}} & \frac{\partial\tilde{\Phi}_{12,k}}{\partial v_{f,k}} & \frac{\partial\tilde{\Phi}_{12,k}}{\partial\delta_{l,k}} & \frac{\partial\tilde{\Phi}_{12,k}}{\partial\delta_{f,k}} \end{bmatrix}=\begin{bmatrix} u_{11} & u_{12} & u_{13} & u_{14} \\ u_{21} & u_{22} & u_{23} & u_{24} \\ u_{31} & u_{32} & u_{33} & u_{34} \end{bmatrix} \quad (5-16)$$

where

$$u_{11} = -\frac{\tan\delta_{l,k}}{L}T_s \quad , u_{12} = \frac{\tan\delta_{f,k}}{L}T_s \quad , u_{13} = -\frac{v_{l,k}}{L}\sec^2\delta_{l,k}T_s \quad , u_{14} = \frac{v_{f,k}}{L}\sec^2\delta_{f,k}T_s$$

$$u_{21} = (b - av_{l,k}u_{11})T_s \quad , u_{22} = -[a(\sin\tilde{\theta}_{f\_L,k} + v_{l,k})u_{12} + b\cos\tilde{\theta}_{f\_L,k}]T_s$$

$$u_{23} = -av_{l,k}u_{13}T_s \quad , u_{24} = -av_{l,k}u_{14}T_s \quad , u_{31} = \frac{1}{\hat{d}_{12,k-1}}(bv_{l.k}u_{11} - a)T_s$$

$$u_{32} = \frac{1}{\hat{d}_{12,k-1}}[a\cos\tilde{\theta}_{f\_L,k} - b(\sin\tilde{\theta}_{f\_L,k} + v_{l,k}u_{12})]T_s - \frac{u_{12}}{T_s}$$

$$u_{33} = \frac{1}{\hat{d}_{12,k-1}}[bv_{l,k}u_{13}T_s] \quad , u_{34} = \frac{1}{\hat{d}_{12,k-1}}[-bv_{l,k}u_{14}]T_s - \frac{u_{24}}{T_s}$$

For the state observation vector Z_k, and following the LRF-landmark method as described above, the leader-follower relative state observation problem can be found as:

$$Z_k = [-\beta_k, d_{3,k}, \alpha_{3,k}]^T \tag{5-17}$$

Based on the above observation function equation (5-17) and the LRF-landmark observation calculation in equation (3-2) and (3-3), the observation Jacobean H_k and $J_{w,k}$ can be given:

The observation Jacobean H_k and $J_{w,k}$ can be given:

$$H_k = \begin{bmatrix} \frac{\partial\theta_{flaser\_L,k}}{\partial\tilde{\theta}_{f\_L,k}} & \frac{\partial\theta_{flaser\_L,k}}{\partial\tilde{d}_{12,k}} & \frac{\partial\theta_{flaser\_L,k}}{\partial\tilde{\Phi}_{12,k}} \\ \frac{\partial d_{laser,k}}{\partial\tilde{\theta}_{f\_L,k}} & \frac{\partial d_{laser,k}}{\partial\tilde{d}_{12,k}} & \frac{\partial d_{laser,k}}{\partial\tilde{\Phi}_{12,k}} \\ \frac{\partial\Phi_{laser,k}}{\partial\tilde{\theta}_{f\_L,k}} & \frac{\partial\Phi_{laser,k}}{\partial\tilde{d}_{12,k}} & \frac{\partial\Phi_{laser,k}}{\partial\tilde{\Phi}_{12,k}} \end{bmatrix} = \begin{bmatrix} 1 & 0 & 0 \\ 0 & 1 & 0 \\ 0 & 0 & 1 \end{bmatrix} \tag{5-18}$$

and

$$J_{w,k}=\begin{bmatrix} \frac{\partial \theta_{flaser\_L,k}}{\partial d_{1,k}} & \frac{\partial \theta_{flaser\_L,k}}{\partial d_{3,k}} & \frac{\partial \theta_{flaser\_L,k}}{\partial \alpha_{3,k}} \\ \frac{\partial d_{laser,k}}{\partial d_{1,k}} & \frac{\partial d_{laser,k}}{\partial d_{3,k}} & \frac{\partial d_{laser,k}}{\partial \alpha_{3,k}} \\ \frac{\partial \Phi_{laser,k}}{\partial d_{1,k}} & \frac{\partial \Phi_{laser,k}}{\partial d_{3,k}} & \frac{\partial \Phi_{laser,k}}{\partial \alpha_{3,k}} \end{bmatrix}=\begin{bmatrix} h_{11} & h_{12} & -1 \\ 0 & 1 & 0 \\ 0 & 0 & 1 \end{bmatrix} \quad (5\text{-}19)$$

where

$$h_{11}=-\frac{l_3^2-d_{3,k}^2-d_{1,k}^2}{d_{3,k}\sqrt{(2l_{3,k}d_{3,k})^2-(l_3^2+d_{3,k}^2-d_{1,k}^2)^2}} \quad ,$$

$$h_{12}=-\frac{2d_{1,k}}{\sqrt{(2l_3d_{3,k})^2-(l_3^2+d_{3,k}^2-d_{1,k}^2)^2}}$$

The system and observation functions was defined and Jacobeans functions were calculated. Once the Jacobeans functions are known, Kalman gain, the leader-follower relative state observation, and state error covariance matirx can be found using equation (5-3,4,5,6,7,8).

In this research, the input of system function $f(\cdot)$ is the encoder information of steering angle and velocity. Under farmland conditions, the noise covariance matrix Q for the encoders can be defined as:

$$Q=\begin{bmatrix} \sigma_{vl}^2 & 0 & 0 & 0 \\ 0 & \sigma_{vf}^2 & 0 & 0 \\ 0 & 0 & \sigma_{\delta l}^2 & 0 \\ 0 & 0 & 0 & \sigma_{\delta f}^2 \end{bmatrix} \quad (5\text{-}20)$$

Besides, the observation was assumed to be provided by the LRF (SICK LMS 211), and data were relative distance and angle of each landmark from the LRF. The observation noise covariance matrix R for the LRF can be expressed as:

$$R = \begin{bmatrix} \sigma_d^2 & 0 & 0 \\ 0 & \sigma_d^2 & 0 \\ 0 & 0 & \sigma_{ang}^2 \end{bmatrix} \tag{5-21}$$

where

$\sigma_{vl} = \sigma_{vf} = 0.198 m/s$, $\sigma_{\delta l} = \sigma_{\delta f} = 0.105 rad/s$

$\sigma_d = 0.0013m$, $\sigma_{ang} = 0.0038rad$

As noted above, the LRF observation information is not always available because of its low update frequency (compared with odometry system) and propagation delay of LRF signals. Thus, the correction step is only processed when the LRF observation is available. This means that:

If LRF observation is available:

The posteriori estimate $\hat{X}_k$ and state error covariance matrix $\hat{P}_k$ could be calculated by fusing the odometry based priori estimate state $\tilde{X}_k$ and LRF-based observation results Z_k using equation (5-7) and (5-8).

If LRF observation gets delayed:

The posteriori estimate $\hat{X}_k$ and state error covariance matrix $\hat{P}_k$ approximately adopt the priori estimate state $\tilde{X}_k$ and state error covariance matrix $\tilde{P}_k$ for calculating next time instant *k+1*:

$$\hat{X}_k = \tilde{X}_k \tag{5-22}$$

$$\hat{P}_k = \tilde{P}_k \tag{5-23}$$

5.3 Simulation results

Simulation were executed to evaluate the performance of EKF to reduce sensor noise for relative position estimate by fusing the LRF and odometry data. In the

simulation the EKF estimated leader-follower relative position would supply to the follower controller and evaluate on case of leader-follower formation tracking. The simulation was conducted for a leader equipped with encoders on the rear and front wheels to record velocity and steering angle of the tractor, and the autonomous follower equipped with encoders and LRF.

In the simulation, sensor noise was selected based on the farmland condition and previous studies. The noise of odometry (encoders) was generated by random functions, and added to the velocity and steering angle of the leader and the follower were around 0.032 m/s and 0.0524 rad/s (Yu et al., 2009; Qi et al., 2010). The noise of LRF was also generated by random functions, and added to the distances and angles between the LRF and each landmarks were around 5 cm and 0.035 rad under a distance around 4 m (Ahamed et al., 2006).

In the simulation, the global position of the follower was unavailable and the only information transmitted from the leader to the follower was the velocity and steering angular velocity of the leader (simulating LRF-based and GPS-free autonomous driving). During farmland operations the transmition of the leader velocity and steering angular velocity could be transmitted using the wireless LAN.

The time for data transmission using wireless LAN and LRF scan interval was simulated as 20 ms and 200 ms, respectively. Note that the laser detection frequency was set lower than the usual frequency of LMS 211. And the time interval Ts was 100 ms. Simulations on small and large sinusoidal curvature paths were performed (Fig 5.3 and 5.4).

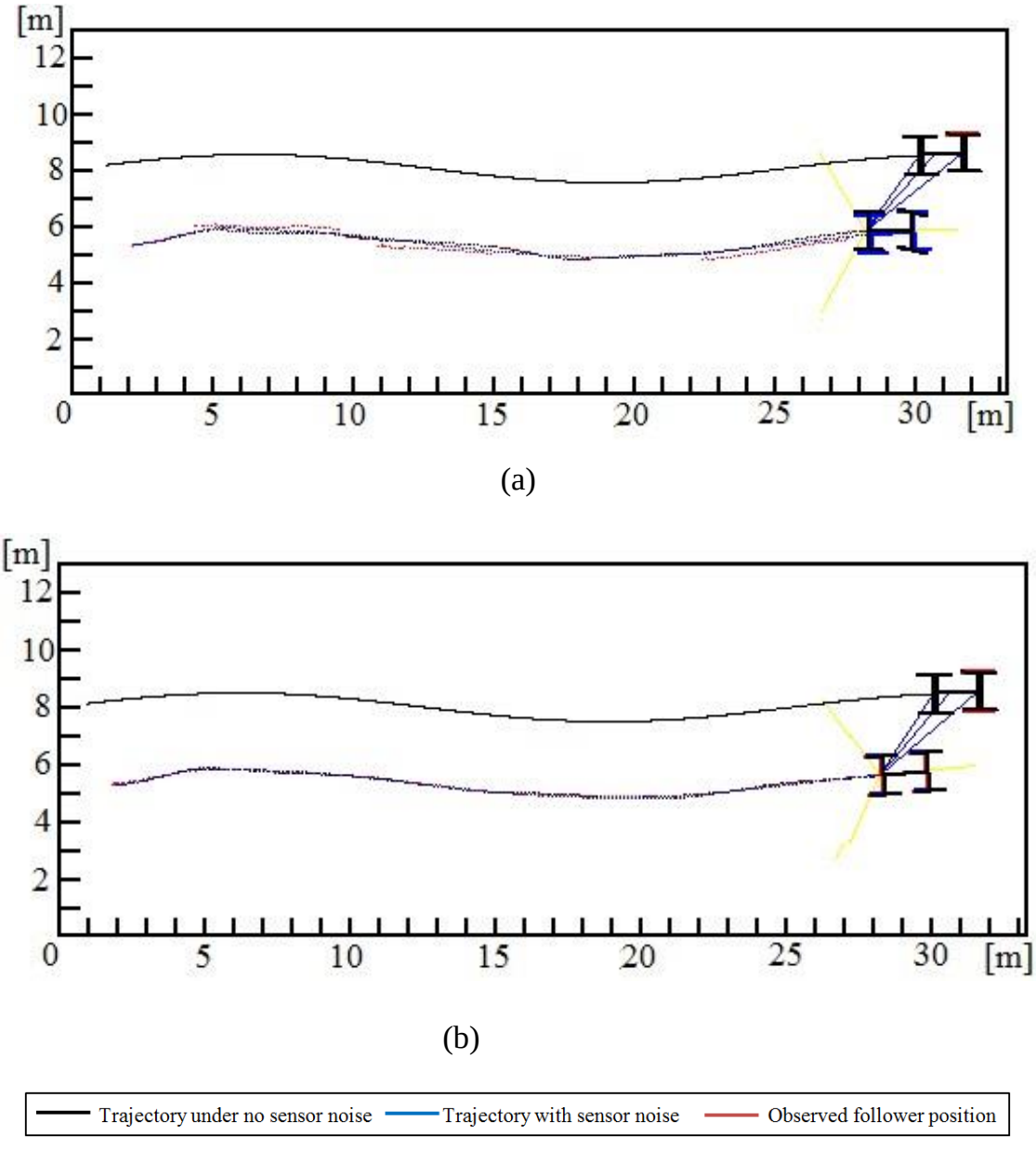

Fig. 5.3 Leader-follower formation tracking on small sinusoidal curved path.

(a)With sensor noise; (b) Sensor data fusion by EKF.

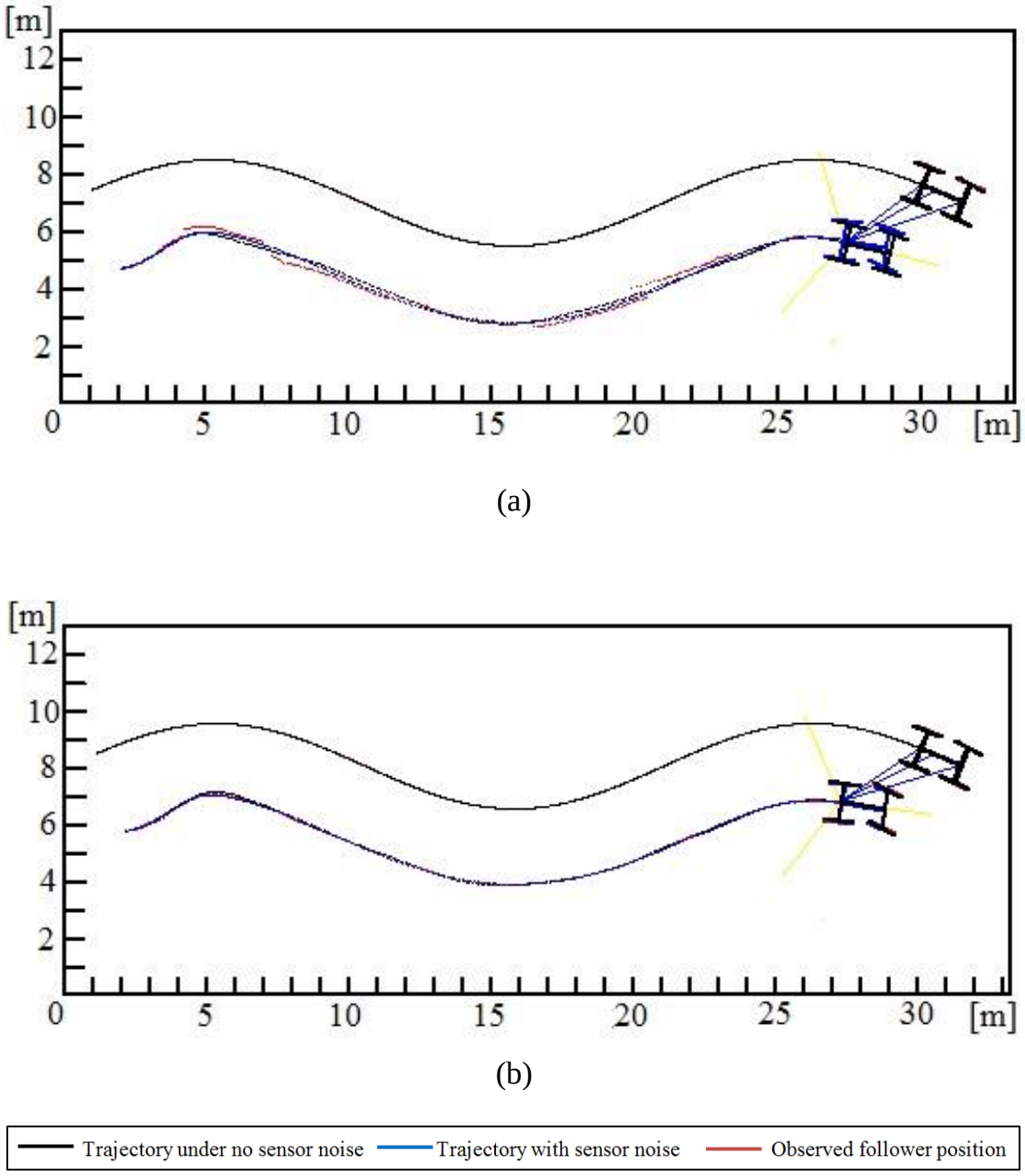

Fig. 5.4 Leader-follower formation tracking on large sinusoidal curved path.

(a)With sensor noise; (b) Sensor data fusion by EKF.

The results of formation tracking were compared for three cases: excluding sensor noise, including sensor noise, and fusion of sensor data using the EKF. In the second case, the odometry positioning was used while the LRF positioning was not available. In the third case, the fusion was performed with odometry and LRF-observed position data using the EKF algorithm. In the first case, the ideal case was assumed, where both the LRF and odometry were noise-free. In the simulated experiment results, it was clearly observed that the small and large curvature paths were affected by sensor noise. Furthermore, the trajectory of the follower was not smooth and deviated from the ideal trajectory. After fusing sensor data using EKF algorithm, the trajectory of the follower was smooth. The formation tracking and observation accuracies were also improved.

In the case of leader-follower relative positioning, error was observed while there was sensor noise (Fig 5.5 and 5.6). Consequently, instability in the velocity and steering angle of the follower was observed.

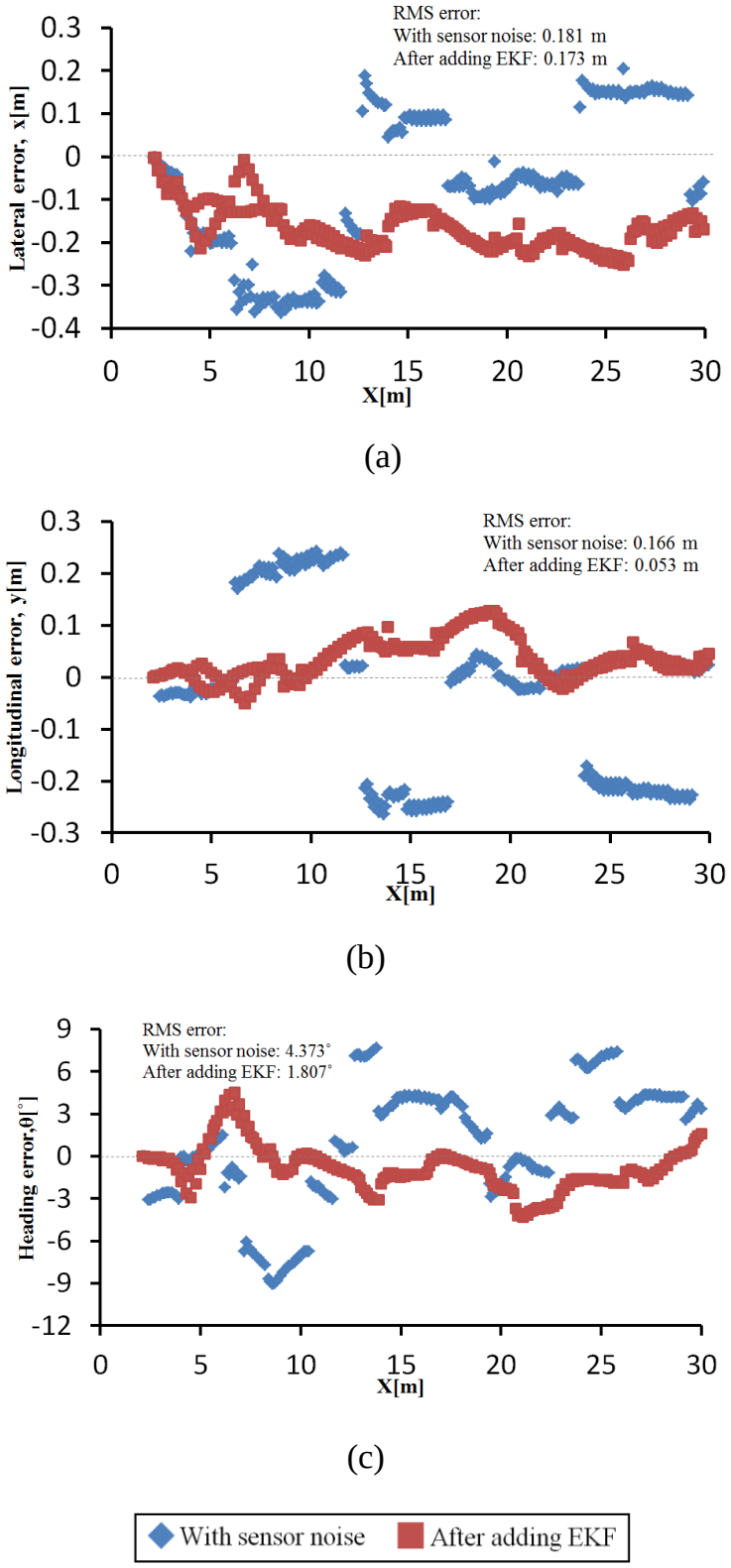

Fig. 5.5 Leader-follower relative position error on small sinusoidal curved path. (a) Lateral error; (b) Longitudinal error; and (c) Heading error.

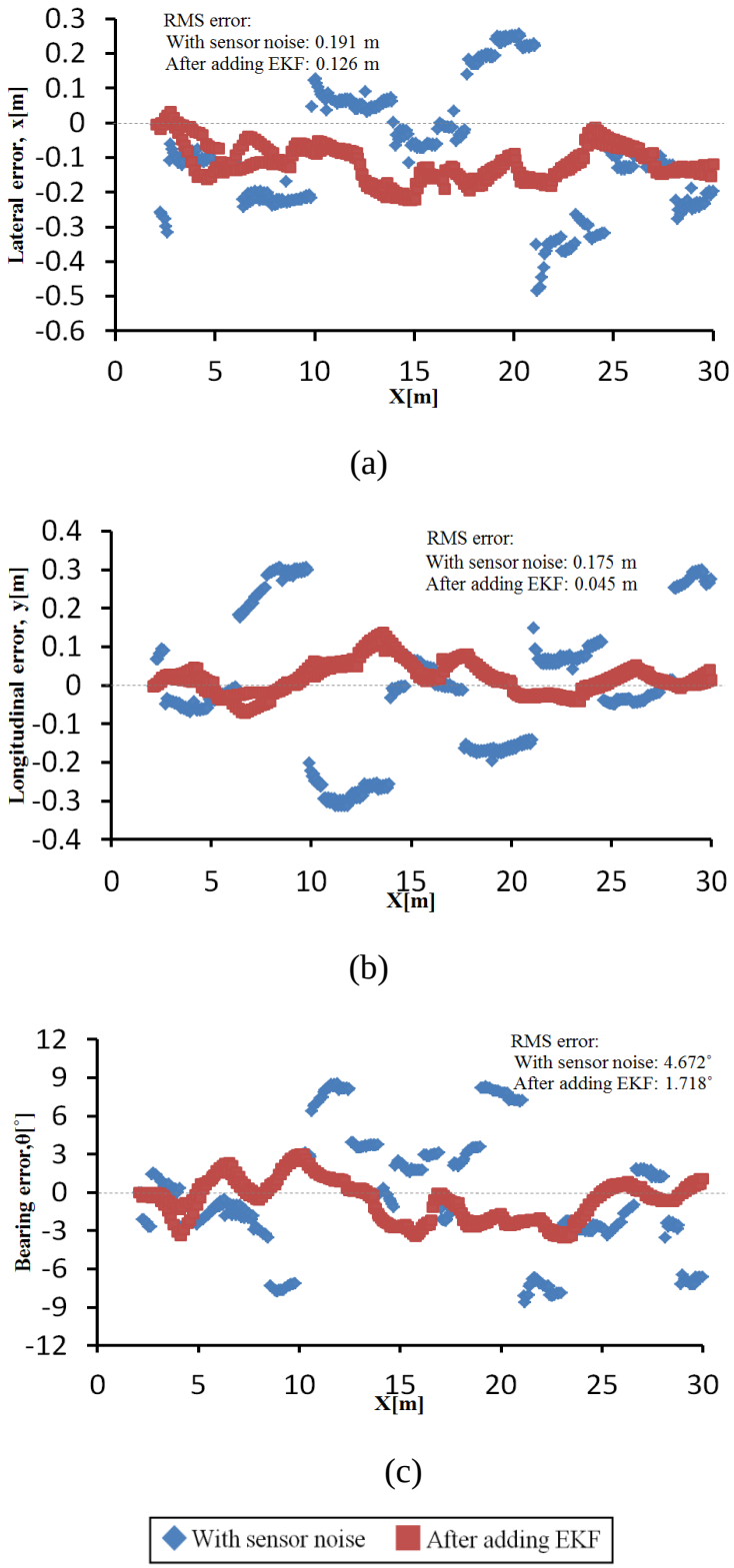

Fig. 5.6 Leader-follower relative position error on large sinusoidal curved path. (a) Lateral error; (b) Longitudinal error; and (c) Heading error.

To improve the relative positioning error, the EKF algorithm was implemented for motion stability (Fig 5.7 and 5.8). After adding the EKF, the observation error was decreased. As a result, the velocity and steering angle of the follower was stable and close to the value similar to the case with no noise.

After adding the EKF for the small sinusoidal curved path, the RMSEs of lateral, longitudinal, and heading observation error was reduced from 0.181 to 0.173 m, 0.166 to 0.053 m, and 4.373 to 1.807˚, respectively. The RMSEs of the velocity and steering angle of the follower were reduced from 0.167 to 0.053 *m/s* and 6.029 to 2.406˚, respectively. In the case of large curvature path, the RMSEs for lateral, longitudinal, and heading observation error were reduced from 0.191 to 0.126 m, 0.175 to 0.045 m, and 4.672 to 1.718˚, respectively. The RMSEs of velocity and the steering angle of the follower were also reduced from 0.176 to 0.039 m/s and 7.659 to 3.157˚, respectively.

Because observation accuracy was improved significantly along with stable velocity and steering angle, the tracking accuracy was improved for small and larger curved paths (Fig 5.9 and 5.10). On the small curved path after adding the EKF, the RMSEs of lateral, longitudinal, and heading tracking error was reduced from 0.295 to 0.251 m, 0.135 to 0.11 m, and 4.856 to 3.938˚, respectively. On the large curved path, the RMSEs of lateral, longitudinal, and heading tracking error were reduced from 0.303 to 0.227 m, 0.259 to 0.228 m, and 13.416 to 13.198˚, respectively.

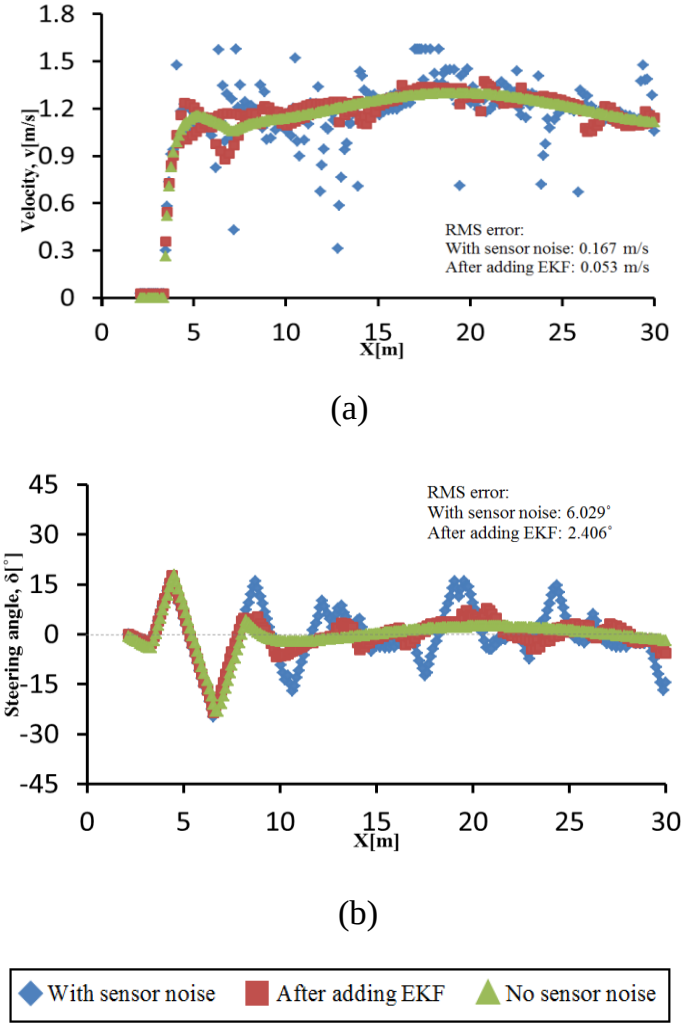

Fig. 5.7 Velocities and steering angle of the follower under no sensor noise, with sensor noise, and EKF conditions on small sinusoidal curved path.

(a) Velocity; (b) Steering angle.

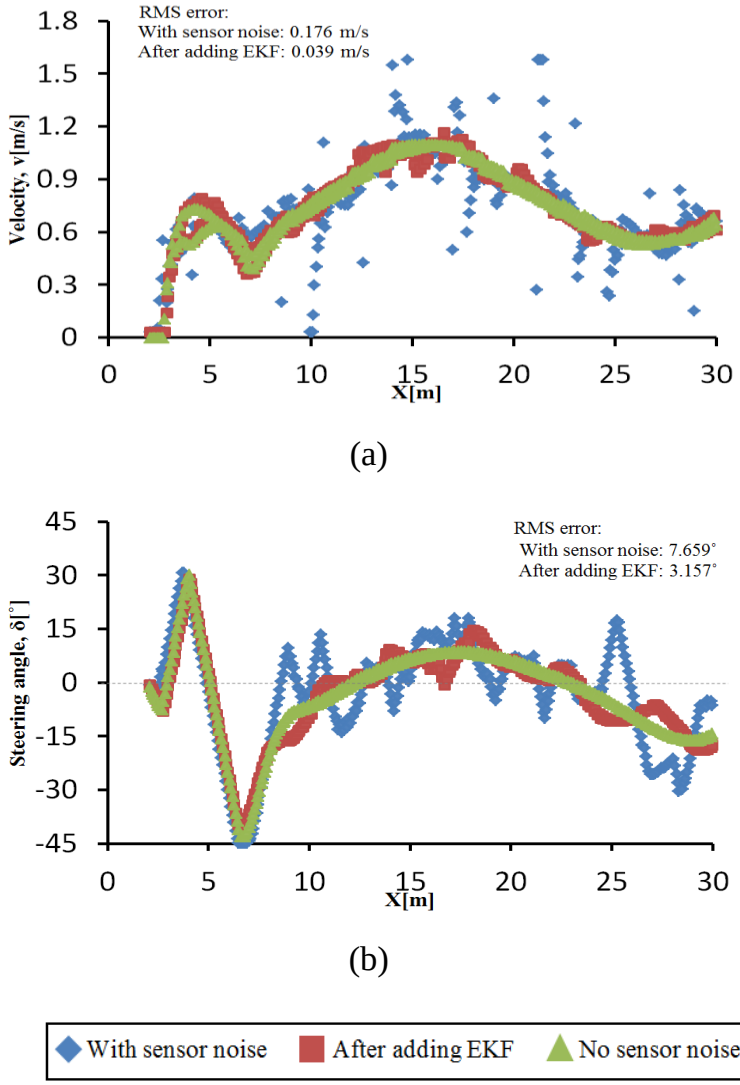

Fig. 5.8 Velocities and steering angle of the follower under no sensor noise, with sensor noise, and EKF conditions on large sinusoidal curved path.

(a) Velocity; (b) Steering angle.

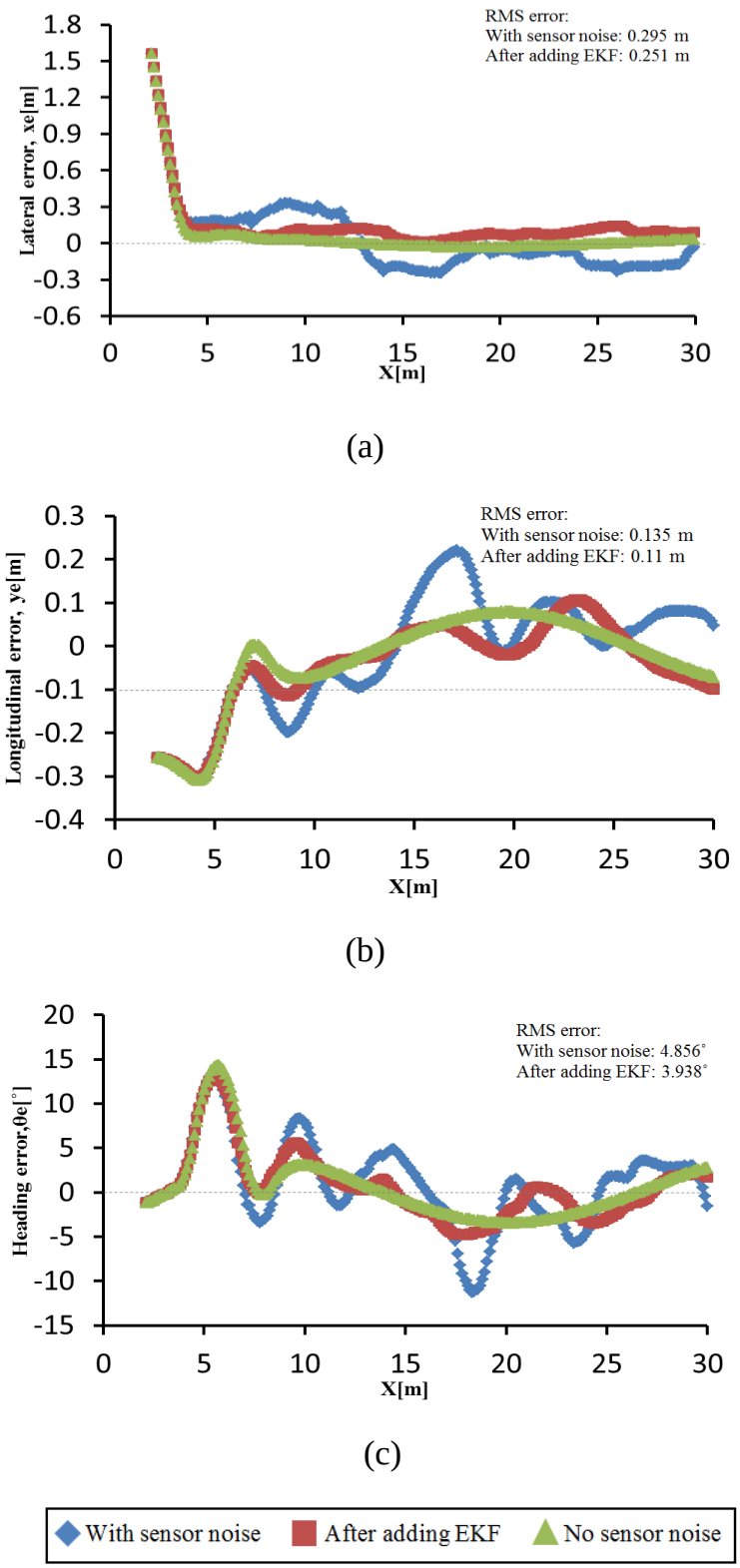

Fig. 5.9 Formation tracking error on small sinusoidal curved path.

(a) Lateral error; (b) Longitudinal error; and (c) Heading error.

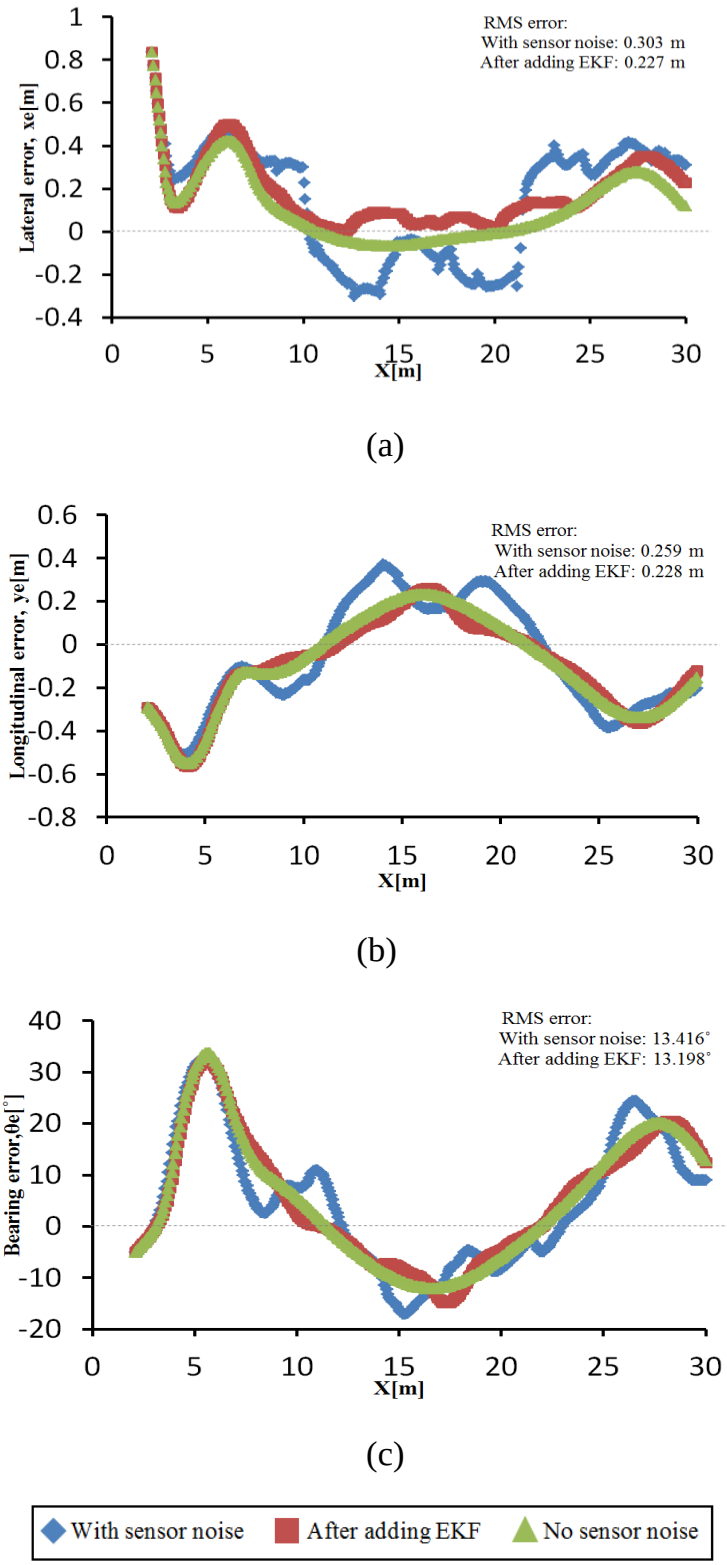

Fig. 5.10 Formation tracking error on large sinusoidal curved path.

(a) Lateral error; (b) Longitudinal error; and (c) Heading error.

5.4 Conclusion

In this chapter, an EKF estimation algorithm was developed and proven to have good performance for reducing noise. After integrating the EKF, the LRF noise was decreased and updated relative positional information between the leader and the follower quickly and with high accuracy. As a result, stable velocity and steering angle of the follower and high accuracy of formation tracking was established.

Chapter 6

Structure of Experimental Vehicle System

In the previous chapters, simulation results have verified the developed leader-follower vehicle tracking system could drive a follower vehicle to realize stable and accuracy tracking. Considering the sensor noise was more complex than in simulation and the limitation of mechanic mechanical components, field experiment should be conducted to further examine performance of the developed tracking system under real condition.

In this study, main platform and supporting means have been selected, with respect to economical and practical aspects. Two four-wheel drive vehicles with same model have been used as experiment vehicles, one as a leader and another as a follower. The marker plane was equipped on the leader vehicle, camera and odometry system was installed on the follower vehicle. In detail, all of experimental apparatus were described as follows.

6.1 Experiment vehicle

The experimental leader and follower vehicle were modified from electric vehicle EJ-20 which was produced by CHIKUSUI CANYCOM Company. In Figure 6.1 the leader vehicle was installed a marker and a reflector, the follower vehicle was modified to be an autonomous vehicle including local sensing part, data collection part, steering part, velocity adjusting part, data transmission and calculation part. The basic instrumentation system of the autonomous follower vehicle was described in Fig. 6.2.

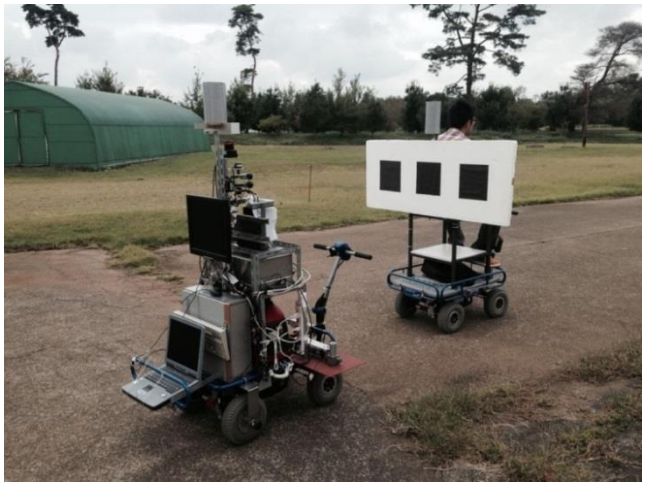

Fig. 6.1 The experimental leader and follower vehicle system

6.1.1 Steering system

Steering of the autonomous vehicle was conducted by an electronic cylinder (Tsubaki LPF040L2.0VK2J). The length of piston rod was 200 mm and maximum speed of 40mm/s. It could provide stable thrust power up to 204 kgf. Control of the electronic cylinder was through a set of relay according to the DIO board signal, including enable, holding, extending and shrinking. It could found in figure 4.3 that the vehicle could steer left and right by extending and shrinking the electronic cylinder. The maximum steering angle of the vehicle was limited at 40˚.

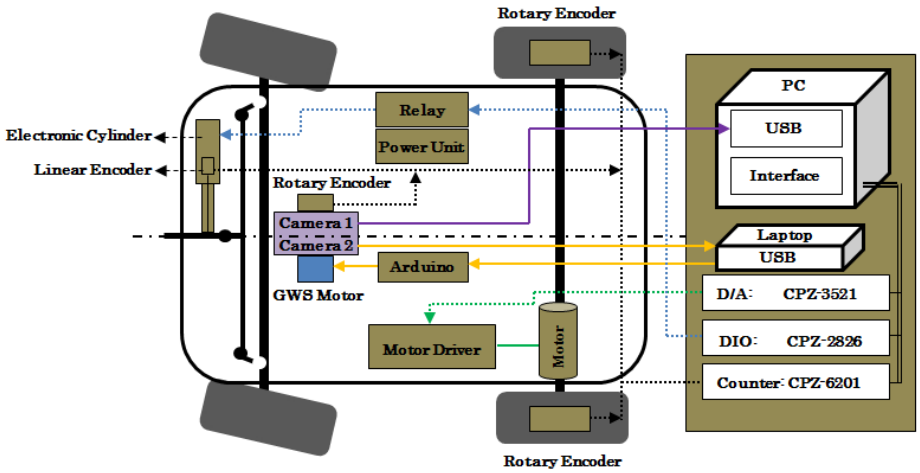

Fig. 6.2 Structure of autonomous vehicle

A linear encoder (Mutoh DX-025) own a resolution of 25 pulse/mm was installed on the electronic cylinder to measure the motion length of piston rod, and could be further utilized to calculate the steering angle. The signal of linear encoder was interfaced to the computer through a counter board. With the limitation of system respond speed, steering accuracy of the vehicle was about 0.3˚. The steering control configuration was shown in Fig 6.4

Fig 6.3 Structure of Steering system

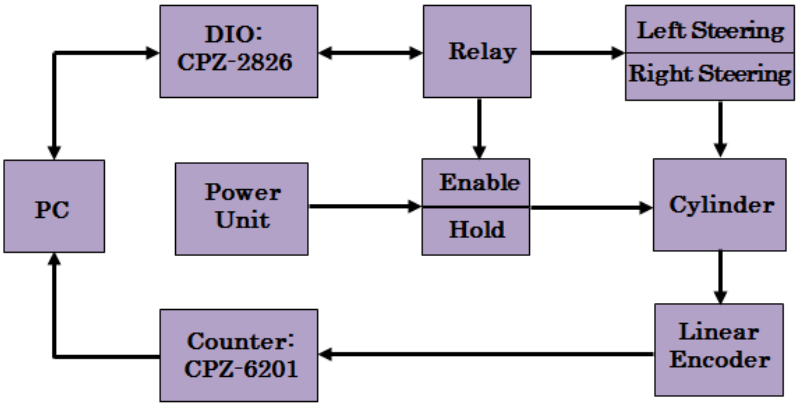

Fig. 6.4 Configuration of Steering system

6.1.2 Velocity control system

In this study, the vehicle was driven using a 350 W electronic motor, thus, its velocity could be adjusted by controlling the motor speed. Input signal of motor driver was generated through a DA board. As shown in Fig 4.5, a relay was used

to control motion direction of the vehicle by interfacing a DIO board.

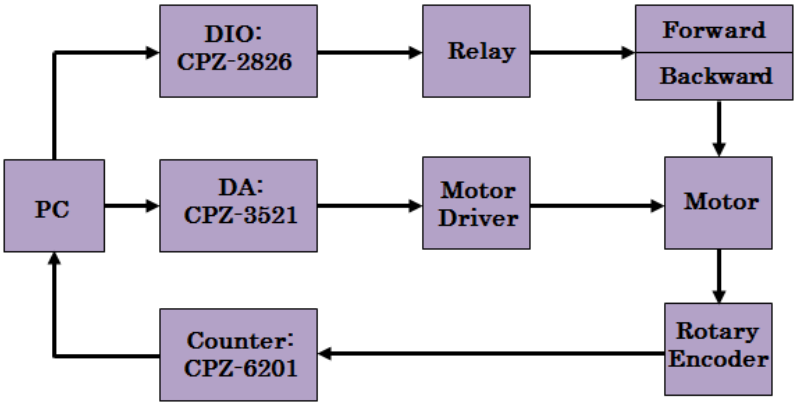

Fig. 6.5 Configuration of velocity control system

Pair of Omron E6B2-CWZ6C incremental rotary encoder was installed on the rotary center of each rear wheel Fig 4.6. The output signal consists of A-phase, B-phase and Z-phase. Difference between the A-phase and the B-phase was 90˚, and the Z-phase was the reference output. Pulse would be generated and counted by a counter board interfaced with the computer. Corresponding to wheel size of the vehicle, the velocity of the vehicle and traveling distance could be estimated. As the two rear wheels were independents, the velocity and traveling distance of the vehicle were calculated using averaging velocity of left and right wheel.

Fig. 6.6 Incremental rotary encoder in velocity control system

The important technical data of the experimental vehicles were described in Table 6.1 as follow.

Table 6.1 Technical data of experiment vehicle

Model	CHIKUSUI EJ-20
Motor	24V350W
Velocity (km/h)	0~4.5
Length (mm)	1040
Width (mm)	610
Height (mm)	940
Wheel base (mm)	600
Ground clearance (mm)	60
Length of drawbar (mm)	Front: 460/ Rear: 490

6.1.3 Camera system

A Logitech Pro 9000 camera was equipped on the autonomous follower vehicle to provide monocular vision information. It could provide 2 million effective pixels with a maximum 30 frame rate.

Due to limitation of camera view angle it exciting potential risk of losing target during tracking the leader vehicle, especially on a large curvature path. To overcome this problem a camera servo system was designed to maintain the target in the camera view field center. The camera servo was composed by a GWS servo motor, a rotary encoder (SUNX ORE-38) and camera (Fig 4.7). Rotation of the servo motor was controlled by an Arduino micro-controller (Fig 4.8).

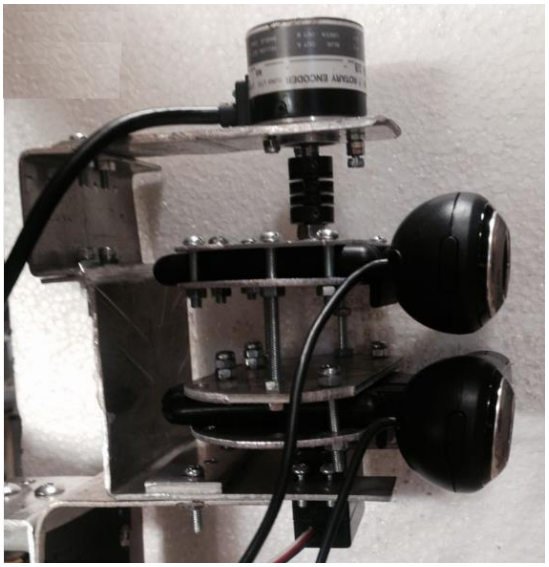

Fig. 6.7 Camera servo system

In the figure 6.7 one camera was connected with the control computer for vehicle control, another one was connected with a laptop to control the GWS servo motor through the Arduino micro-controller.

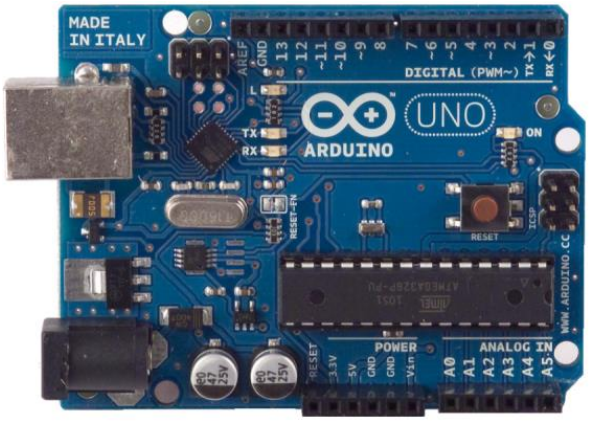

Fig. 6.8 Arduino micro-controller

Reason of using additional camera to drive the GWS servo motor was that, when the servo motor need to turn a relative large angle USB port of control computer was impossible to provide the requirement electric current. This would lead to unstable of the control system. The laptop calculated the offset angle between the target and the camera optic axis, then online transforms the offset angle to the

Arduino micro-controller through USB Serial Communications at 9600 baud rate. The PWM port in the Arduino micro-controller could drive the GWS servo motor rotary a correct angle to ensure the target always locate on the camera view field center.

The marker was composed by a white polystyrene block as background and three black square paper pasted with equal interval. Length of square side was 0.25 m and distance between two adjacent squares was 0.44 m. Length and width of the polystyrene block was1.55 m and 0.6 m, respectively.

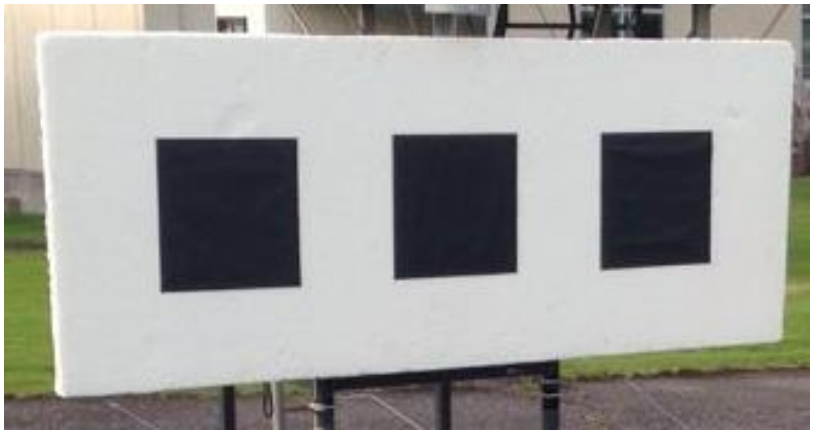

Fig. 6.9 White background and black square marker

6.1.4 Laser sensor

A SICK LMS 511 laser ranger finder (LRF) was used to provide reference data for system performance evaluation (Fig 4.10). The LMS 511 LRF operates according to the time of flight principle. A pulsed laser beam is emitted and reflected once met an object. The maximum scanning angle was 190˚ and maximum measurement range of sensor was about 80 m. The minimum angular resolution of the sensor for scanning the target could be set as 0.167˚. The system error in rang of 10 m was ±25 mm and the statistical error (1 sigma) in rang of 10m was ±7 mm.

Fig. 6.10 SICK LMS 511 Laser ranger finder

Cylinder reflector used in the research was fabricated using plastic reflective sheet pasting on a 15cm diameter PPR cylinder as shown in figure 6.11. Both of the leader and the follower vehicle were installed such reflector above their rear wheel bear center.

Fig. 6.11 Cylinder reflector

6.2 Programming process

The control program was corded with C++ Builder 6.0 on a Windows platform

and OpenCV library was used for image processing. The program composed by function of image frame catch, image processing, leader-follower relative position calculation, I/O board operation and hardware control, vehicle velocity and steering angle calculation.

6.3 Conclusion

The autonomous vehicle was rationally modified from an electronic vehicle. The relationship between voltage of DA board output and the vehicle motion velocity, and relationship between electronic cylinder motion length and steering angle were fully calibrated. The designed low cost monocular vision system possible to provide stable and accuracy observation for navigation a follower to track a leader vehicle.

Chapter 7

Field Evaluation Experiments

Experiments for verifying the stability and accuracy of the camera-marker sensing system and leader trajectory tracking accuracy were conducted. Camera-marker sensing system evaluation experiments included a static evaluation experiment and a dynamic evaluation experiment in two parts. The static evaluation experiment was intent to verify the stability and accuracy of the designed observation method, optimize the camera coefficients, and determine the threshold values for data smoothing. The dynamic evaluation experiment was designed to analyze the observation stability and accuracy when both the leader and the follower were driving, and verify the effectiveness of the least squares method-based data smoothing solution. As a reference the LMS 511 LRF was used to measure the relative position between the camera and the marker in camera-marker sensing system evaluation experiments, and record leader and follower vehicle driving trajectory in tracking performance evaluation experiment.

7.1 Stabilization of camera observation

7.1.1 Camera servo system

Owing to the limitation of the view angle, the camera has a potential risk of losing the target during tracking of the leader vehicle, especially on a large curvature path. To overcome this problem a camera servo system was designed to maintain the marker in the camera view field center. The camera servo was composed of a GWS servo motor and a rotary encoder with the camera (Fig 7.1).

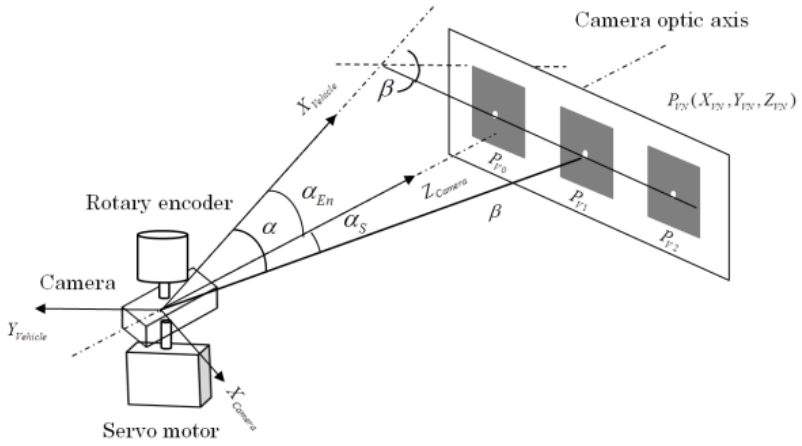

Fig.7.1 Camera servo system

By minimizing angle α_s formed between the middle square center to the camera optic axis, the servo motor could rotary the camera and towards the marker center. The rotation angle α_{En} of camera could be monitored by a rotary encoder installed above the camera. Existing relationship as:

$$\alpha = \alpha_s + \alpha_{En} \tag{7-1}$$

Then the transformation of coordinates between the camera and the follower vehicle could be expressed as follows:

$$X_{VN} = \frac{X_{CN}}{\cos\gamma}\sin\alpha_{En} + Z_{CN}\cos\alpha_{En} \tag{7-2}$$

$$Y_{VN} = -\frac{X_{CN}}{\cos\gamma}\cos\alpha_{En} + Z_{CN}\sin\alpha_{En} \tag{7-3}$$

Where, $P_{VN}(X_{VN}, Y_{VN})$ was the coordinates of the square centers in the follower vehicle based local coordinates.

Relative position between the leader and the follower described in equation (3-13, 14 and15) could be written as:

$$x_{l\_F} = X_{V2} \tag{7-4}$$

$$y_{l\_F} = Y_{V2} \tag{7-5}$$

$$\theta_{l\_F} = \beta \tag{7-6}$$

Where, (X_{V2}, Y_{V2}) was the follower vehicle based local coordinates of the middle square center, β was calculated from the dip angle of the straight line composed by P_{VN} in the follower vehicle local coordinates.

7.1.2 Observation smoothing using least square method

In this study, limited by the camera performance and monocular vision the observed leader-follower relative position was noisy under the worst farm conditions, and in some cases large observed error would occur or there was even a failure to detect the marker plane. Smoothing of observation data was necessary to ensure the accurate tracking of the leader vehicle and also to improve the motion stability of the follower vehicle. The commonly used method of least square was introduced to smooth the relative distance D and the relative heading angle β by fitting a quadratic curve separately.

During the process of data smoothing, predicted data could be obtained by fitting the stored latest certain times of observation data to a quadratic curve using the least square method. The quadratic curve could be written as:

$$Q(s) = as^2 + bs + c \tag{7-7}$$

Where, the s was number of observation times used to store and fit, and $Q(s)$ was the sequence of stored observation data.

As the motion of the two vehicles was continuous, the relative distance and angle between them would not existence jumping during camera observation. To improve the fitting effect and maintain the original transfer tendency the appropriate handing of the stored data used for fitting was the key point.

Once a new camera observation was available the sequence of stored observation

data would be updated and the latest stored data after updating was temporarily determined as follows:

$$q_{Store\_i} = q_{Store\_i+1} \qquad i \in (1,2.....n) \tag{7-8}$$

$$q_{Store\_n} = \begin{cases} q_{Raw} & q_{Error1} < M_1 \\ q_{Store\_n-1} & q_{Error1} > M_1 \end{cases} \tag{7-9}$$

$$q_{Error1} = \left| q_{Store\_n} - q_{Fit} \right| \tag{7-10}$$

After fitting to the quadratic curve using the least square method, the difference between the predicted data and the latest stored data would be calculated and compared with a threshold value, andthe latest stored data could be finally determined as follows:

$$q_{Store\_n} = \begin{cases} q_{Raw} & q_{Error2} < M_2 \\ q_{Fit} & q_{Error2} > M_2 \end{cases} \tag{7-11}$$

$$q_{Error2} = \left| q_{Store\_n} - q_{Fit} \right| \tag{7-12}$$

The current relative position between the leader and the follower vehicle was described by the predicted data q_{Fit}.

Where, q_{Raw} was raw vision data obtained currently, the q_{Fit} was predicted by quadratic curve fitting using the stored latest n times of observation data, q_{Store_i} was stored i_{th} observation data, and M_1 and M_2 were threshold values.

7.2 Evaluation for camera observation stability and accuracy

7.2.1 Static evaluation

In the static evaluation experiment, the position of the marker was expected to

cover the entire camera view field and a large relative angle scope. Thus, the calibrated camera coefficients could be fully adjusted to offset image distortion. The marker position was obtained from the LRF and shown in the camera based local coordinates (Fig 7.2). The maximal distance from the camera to the marker was approximately 6 m and the relative angle formed between the marker and the camera axis ranged from -40˚ to 40˚.

Referenced with the LRF data, the camera observation error of the relative position could be calculated (Fig 7.3). It showed that the accuracy of the orientation angle was relatively stable and had a very low error. However, the accuracy of distance and relative angle was degraded with increasing the relative distance from the camera to the marker. As the reason for this phenomenon, besides the limitation of the camera, the pitch angle of the vehicle also potentially caused observation error on uneven ground. In a real farm task, a larger sized tractor and larger tires would be expected to form a smaller pitch angle, so that the observation error would be limited. Further analysis showed that the accuracy of the camera observation was very high over a distance range of 0~4 m. In more than 89% of observations, the distance and relative angle errors were smaller than 0.05 m and 5˚, respectively; and in more than 97% of observations, these errors were smaller than 0.10 m and 10˚, respectively (Table 7.1); The RMS errors of the distance and relative angle observation errors were 0.036 m and 3.01˚ respectively (Table 7.2).

Table 7.1 Proportions of observation numbers located in certain error scope.

Distance scope	**Proportions of observation numbers in certain error scope**					
	Distance accuracy		**Relative angle accuracy**		**Orientation accuracy**	
	-10~10 cm	**-5~5 cm**	**-10~10 °**	**-5~5 °**	**-0.4~0.4 °**	**-0.25~0.25 °**
0~6m	92.2 %	66 %	96.7 %	64.4 %	93.3 %	80 %
0~4m	97.3 %	89.2 %	100 %	89.2 %	91.8 %	78.3 %

Table 7.2 RMSEs of relative position observation error.

Distance scope	**RMSE**		
	Distance error	**Relative angle error**	**Orientation error**
0~6m	0.058 m	5.07 °	0.228 °
0~4m	0.036 m	3.01 °	0.239 °

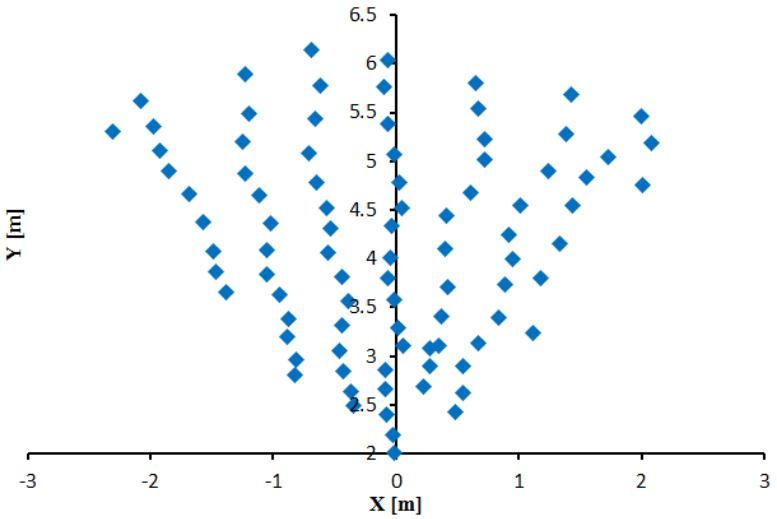

(a)

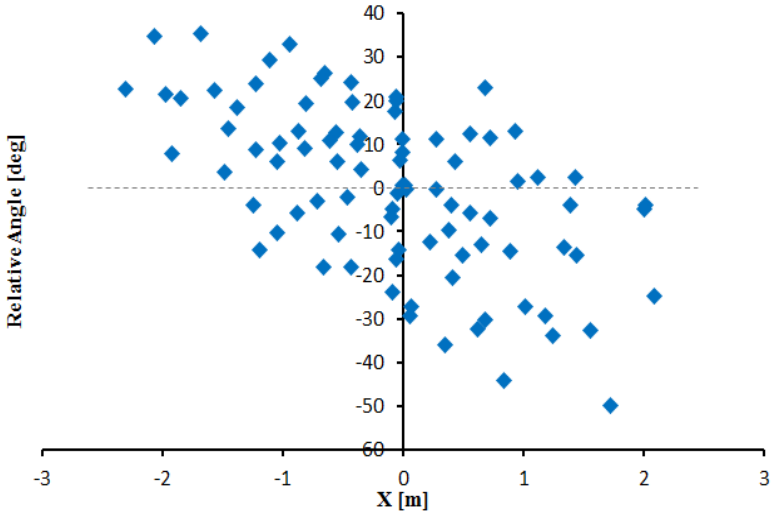

(b)

Fig. 7.2 Position of the marker. (a) Location of the marker.

(b) Relative angle between the marker and the x-axis.

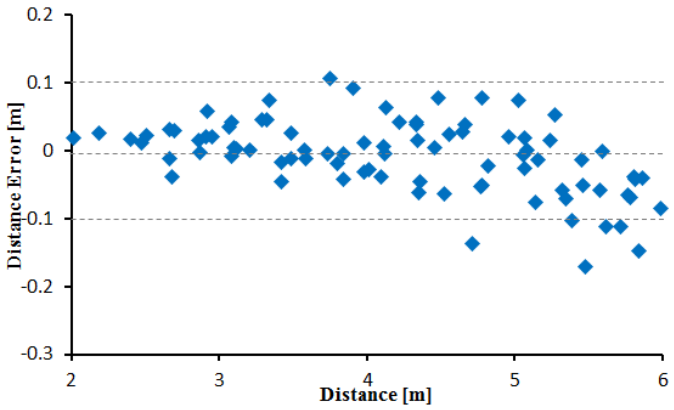

(a)

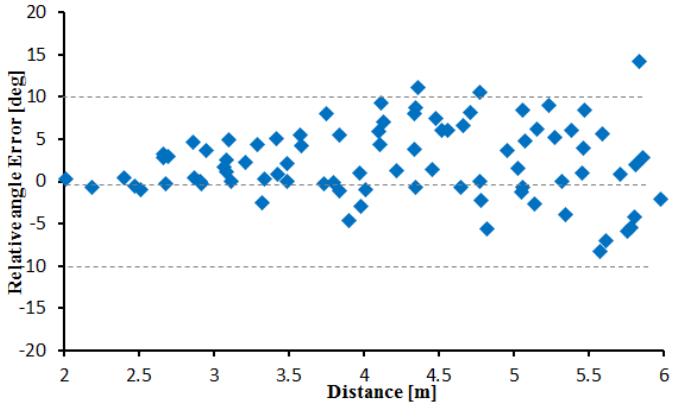

(b)

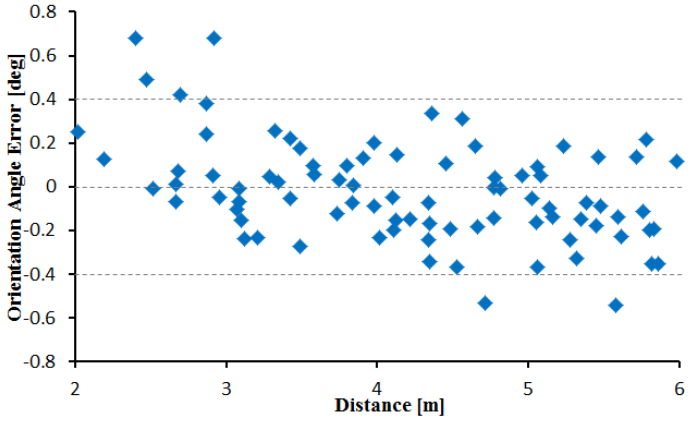

(c)

Fig. 7.3 Accuracy of camera observation.

(a) Distance error. (b) Relative angle error. (c) Orientation error.

7.2.2 Dynamic evaluation

From the static evaluation experiment it was found that for the raw camera observation the orientation angle was stable and of sufficient accuracy, whereas the distance and relative angle were noisy. Thus, the dynamic evaluation was focused mainly on analyzing the distance and relative angle observations. In the dynamic evaluation experiment, the leader vehicle was driven along a zigzag path and the follower vehicle was controlled in remote mode to follow the leader. Raw camera observation data, data smoothed by least square method based curve fitting and LRF observation data were recorded during driving.

The results showed that both the raw and smoothed camera data closely matched the LRF data (Fig 7.4). The RMS errors of relative position error obtained from the raw camera observation were 0.048 m and 3.15˚ for the relative distance and relative angle, respectively. These were coincident with the results under static conditions, meaning that the motion of the marker and the camera did not affect the observation accuracy.

In the experiment, the raw camera observed data were smoothed by fitting a curve using the least square method. After data smoothing, the raw camera observation data was observably smoothed, as was clearly shown by the sample data circled in figure 7.4. Furthermore, the accuracy of relative position observation was improved after data smoothing and RMS errors of the relative distance and relative angle were reduced to 0.046 m and 2.87˚, respectively (Fig 7.5). Compared with the raw camera observation data the dispersion of the smoothed data was also reduced, with the standard deviations of the relative distance and relative angle reduced from 0.049 m to 0.042 m and 3.74˚ to 2.55˚,

respectively (Fig 7.6).

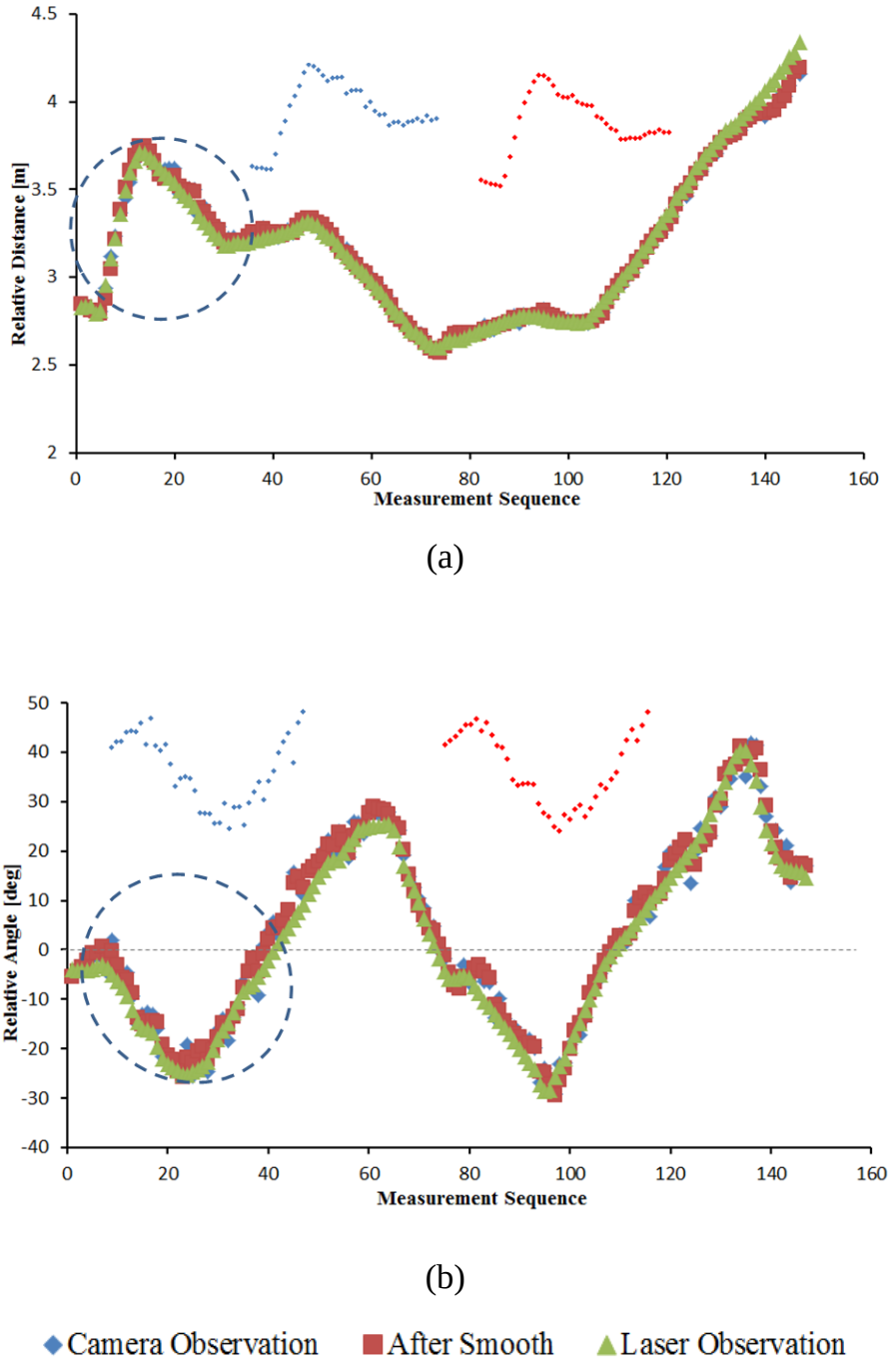

Fig. 7.4 Relative position described by raw camera, smoothed and LRF.

(a) Relative distance. (b) Relative angle.

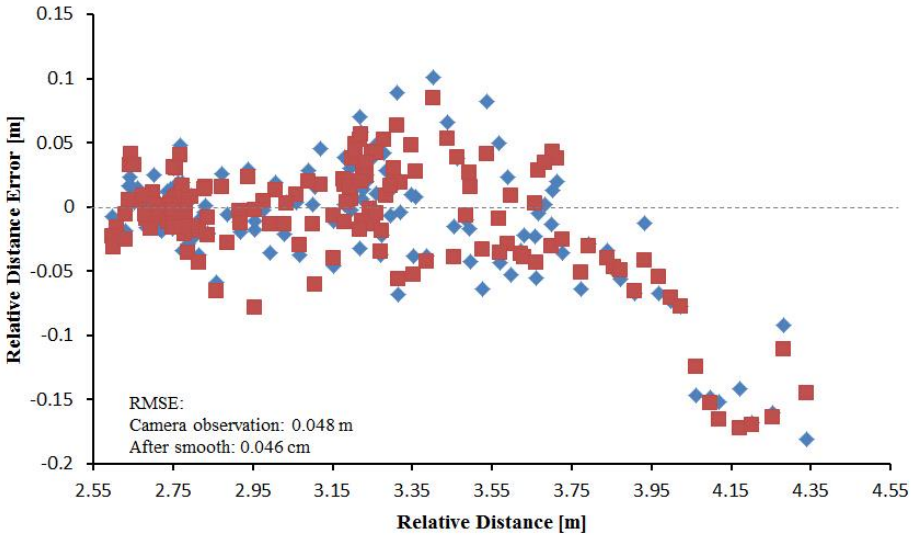

(a)

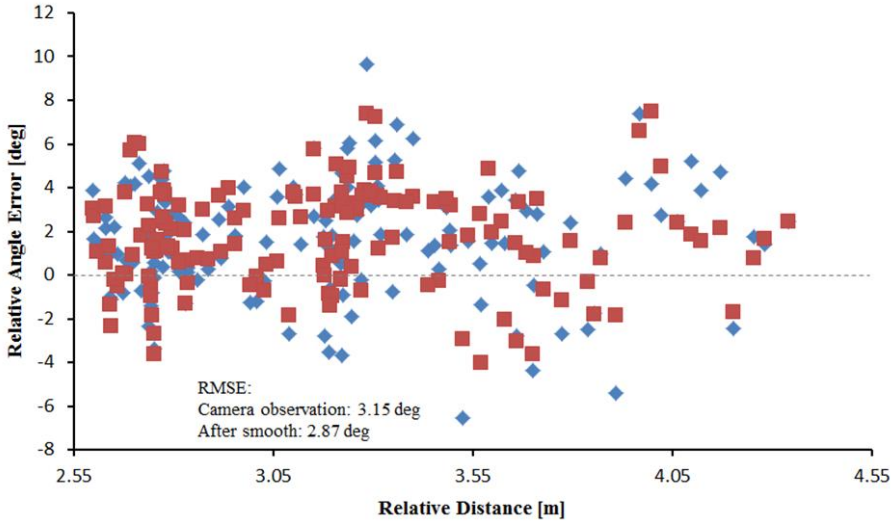

(b)

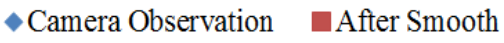

Fig. 7.5 Relative position error of camera observation.

(a) Relative distance error. (b) Relative angle error.

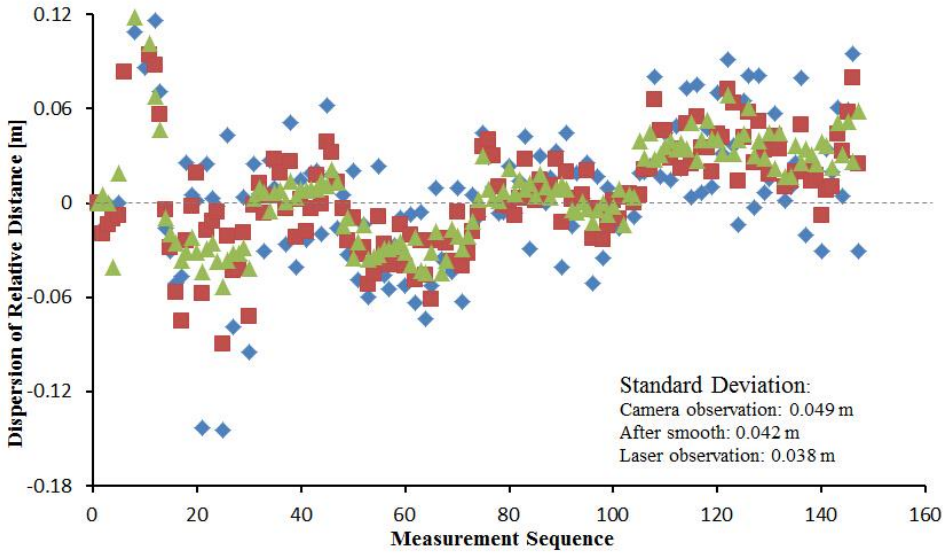

(a)

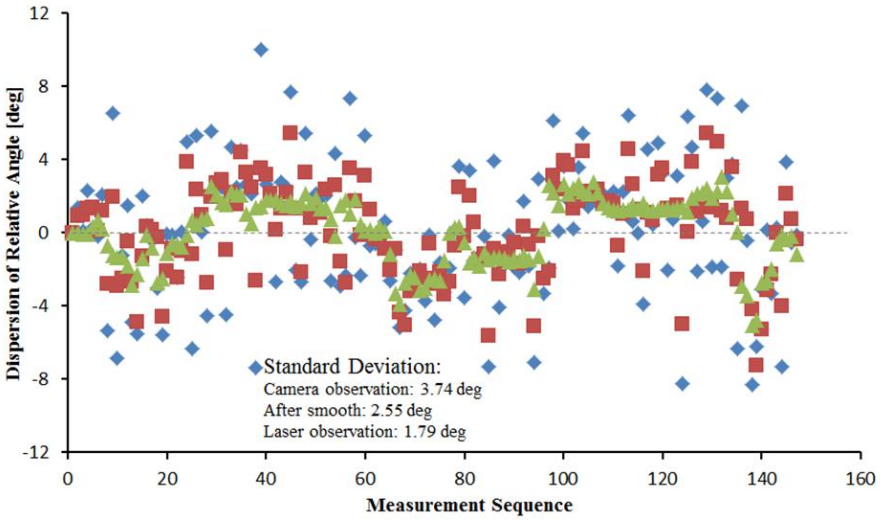

(b)

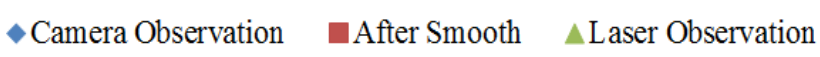

Fig. 7.6 Dispersion of camera observation data.

(a) Dispersion of relative distance. (b) Dispersion of relative angle.

7.3 Evaluation of tracking performance

7.3.1 Evaluation of tracking accuracy

For evaluation of tracking accuracy, linear and parallel tracking experiments were conducted on straight, turning and zigzag paths (Fig 7.7, 10 and 13). Cylindrical markers were mounted above the rear wheel centers of the leader and follower vehicles and a LMS 511 LRF was used to record their trajectores at a frequency of 25HZ. The experiments were conducted on a concrete ground concludes grass, gaps and soil blocks. This will cause a relative large roll angle of the experimental vehicle as reason of its small size. Another set of comparative experiments using the raw camera observation data was conducted for evaluation of efficacy of motion stabilization using the least square method based data smoothing. The leader vehicle was driven at a velocity of 0.25 m/s.

The required distance d_{01} between the leader and follower vehicle was 4 m in linear tracking. In parallel tracking the required lateral and longitudinal distance offsets of the follower vehicle were set at 4 m and 2 m from the leader vehicle, so that the trajectory of the follower vehicle was expected to parallel that of the leader vehicle at a 2 m interval.

According to Figures (7.7, 10 and 13), the follower vehicle could adjust its state and arrive at the required position related to the leader rapidly and smoothly. Tracking accuracy was evaluated by the relative distance between the leader and the follower vehicle, and the interval space between the leader and follower vehicle trajectories, where the trajectory segments of AB and CD were used to calculate this interval space.

Figures (7.8, 11 and 14) show that after the follower vehicle arrived at its

required position the relative distance to the leader vehicle could be maintained. When tracking on a straight path, the average relative distance between the leader and the follower were 4.35 m and 4.79 m for linear and parallel tracking, respectively (Fig 7.8). When tracking on a turning path, the average relative distances were 4.30 m and 4.79 m for linear and parallel tracking, respectively (Fig 7.11). When tracking on a zigzag path, the average relative distances were 4.28 m and 4.75 m for linear and parallel tracking, respectively (Fig 7.14). There was a relative distance error of around 0.3m for both linear tracking and parallel tracking. This error arose because control command of the follower velocity and steering angle could rely only on the relative position between the leader and the follower. From capturing a camera frame to generating a control command, the program needed approximately 200 ms. This delay meant that when the follower responded to compensate the position offset, a new position offset was formed. Adjusting velocity and steering angle also introduced a time delay and noisy camera observations also caused tracking error. However, under different path types in both linear and parallel tracking, the relative distance could be maintained, showing the stability of the tracking system and conforming to the requirements of agricultural operation.

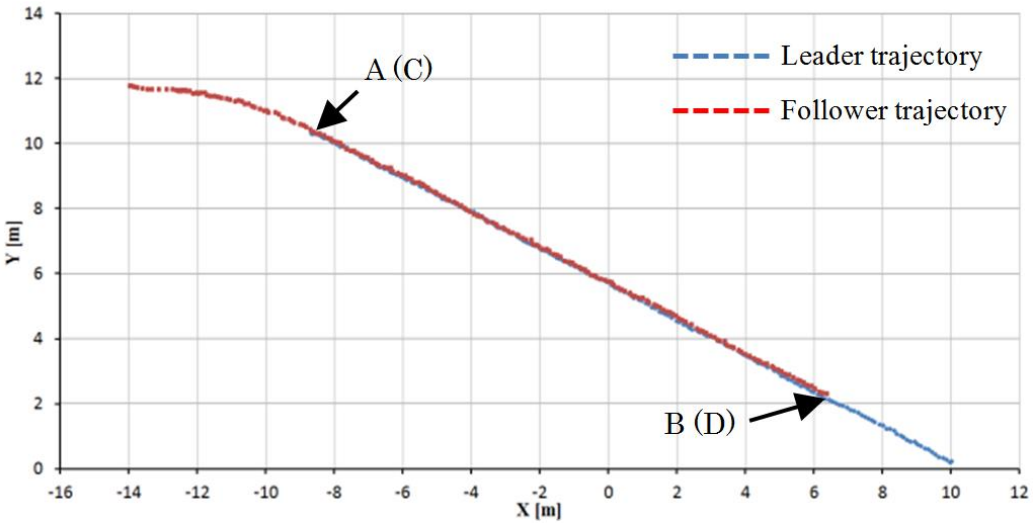

(a)

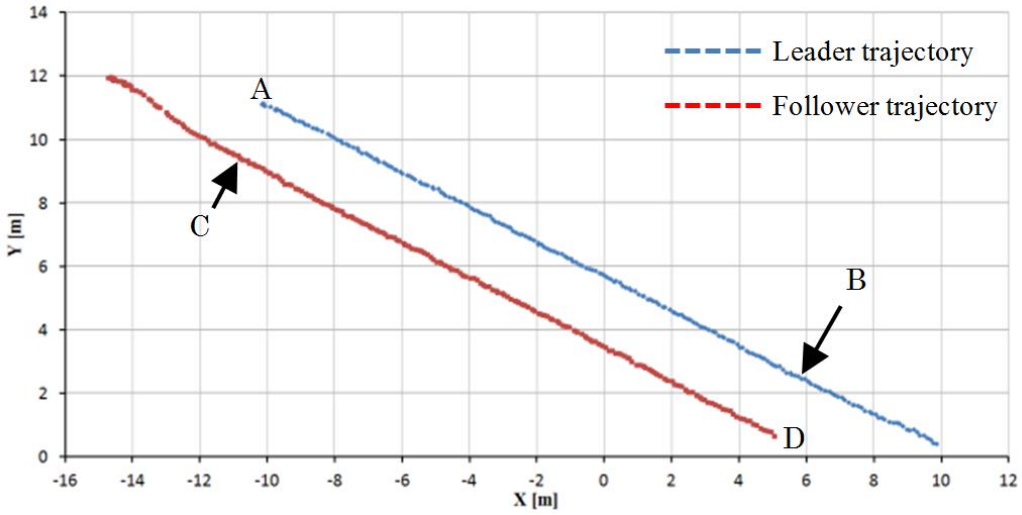

(b)

Fig. 7.7 Leader trajectory tracking on a straight path.

(a) Linear tracking. (b) Parallel tracking.

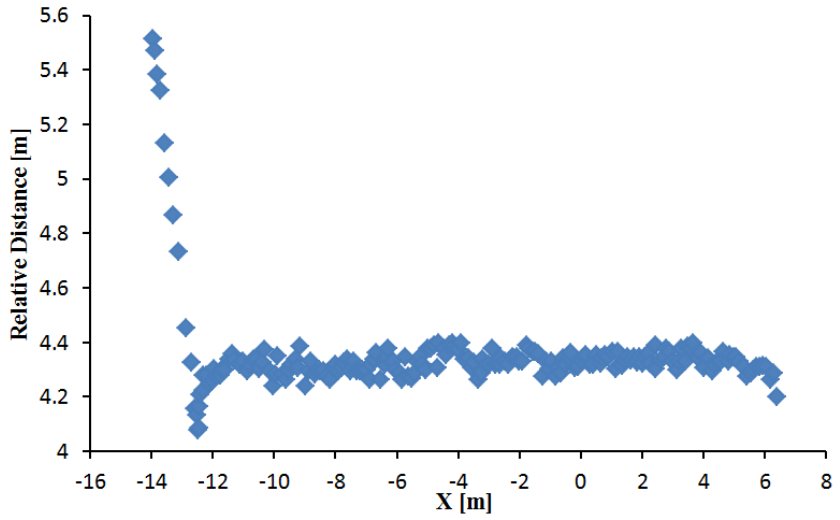

(a)

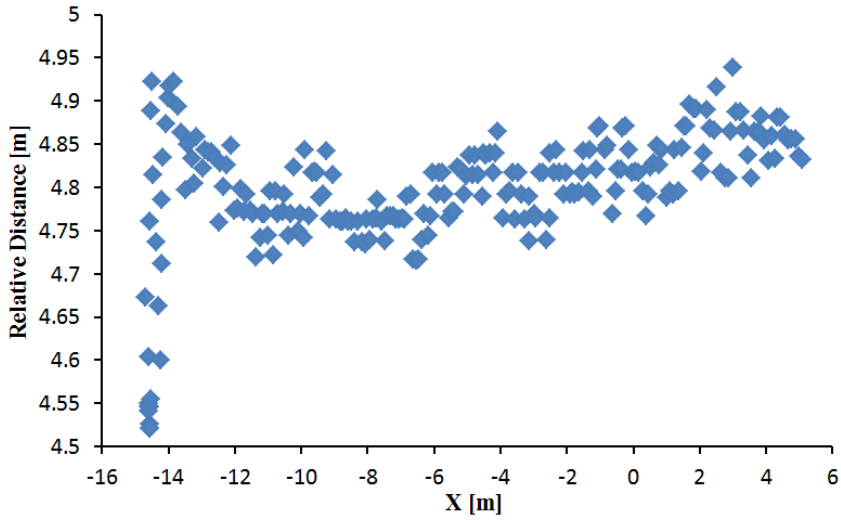

(b)

Fig. 7.8 Relative distance between leader and follower tracking during tracking on a straight path.

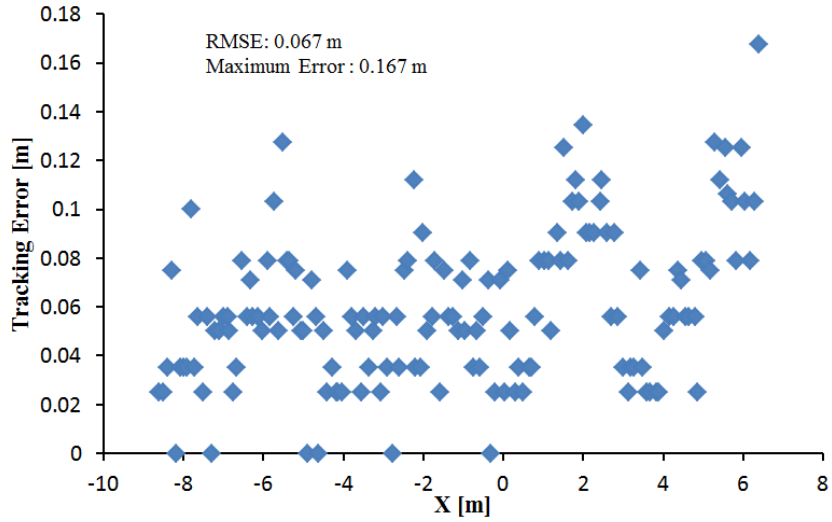

(a)

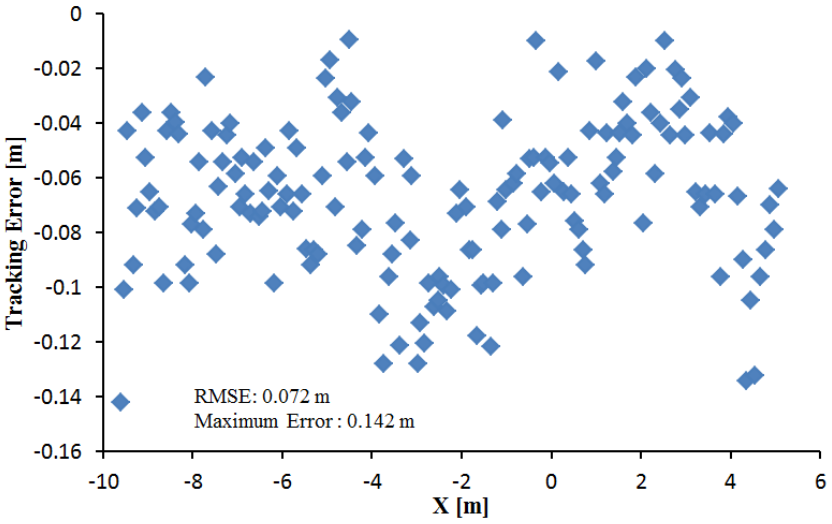

(b)

Fig. 7.9 Tracking error between leader and follower trajectories during tracking on a straight path. (a) Linear tracking. (b) Parallel tracking.

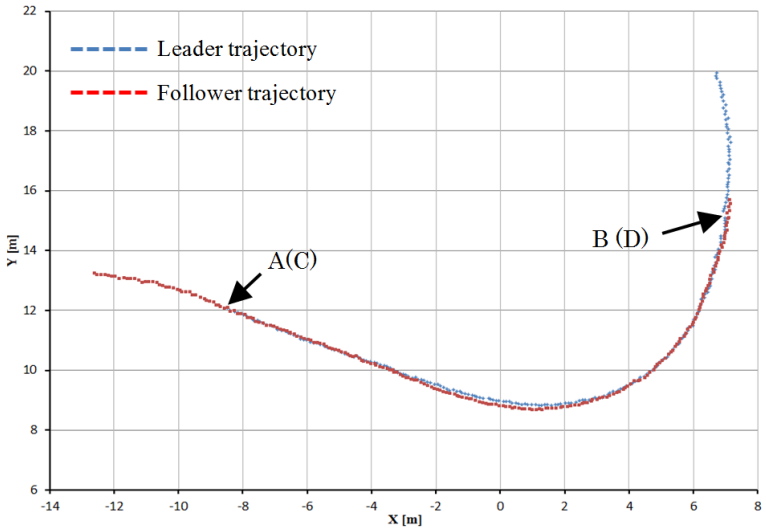

(a)

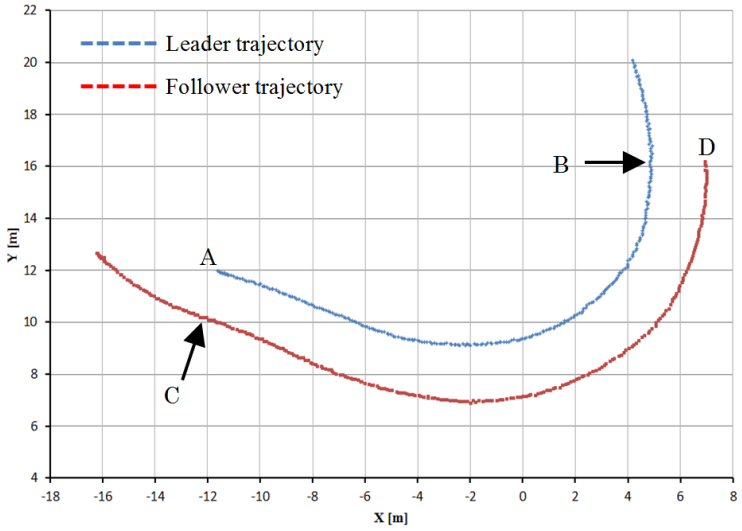

(b)

Fig. 7.10 Leader trajectory tracking on a turning path.

(a) Linear tracking. (b) Parallel tracking.

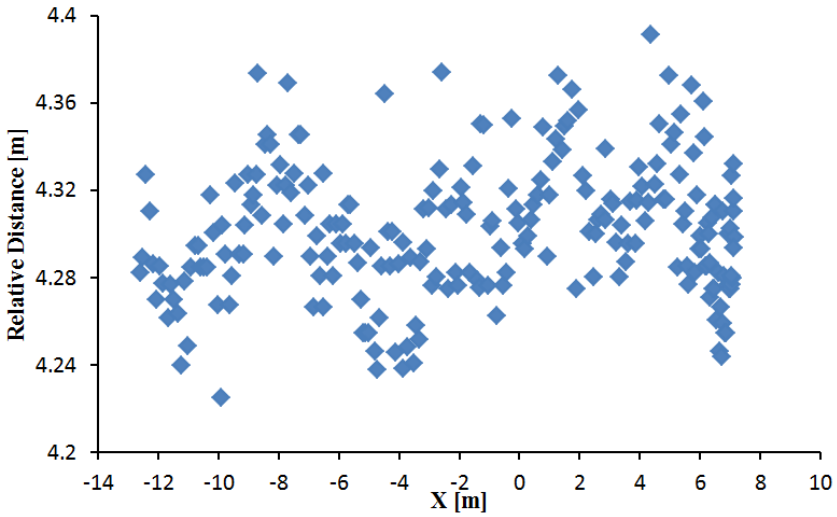

(a)

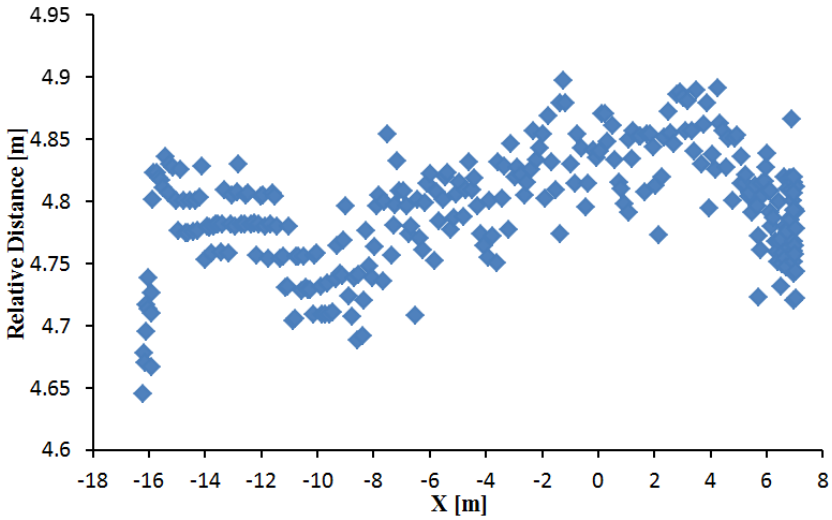

(b)

Fig. 7.11 Relative distance between leader and follower tracking during tracking on a turning path. (a) Linear tracking. (b) Parallel tracking.

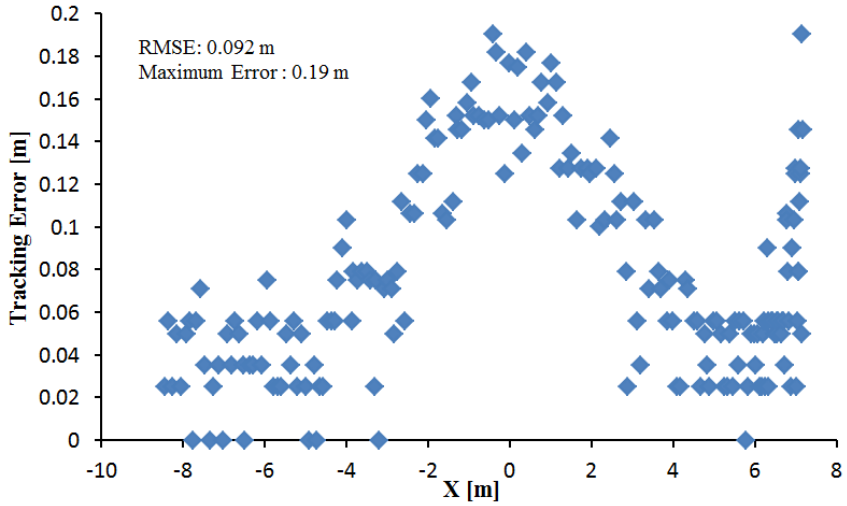

(a)

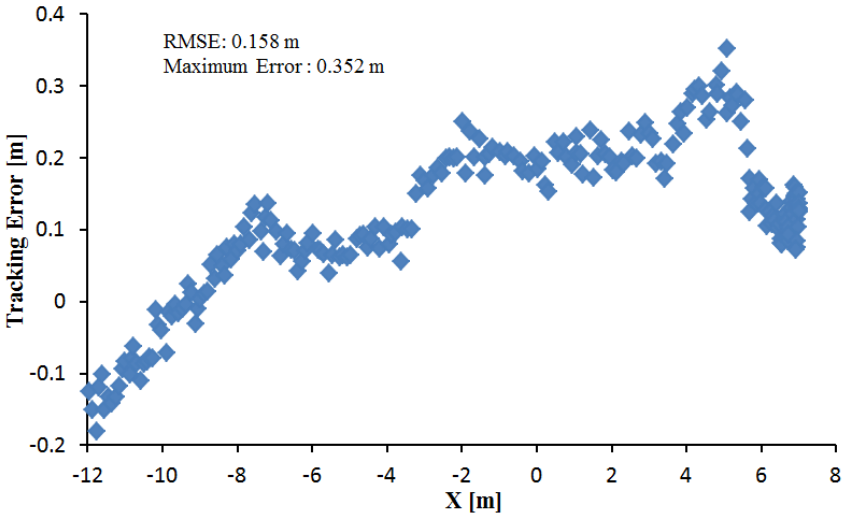

(b)

Fig. 7.12 Tracking error between leader and follower trajectories during tracking on a turning path. (a) Linear tracking. (b) Parallel tracking.

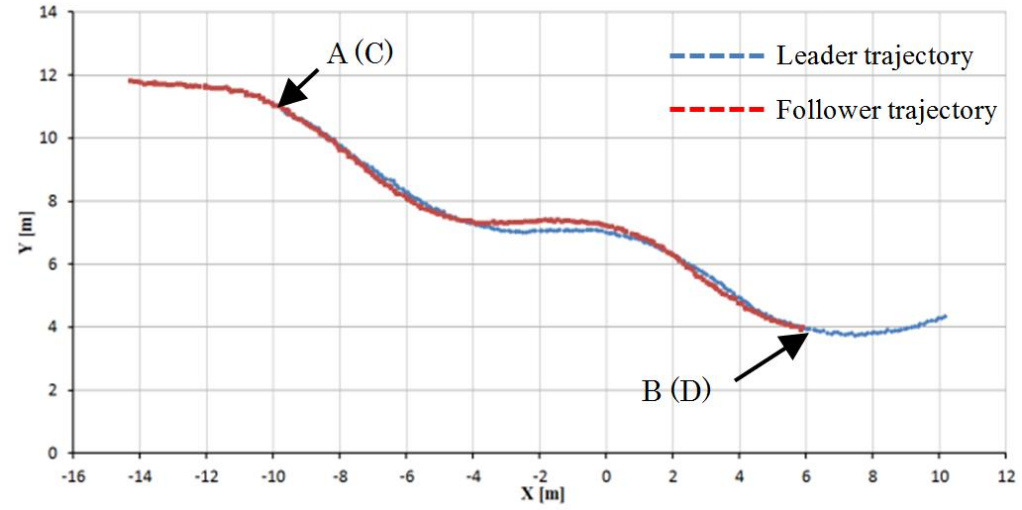

(a)

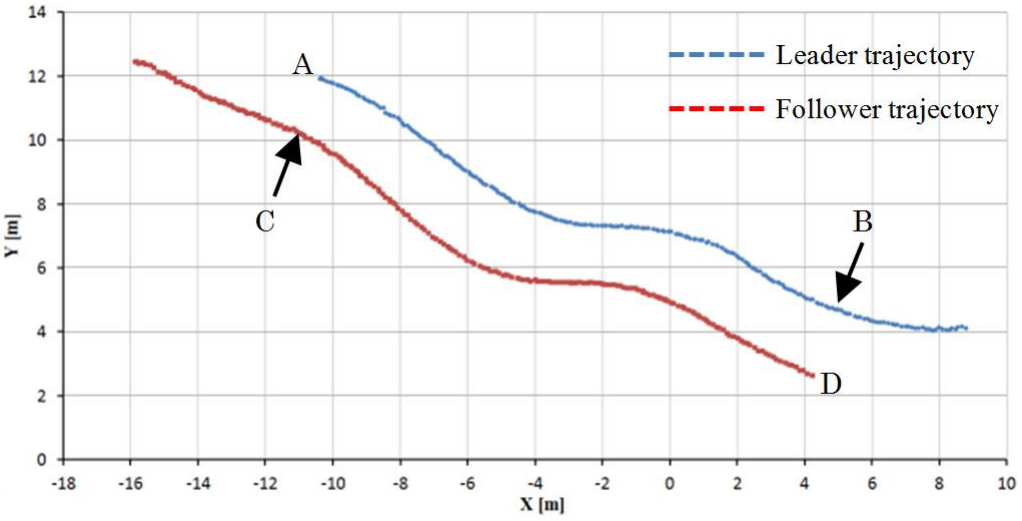

(b)

Fig. 7.13 Leader trajectory tracking on a zigzag path.

(a) Linear tracking. (b) Parallel tracking.

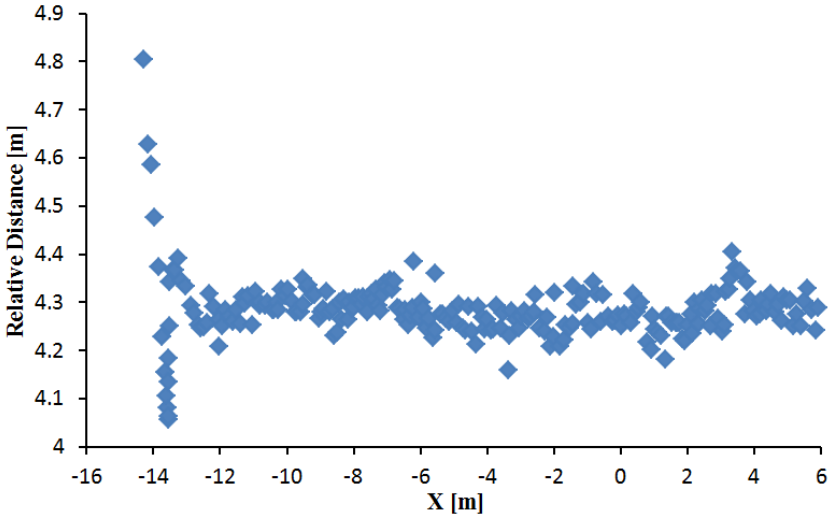

(a)

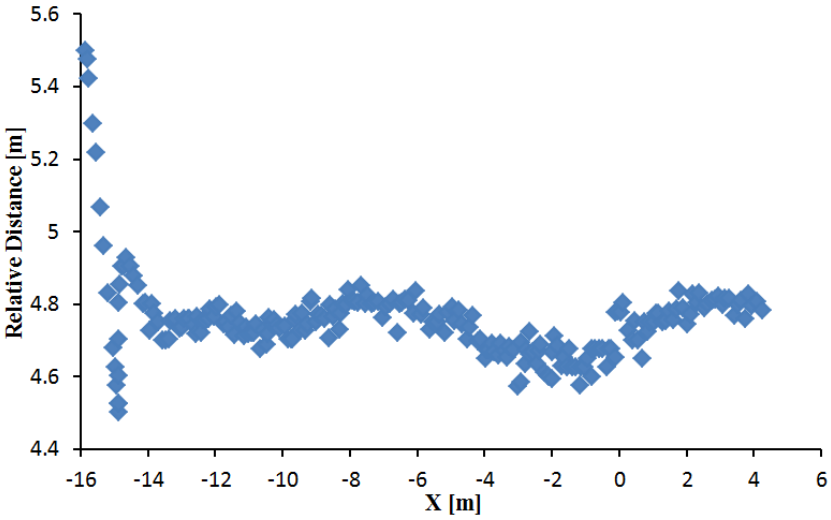

(b)

Fig. 7.14 Relative distance between leader and follower tracking during tracking on a zigzag path. (a) Linear tracking. (b) Parallel tracking.

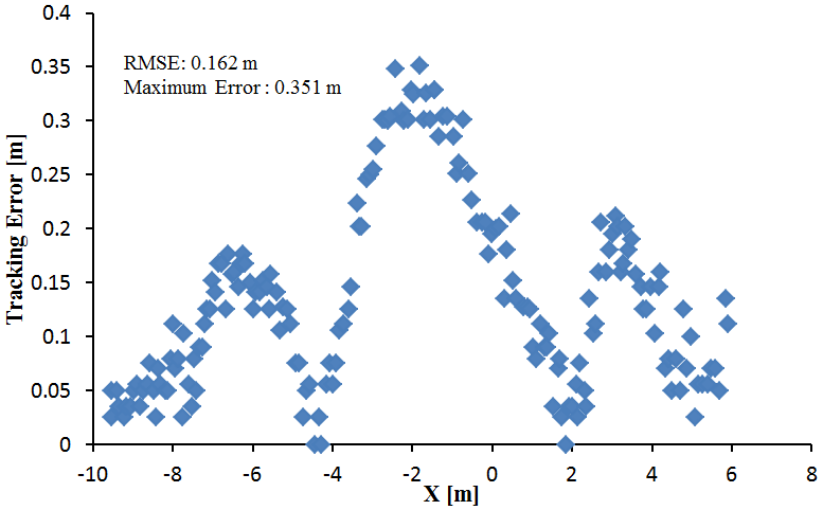

(a)

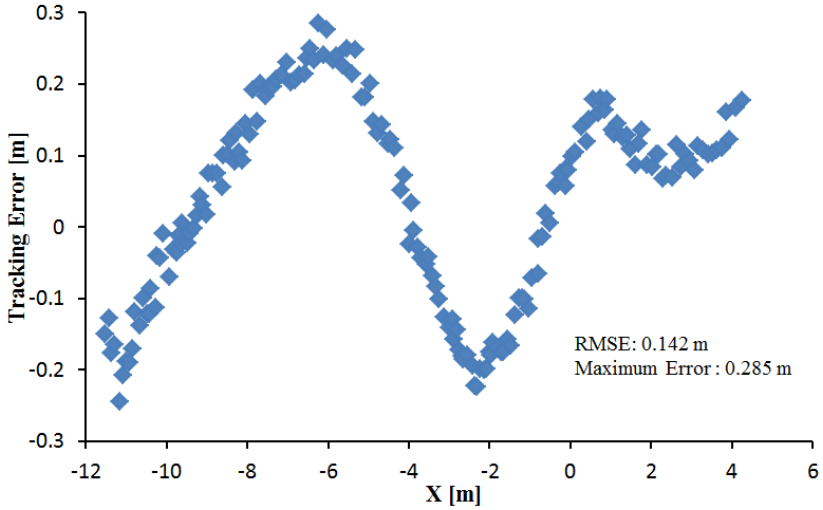

(b)

Fig. 7.15 Tracking error between leader and follower trajectories during tracking on a zigzag path. (a) Linear tracking. (b) Parallel tracking.

The interval space between the leader and follower vehicle trajectories is shown in Figures (7.9, 12 and 15). During tracking on a straight path, a very low tracking error between the trajectories of the leader and follower vehicles could be achieved, and the maximum and RMS tracking errors between these trajectories were 0.167 and 0.067 m for linear and 0.142 and 0.072 m for parallel tracking (Fig 7.9). During tracking on a turning path, the maximum and RMS tracking errors between the trajectories were 0.19 and 0.092 m for linear and 0.352 and 0.158 m for parallel tracking (Fig 7.12); During tracking on a zigzag path, the maximum and RMS tracking errors between the trajectories were 0.351 and 0.162 m for linear and 0.285 and 0.142 m for parallel tracking (Fig 7.15); compared with the straight path, turning and zigzag path tracking showed higher error. Figures (7.10 and 13) show that larger variant the direction of the leader vehicle would result in larger tracking error. This error remained at a low level when the leader vehicle was driven on a constant-curvature path. Considering road space and agricultural operations, the tracking accuracy was sufficient to ensure safe tracking and precision operation.

7.3.2 Evaluation of driving stability

Another set of comparative experiments using raw camera observation data was conducted on the same straight, turning and zigzag paths. To evaluate the stability of the velocity and steering angle of the follower vehicle, the standard deviations of the velocity and steering angle dispersion were calculated and compared with those of the experiment using the least square method based smoothing of camera observation data. Figure 7.16 and 7.17 shows that after smoothing the camera observed data the stability of velocity and steering angle

was significantly improved, table 7.3 shows the improvement of driving stability in straight, turning and zigzag paths. Notice that on parallel tracking the velocity and steering angle showed larger dispersion compare with the linear tracking. The reason was concluded to be that during tracking on parallel the distance from the camera to the marker plane was greater than during tracking on linear. With the limitation of the camera view angle, the servo system would turn the camera to keep the marker located in the image center. Thus, compared with the linear tracking the relative angle between the camera and the marker plane was larger during tracking on parallel. The greater distance and larger relative angle between the camera and the marker plane would introduce greater noise in the camera observation and increase the variation of velocity and steering angle.

7.4 Conclusion

In this chapter, fully experiments were done for evaluation the performance of the camera-marker sensing system and leader trajectory tracking. The results showed that the camera-marker sensing system was enough stability and accuracy to measure the leader-follower relative position for supporting the tracking task, and the leader trajectory tracking algorithm could control the follower stably and realize accuracy tracking.

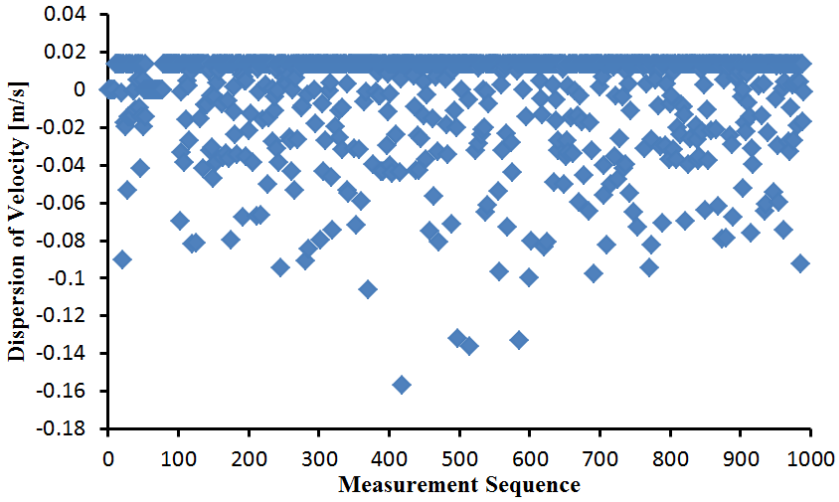

(a)

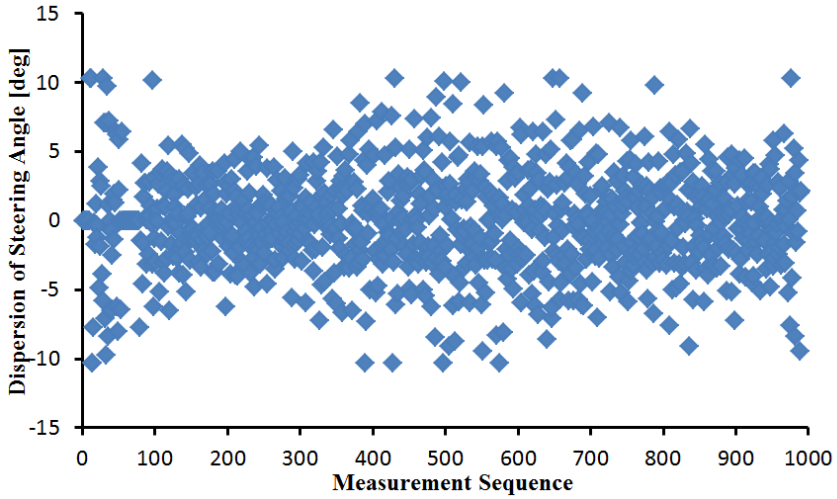

(b)

Fig. 7.16 Dispersion of velocity and steering angle before data smooth.

(a) Velocity Dispersion. (b) Steering angle Dispersion.

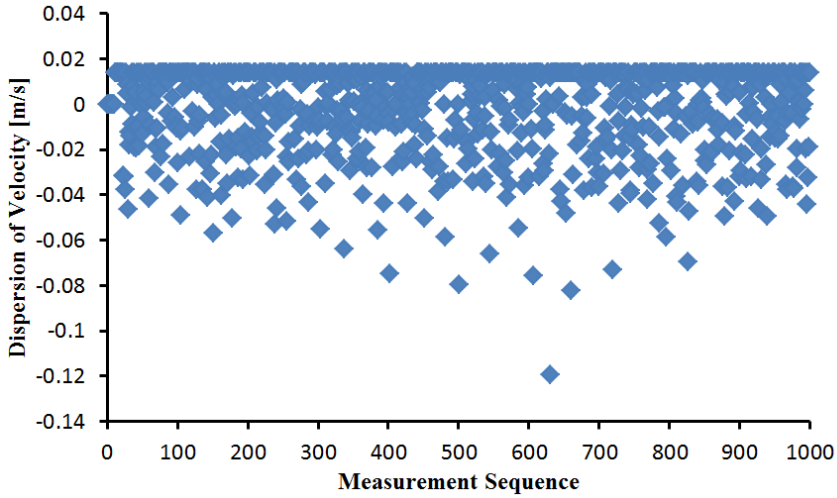

(a)

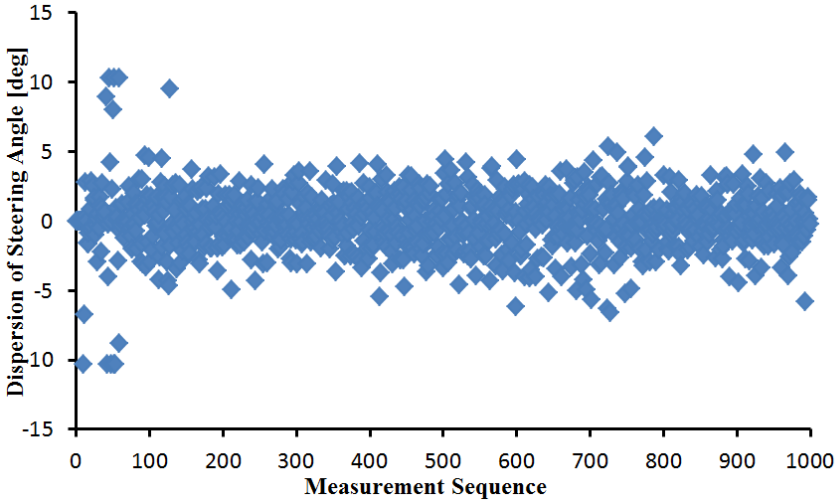

(b)

Fig. 7.17 Dispersion of velocity and steering angle after data smooth.

(a) Velocity Dispersion. (b) Steering angle Dispersion.

Table 7.3 Standard deviation of velocity and steering angle dispersion.

		Standard deviation					
		Straight Path		Zigzag path		Turning path	
		Without Smoothed	Smoothed	Without Smoothed	Smoothed	Without Smoothed	Smoothed
Linear tracking	**Velocity**	0.023 m/s	0.017 m/s	0.021 m/s	0.016 m/s	0.02 m/s	0.0169 m/s
	Steering Angle	3.219 ˚	1.598 ˚	2.152 ˚	1.33 ˚	2.175 ˚	1.194 ˚
Parallel tracking	**Velocity**	0.024 m/s	0.019 m/s	0.024 m/s	0.022 m/s	0.026 m/s	0.019 m/s
	Steering Angle	3.456 ˚	2.048 ˚	3.705 ˚	2.257 ˚	3.539 ˚	2.183 ˚

Chapter 8

Conclusions

This thesis aimed to develop a stable tracking system for multiple agriculture vehicles to improve working efficiency and safety driving. Series of works including sensing system design, control algorithms development and field experiments have been done. The mainly contribution of this study and future work was drawn as follow.

8.1 Summary of contribution

8.1.1 Designed local sensing system

Local sensing systems based on the triangulation principle were developed for LRF and monocular camera. The artificial landmark could ensure the robust recognition by a LRF and camera, and also facilitate to measurement the relative position between the leader and follower vehicles. A least square method based data smooth method was proposed and evaluation experiments showed it could significantly smooth the noisy camera observation data without losing of accuracy.

8.1.2 Applicate the EKF to decrease sensor noise

Under the agricultural environment condition leader-follower relative position measured by local sensing system was easily suffered by external disturbers and would be noisy. An EKF estimation algorithm was developed and proven to have good performance for reducing noise. EKF model for LRF-landmark based local sensing and odometry data fusing was conducted in simulation experiment. After integrating the EKF, the LRF noise was decreased and updated relative positional

information between the leader and the follower quickly and with high accuracy. As a result, stable velocity and steering angle of the follower and high accuracy of formation tracking was established. By estimating the relative position between the leader and the follower in the local coordinate system, the follower could update positional information independently, particularly without GPS and Gyroscope sensors to define its position for tracking the leader. Therefore, a low-cost, reliable navigation system for the leader and the follower could be available.

8.1.3 Development of leader-follower formation tracking algorithm

Tasks as harvesting require a truck driving follow with the harvester to unload the harvested crops. For driving safety and successful task carrying out it was essential to maintain a relative formation with between the leader and follower vehicle. A virtual follower-based feedback control algorithm was development to solve this problem. Simulation experiment showed that under a small curved path the RMSEs of lateral, longitudinal, and heading tracking error was 0.166 m, 0.104 m, and 4.045˚, and on large curved path was 0.195 m, 0.234 m, and 13.613˚, respectively. The results conformed the follower vehicle could realize the stable and accuracy formation tracking with the leader vehicle.

8.1.4 Development of leader vehicle trajectory tracking algorithm

Tracking of the leader vehicle trajectory could was considered as an effective way to ensure the safety driving and precision agricultural task operation for the limited information available autonomous follower vehicles. In this study a control point based simple feedback control algorithm was developed. As the algorithm was only relay on the input of the leader-follower relative position,

thus it was communication free between the leader and the follower. By adjusting the control point location on the follower vehicle centerline and control parameter the follower vehicle could tracking the leader with a requirement distance and trajectory interval. Filed experiments conducted on concert road surface for tracking a leader vehicle driving on straight, turning and zigzag path has been done, and the results showed that both on linear and parallel tracking the algorithm showed excellently performance on tracking accuracy and tracking stability.

8.2 Future work

To complete the work have done in this thesis and further extending the research scope, follow study was expected to continual.

8.2.1 Flexible local sensing system development

Artificial landmark could assist to ensure accuracy and stable of the leader-follower relative position observation. However this method required implement of landmark on the leader vehicle and sometimes was inconvenient. A stable local sensing system based on leader feature was expected to develop in order to improve the flexibility.

8.2.2 Robust tracking system development

The formation tracking and the leader trajectory tracking developed in this study have not considered distributes such as motion obstacles. From the robust point of view the follower vehicle should own performance to cover both obstacle avoiding and the leader vehicle tracking. For this object, the follower vehicle need to improve its sensing capacity then could not only detect the leader vehicle but also the motion obstacles, flexible tracking algorithm was also necessary to

switch between tracking and separation.

8.2.3Tracking control of multiple tractor-trailer system

The present tracking model was developed based on vehicles without trailer. Coordinate driving of multiple tractor-trailer system also own great realistic significance. Based on the knowledge obtained in this study tracking system for multiple tractor-trailer system was expected to study.

Acknowledgements

First, I would like to express indebtedness, deepest sense of gratitude, sincere appreciation to my academic advisor, Professor Tomohiro Takigawa, who introduced me to a most compelling research avenue. His kind advice, scholastic guidance, sympathetic supervision, and encouragement guided me to walk on this avenue.

I also would like to express my profound gratitude and sincere appreciation to my favorite teacher Assoc. Professor Ryozo Noguchi and Assoc. Professor Tofael Ahamed, for their availability, expertise and advice motivation, and encouragement to move forward.

I am pleased to express my cordial respect and gratitude to Professor Atsushi Ishii, my dissertation committee member. His valuable suggestions and corrections helped me to improve this research.

Special gratitude is express to staffs of Agricultural and Forestry Research Center, University of Tsukuba: Mr. Tsuyoshi Honma and Mr. Yasuhiro Matsumoto. Thanks for their helps on experimental vehicle modification.

Sincere gratitude and thanks to my juniors Mr. Nugroho Adi Sasongko, Mr. Gao Peng Bo, Mr. Gan Jing Lin for their great support. Special thanks are extended to all my laboratory's members for their great camaraderie.

Acknowledgement is also due to the Japanese Government for providing a scholarship for my study here.

Finally, my deep gratitude is to my beloved parents, wife and son, sister and brother for their love and mental support.

Reference

Ahamed,T., Takigawa,T., Koike.M., Honma.T., Hasegawa.H., Q. Zhang., 2006. Navigation using a Laser Range Finder for Autonomous Tractor (Part 1)-Positioning of Implement. Journal of the Japanese Society of Agricultural Machinery. 68(1).

Ahamed,T., Tian,L.,Takigawa,T.,Zhang,Y., 2009. Development of Auto-Hitching Navigation System for Farm Implements using Laser Range Finder, Transactions of the American Society of Agricultural and Biological Engineering, 52(5):1793-1803.

Barshan,B., Durrant-Whyte,H.F., 1995. Inertial navigation system for mobile robots. IEEE Transaction on Robotics and Automation, 11(3), 328-342

Barawid Jr., O.C., Mizushima,A., Ishii, K. and Noguchi,N. 2007. Development of an autonomous Navigation System using a Two dimensional Laser Scanner in an Orchard Application. Biosystems Engineering, 96(2), 139-149.

Chen,C., Wang H.., Chew.N.T., Guzm ́an.J.I., Sh.J., Wah.C.C., 2004. Target-tracking and path planning for vehicle following in jungle environment Control, Automation, Robotics and Vision Conference, ICARCV 2004 8th 455 - 460 Vol. 1.

Cho,B.S., Moon,W.S., Seo,W.J., Beak,W.R., 2011. A dead reckoning localization system for mobile robots using inertial sensors and wheel revolution encoding. Journal of Mechanical Science and Technology. 25 (11), 2907-2917.

Chen,J., Sun,D., Yang,J., 2008. A receding-Horizon formation tracking controller with leader-follower strategies. Proceedings of the 17th World Congress The international Federation of Automatic Control Seoul,Korea, July 6-11.

Chateau,T.,Debain,C., Collange,F., Trassoudaine,L., Alizon,J., 2000. Automatic guidance of agricultural vehicles using a laser sensor. Computers and Electronics in Agriculture, 28, 243–257.

Dunbar,W.B., 2007. Distributed receding horizon control of dynamically coupled nonlinear systems. IEEE Transactions on Automatic control, 52(7), 1249-1263.

Fu,H.D., Olaf,P., Wolfgang,H., Roland,K., 2013. “Time-optimal guidance control for an agricultural robot with orientation constraints, Computers and Electronics in Agriculture, 99, pp.124-131.

Gou, A., Akira, M., Noguchi,N., 2005. Study on a Straight Follower Control Algorithm based on a Laser Scanner. Journal of the Japanese Society of Agricultural Machinery, 67(3), 65 -7.

Guo,L.S., He,Y., Zhang,Q., Han, S.F., 2002. Real-Time Tractor Position Estimation System Using a Kalman Filter. CSAE Transactions, 18(5), 96-101.

Hague,T., Marchant,J.A., Tillet,N.D., 2000. Ground based sensing system for autonomous agricultural vehicles. Computer and Electronics in Agricultural, 25: 11-28.

Han, S., Zhang, Q., Ni, B., Reid, J.F., 2004. A guidance directrix approach to vision-based vehicle guidance system. Computers and Electronics in Agriculture, 43,179-195.

Kise.M., Noguchi.N., Ishii. K., Terao.H., 2001. Development of robot tractor based on RTK-GPS and Gyroscope. ASAE Paper 01-1195.

Kannan.S.K., Johnson.E.N., Watanabe.Y., Sattigeri.R., 2011. Vision-Based Tracking of Uncooperative Targets. International Journal of Aerospace Engineering.

Li,M., Imou,K., Wakabayashi,K., Yokoyama,S., 2009. Review of research on agricultural vehicle autonomous guidance. International Journal of Agricultural and Biological Engineering, 2(3), 1-26.

Morin,P., Samson,C., 2008. Motion control of wheeled mobile robots. In, Springer Handbook of Robotics , 799-826.

Maeyama,S., Ohya,A., Yuta,S., 1997. Robust Dead Reckoning System by Fusion of Odometry and Gyro for Mobile Robot Outdoor Navigation. Journal of the Robotics Society of Japan, 15(8), 1180-1187.

Morbidi,F., Parttichizzo,D., 2008. Sliding mode formation tracking control of a tractor and trailer-car system", in Proc. Robotics: Science and Systems III, W. Burgard, O. Brock and C. Stachniss Eds., MIT press, Cambridge MA, pp. 113-120, March.

Madhavan,R., Fregene,K., Parker,L,E., 2004. Distributed Cooperative Outdoor Multirobot Localization and Mapping, Autonomous Robots, 17, 23–39.

Noguchi,N., Barawid,O.J., 2011. Robot Farming System Using Multiple Robot Tractors in Japan. International Federation of Automatic Control, 18(1), 633-637.

Noguchi,N., Reid, J.F., Will,J., Benson,E., Stombaugh, T., 1998. Vehicle automation system based on multi-sensor integration. ASAE paper 98311,

St.Joseph, Michigan, USA.

Noguchi,N., Will,J., Reid,J., Zhang,Q., 2004. Development of a master–slave robot system for farm operations. Computers and Electronics in Agriculture, 44, 1–19.

Núñez,P., Vázquez-Martín, R., Toro, J.C.D., Bandera,A., Sandoval,F., 2008. Natural landmark extraction for mobile robot navigation based on adaptive curvature estimation. Robotics and Autonomous System. Vol.56 247-264.

Nagasaka,Y., Taniwaki,K., Otani,R., Shigeta,K., 2002. An automated rice transplanter with RTKGPS and FOG. Agricultural Engineering International: the CIGR Journal of Scientific Research and Development. Manuscripit PM 01 003. Vol.IV. October.

Qi,J.T., Zhang,S.H., Yu,Y.J., Li,Y., Xu,Y., 2010. Experimental Analysis of Ground Speed Measuring Systems for the intelligent Agricultural Machinery. In: Seventh International Conference on Fuzzy System and Knowledge Discovery (FSKD 2010), 668-671.

Sutiarso, L., Kurosaki,H., Takigawa,T., Koike,M., Yukumoto,O., Hasegawa,H., 2002. Trajectory control and its application to approach a target: Part II. Target approach experiments. ASAE Transactions, 45 (4), 1199-1205.

Torii,T., Kanuma,T., Okamoto,T., Kitani,O., 1996. Image analysis of crop row for agricultural mobile robot. Processding of AGENG96, Madrid, Spain, EurAgEng, 1045-1046.

Thrun,S., Burgard,W., Fox,D., 2005. Probabilistic Robotics (Intelligent Robotics and Autonomous Agents). The MIT Press,USA.

Van Zuydam,R.P., 1999. A driver's steering aid for an agricultural implement,

based on an electronic map and Real Time Kinematic DGPS. Computers and Electronics in Agricultural. 24(3), 153-163.

Wu,D., Zhang, Q., Reid,J.F., Qiu,H., 1999. Adaptive control of electrohydraulic steering system for wheel-type agricultural tractors. ASAE Paper 993079.

Yang,E.,Gu,D.B., 2007. Nonlinear Formation-Keeping and Mooring Control of Multiple Autonomous Underwater Vehicles. IEEE/ASME transactions on mechatronics, 12(2).

Yamaguchi,H., Tamio,A., 2003. A Path Following Feedback Control Method for a Cooperative Transportation System with Two Car-Like Mobile Robots. The Society of Instrument and Control Engineers, 39(6), 575-584.

Yu,Y.J., Zhang,S.H., Qi,J.T., Zhang,L.H., 2009. Positioning Method of Variable Rate Fertilizer Applicator Based on Sensors. Transactions of the CSAM, 40(10), 165-168.

Zhang,X., Geimer,M., Noack,P.O., Grandl,L., 2010. A semi-autonomous tractor in an intelligent master–slave vehicle system. Intelligent Service Robotics, 3(4), 263-269.

Zhou,J.J., Wang,X., Wang,X.F., Liu,G., Li,S., 2013. Autonomous Navigation system based on GPS for Agricultural Vehicles. Advanced Materials Research Vols.774-776, 1404-1408.